MODELLING OF PULVERISED COAL SWIRLING FLAMES IN AXI-SYMMETRIC FURNACES

Final Report to Thermal Sciences Limited

F. C. Lockwood and M. A. Yehia

ThermoFluid Section
Mechanical Engineering Department
IMPERIAL COLLEGE

January 1992

93-01528/

ABSTRACT

A mathematical model of pulverised coal combustion is developed and applied to predict the flow and combustion characteristics of swirling flames in axi-symmetric furnaces. The model is based on the solution of the time-averaged equations for the conservation of mass, momentum, species and energy for gaseous and particulate phases.

The model validation involved an extensive predictive study that used data gathered from three large scale experimental furnaces at three laboratories: the Imperial College for Science Technology and Medicine (ICSTM), the International Flame research Foundation (IFRF) and the Canadian Combustion Research Laboratory (CCRL). The data collected in the ICSTM laboratory was expressly for validation purposes, thus allowing special emphathsis to the near burner region which dominates the flame stability behaviour and emissions of NO.

Comparisons of the simulations with the experimental measurements reveals both predictive strengths and deficiencies. Most of the burner types studied are reasonably well simulated while the performance of one of them is less well reproduced.

A wide ranging study to explore the sensitivities of the predictions to variations of the model parameters was undertaken in an attempt to elucidate the sources of the discrepancies. The difficulty of this detective work was considerably amplified due to the non-existence of a reliable technique for velocity measurements in a dense pulverised coal flow field. Nonetheless, the poor prediction of the aerodynamic field of the 'difficult' burner was ultimately identified as the principal cause of the prediction problems.

CONTRACT SERIAL NO. 23440-7-9130-01-SQ
CONTRACTOR: THERMAL SCIENCES LIMITED
TITLE: MODELLING OF PULVERISED COAL
BY SWIRLING FLAMES IN AXI-SYMMETRIC
FURNACES: FINAL REPORT

see other part of report TITLE: COMPUTATION
OF RADIANT HEAT TRANSFER ON A NON-ORTHOGONAL
MESH USING THE FINITE VOLUME METHOD (Dec. 27/
1991)

219pp

MICROMEDIA

TABLE OF CONTENTS

ABSTRACT

TABLE OF CONTENTS 3

LIST OF FIGURES 6

LIST OF TABLES 10

NOMENCLATURE 11

Roman Symbols 11

Greek Symbols 13

Subscripts 14

Key words 14

1. INTRODUCTION 16

1.1 PREAMBLE 17
1.2 BACKGROUND OF PHYSICAL MODELLING IN PULVERISED COAL FURNACES 19
1.3 OBJECTIVES AND PRESENT CONTRIBUTION 28
1.4 LAYOUT OF THE THESIS 30

2. PHYSICAL MODELLING 33
2.1 INTRODUCTION 34
2.2 TURBULENCE MODEL 36
2.2.1 Eddy Viscosity Models 38
2.2.1.1 Zero-equation models 38
2.2.1.2 One-equation models 39
2.2.1.3 Two-equation models 39
2.2.2 Reynolds Stress Models 41
2.2.3 Algebraic Stress Models 42
2.2.4 Comparison Between k-ε, ASM and RSM 42
2.2.5 Dificiencies of Standard k-ε Model and Their Possible Remedies 44
2.2.5.1 Streamline curvature 44
2.2.5.2 Interaction of particles 45
2.3 RADIATION HEAT TRANSFER MODELLING 47
2.3.1 Radiation Transfer Equation 47
2.3.2 Radiation Solution Methods 49
2.3.2.1 Statistical methods 49
2.3.2.2 Zonal methods 50
2.3.2.3 Flux methods 50

2.3.3 Mathematical Formulation of the Non-Equilibrium Diffusion Model 51
2.4 PARTICLE MOTION EQUATION 55
2.5 PARTICLE ENERGY BALANCE EQUATION 57
2.6 DEVOLATILISATION MODEL 59
2.6.1 Single Reacting Model 60
2.6.2 Two Competing Reaction Model 61
2.6.3 Multiple Parallel Reaction Model 63
2.6.4 Advanced Devolatilisation Models 63
2.6.4.1 Wen and Chen model 63
2.6.4.2 Suuberg model 64
2.6.5 Choice of Devolatilisation Model 65
2.7 VOLATILE COMBUSTION 66
2.8 HETEROGENEOUS CHAR COMBUSTION 68

3. NUMERICAL SOLUTION 71
3.1 INTRODUCTION 72
3.2 THE COMPUTATION GRID 73
3.3. DISCRETISATION OF THE GENERAL DIFFERENTIAL EQUATION 74
3.3.1 The Convection Terms 74
3.3.1 1 The central differencing scheme 76
3.3.1.2 The upwind scheme 76
3.3.1.3 The hybrid scheme 77
3.3.1.4 The QUICK scheme 77
3.3.1.5 Choice of discretisation scheme 79
3.3.1.6 Final form of the convection terms 80
3.3.2 The Diffusion Terms 80
3.3.3 The Source Terms 81
3.3.4 The Final Form of the Discretised Equation 82
3.4 PRESSURE VELOCITY DECOUPLING 84
3.4.1 The SIMPLE Algorithm 84
3.4.2 The SIMPLER Algorithm 85
3.4.3 The PISO Algorithm 86
3.4.4 Choice of Solution Algorithm 88
3.5 SOLUTION OF THE FINITE DIFFERENCE EQUATIONS 89
3.6 THE BOUNDARY CONDITIONS 90
3.6.1 Inlet Boundary Conditions 90
3.6.2 Exit Boundary Conditions 91
3.6.3 Axis of Symmetry 92
3.6.4 The Wall Boundary Conditions 92
3.6.5 The Quarl Boundary Conditions 94
3.7 THE PARTICULATE PHASE 95

4. EXPERIMENTAL FURNACES AND TEST CONDITIONS 99
4.1 INTRODUCTION 100
4.2 THE FURNACES 102
4.2.1 The CCRL Furnace 102
4.2.2 The ICSTM Furnace 102

4.2.3 The IFRF Furnace 106
4.3 TEST CONDITIONS 107
4.3.1 Isothermal Runs 107
4.3.2 CCRL Combustion Runs 108
4.3.3 Near Burner Runs for Flow Type 2 111
4.3.4 Near Burner Runs for Flow Type 3 111
4.4 PREDICTION PARAMETERS 115

5 RESULTS AND DISCUSSION 116
5.1 INTRODUCTION 117
5.2 ISOTHERMAL CASES 118
5.3 COMBUSTION CASES FOR CCRL FURNACES 132

5.4 COMBUSTION CASES FOR FLOW TYPE 2 152

5.4.1 The IFRF Flame Predictions (Case iii-1) 152
5.4.2 The ICSTM Flame Predictions (Case iii-2) 153

5.5 COMBUSTION CASES FOR FLOW TYPE 3 159
5.5.1 Aerodynamic Flow Pattern and Particle Trajectories 159
5.5.2 Particle History 160
5.5.3 Radial Profiles 167
5.6 PARAMETRIC TESTS 169
5.6.1 The Discretisation Scheme 169
5.6.2 The Inlet Conditions 170
5.6.3 Coal Devolatilisation 174
5.6.3.1 Volatile yield 174
5.6.3.2 Devolatilisation kinetics 176
5.6.3.3 Ignition delay 179
5.6.3.5 Secondary cracking 179
5.6.4 Char Reactivity 182
5.6.5 Coal Demoisturisation 183
5.6.6 Gas Combustion 184
5.6.6.1 The empirical constant 184
5.6.6.2 The volatile chemical kinetic rate 185
5.6.6.3 The flammability limit 186
5.6.7 Effect of Other Parameters 189
5.6.7.1 Particle size distribution 189
5.6.7.2 Drag coefficient 192
5.6.7.3 Effects of soot in radiation heat transfer 192
5.6.7.4 Effect of inlet swirl 194
6. CONCLUSIONS AND SUGGESTIONS FOR FUTURE WORK 199
6.1 RECAPITULATION 200
6.2 CONCLUSIONS 202
6.3 SUGGESTIONS FOR FUTURE WORK 204

REFERENCES 206

LIST OF FIGURES

Figure 1.1 Layout of the FAFNIR program.
Figure 2.1 Cylindrical volume element showing the change of radiative energy.
Figure 2.2 Schematic diagram illustrating the two competing reactions model.
Figure 3.1 The staggered grid.
Figure 3.2 The control volume for scalar, U-velocity and V-velocity cells.
Figure 3.3 Standard five point molecule.
Figure 3.4 Extended nine point molecule.
Figure 3.5 Schematic diagram for the grid clusters in one dimensional notation.
Figure 3.6 The particle trajectory for a time step between A and Z showing intersections with the boundaries of the cells.
Figure 4.1 Schematic of the interior of the CANMET tunnel furnace, distances in cm.
Figure 4.2 Schematic diagram of the burner geometries used for the CCRL furnace, distances in cm.
Figure 4.3 Schematic of the interior of the ICSTM furnace, distances in mm.
Figure 4.4 Schematic diagram of the ICSM burners.
Figure 4.5 Schematic diagram of the IFRF furnace.
Figure 5.1 Comparison between measurements and predictions for the radial profiles of the mean axial and tangential velocities for Case i-1 at quarl exit (x/D = 2.06), first port (x/D = 4.29), second port (x/D = 5.81) and third port (x/D = 7.44).

Figure 5.2 Comparison between measurements and predictions for the radial profiles of the mean axial and tangential velocities for Case i-2 at quarl exit (x/D = 2.06), first port (x/D = 4.29), second port (x/D = 5.81) and third port (x/D = 7.44).

Figure 5.3 Comparison between measurements and predictions for the radial profiles of the mean axial and tangential velocities for Case i-3 at quarl exit (x/D = 2.06), first port (x/D = 4.29), second port (x/D = 5.81) and third port (x/D = 7.44).

Figure 5.4 Comparison between measurements and predictions for the radial profiles of the mean axial and tangential velocities for Case i-4 at quarl exit (x/D = 2.06), first port (x/D = 4.29), second port (x/D = 5.81) and third port (x/D = 7.44).

Figure 5.5 Comparison between measurements and predictions for the radial profiles of the mean axial and tangential velocities for Case i-5 at quarl exit (x/D = 2.06) and first port (x/D = 4.29).

Figure 5.6 Comparison between measurements and predictions for the radial profiles of the mean axial and tangential velocities for Case i-6 at quarl exit (x/D = 2.06), first port (x/D = 4.29), second port (x/D = 5.81) and third port (x/D = 7.44).

Figure 5.7 Comparison between measurements and predictions for the radial profiles of the mean axial velocities for Case i-7 at quarl exit (x/D = 2.06), first port (x/D = 4.29), second port (x/D = 5.81) and third port (x/D = 7.44).

Figure 5.8 Comparison between measurements and predictions for the radial profiles of the mean axial and tangential velocities for Case i-8 at quarl exit (x/D = 2.06).

Figure 5.9 Comparison between measurements and predictions for the radial profiles of the mean axial and tangential velocities for Case i-9 at quarl exit (x/D = 2.06).

Figure 5.10 Comparison between measurements and predictions for the radial profiles of the mean axial and tangential velocities for Case i-10 at quarl exit (x/D = 2.06).

Figure 5.11 Comparison between measurements and predictions for the radial profiles of the mean axial and tangential velocities for Case i-11 at quarl exit (x/D = 2.06).

Figure 5.12.a Contours of the stream function, temperature and oxygen concentration for Case ii-1

Figure 5.12.b The axial distribution of temperature, oxygen concentration and burnout for Case ii-1

Figure 5.12.c Comparison between the predictions and measured data of the radial profiles for oxygen concentration and gas temperature for Case ii-1.

Figure 5.13.a Contours of the stream function, temperature and oxygen concentration for Case ii-2

Figure 5.13.b The axial distribution of temperature, oxygen concentration and burnout for Case ii-2.

Figure 5.13.c Comparison between the predictions and measured data of the radial profiles for oxygen concentration and gas temperature for Case ii-2.

Figure 5.14.a Contours of the stream function, temperature and oxygen concentration for Case ii-3

Figure 5.14.b The axial distribution of temperature, oxygen concentration and burnout for Case ii-3

Figure 5.14.c Comparison between the predictions and measured data of the radial profiles for oxygen concentration and gas temperature for Case ii-3.

Figure 5.15.a The predicted near burner aerodynamic flow pattern for Case ii-4

Figure 5.15.b Comparison between the experimental data and the predicted gas temperature for Case ii-4.

Figure 5.15.c Comparison between the experimental data and the predicted oxygen concentration for Case ii-4.

Figure 5.16.a Comparison between the experimental data and the predicted gas temperature for Case ii-5.

Figure 5.16.b Comparison between the experimental data and the predicted oxygen concentration for Case ii-5.

Figure 5.17.a Predicted contours of stream function, oxygen and temperature for case ii-6.

Figure 5.17.b Comparison between the experimental data and the predicted oxygen concentration and gas temperature for Case ii-6.

Figure 5.18 Comparison between the experimental data and the predicted oxygen concentration and gas temperature for Case ii-7.

Figure 5.19.a The predicted gas flow pattern and particle trajectories in the NBR for the IFRF flame (Case iii-1).

Figure 5.19.b Comparison between predicted radial profiles of oxygen concentration and gas temperature and the experimental data for the IFRF flame (Case iii-1).

Figure 5.20.a The predicted gas flow pattern and particle trajectories in the NBR for the ICSTM flame (Case iii-2).

Figure 5.20.b Comparison between predicted radial profiles of oxygen concentration and gas temperature and experimental data for the ICSTM flame (Case iii-2).

Figure 5.21.a The predicted gas flow pattern and particle trajectories in the NBR for Case iv-1.

Figure 5.21.b Comparison between the predictive and experimental radial profiles of oxygen concentration and gas temperature for Case iv-1

Figure 5.22.a The particles weight losses and temperature versus residence time for Case iv-1.

Figure 5.22.b The particles weight losses and temperature versus residence time for Case iv-2.

Figure 5.23.a The predicted gas flow pattern and particle trajectories in the NBR for Case iv-3.

Figure 5.23.b Comparison between the predictive and experimental radial profiles of oxygen concentration and gas temperature for Case iv-3.

Figure 5.24 Contours of stream function for isothermal prediction of the SCO burner using Hybrid and QUICK discretisation schemes.

Figure 5.25 The effect of the discretisation scheme on the prediction of Case iv-1.

Figure 5.26 The effect of the inlet profile on the prediction of Case iv-3.

Figure 5.27 The effect of the volatile yield on the prediction of Case iv-3.

Figure 5.28 The effect of the volatile kinetics on the prediction of Case iv-3.

Figure 5.29 The effect of the devolatilisation model on the prediction of Case ii-2.

Figure 5.30 The effect of the ignition delay on the prediction of Case iv-1.

Figure 5.31 The effect of secondary cracking on the prediction of Case iv-3.

Figure 5.32 The effect of flammability limits on the prediction of Case iv-3.

Figure 5.33.a The particle trajectories for the large size particles (d_p= 125 μ) for Case iii-2.

Figure 5.33.b Comparison between the predictive and experimental radial profiles of oxygen concentration and gas temperature for Case iii-2 using large size particles (.d_p= 125 μ).

Figure 5.34.a The particle trajectories for the small size particles (d_p= 25 μ) for Case iii-2.

Figure 5.34.b Comparison between the predictive and experimental radial profiles of oxygen concentration and gas temperature for Case iii-2 usingsmall size particles (.d_p= 25 μ).

Figure 5.35 Effect of drag coefficient on the predictions of gas concentration.

Figure 5.36.a The particle trajectories for Case iv-3 with inlet swirl of 0.5

Figure 5.36.b Comparison between the predictive and experimental radial profiles of oxygen concentration and gas temperature for Case iv-3 with inlet swirl of 0.5.

Figure 5.37 Comparison between the predictive and experimental radial profiles of oxygen concentration and gas temperature for Case iii-2, showing the effect of reducing the inlet swirl.

LIST OF TABLES

Table 2.1 The k-ε model constants.

Table 3.1 Gas and particulate components of source terms for the solved equations.

Table 4.1 Operating conditions for isothermal cases in the CCRL furnace (stage i).

Table 4.2 Coal characteristics for the combustion cases in the CCRL furnace (stage ii).

Table 4.3 Operating conditions for the CCRL combustion cases (stage ii).

Table 4.4 Coal properties for the IFRF and ICSTM cases (stages iii and iv)

Table 4.5 Operating conditions for Type 2 flame cases (stage iii).

Table 4.6 Operating conditions for Type 3 flame cases (stage iv).

Table 4.7 Model constants for the standard cases.

Table 5.1 Kinetic parameters for the single reaction devolatilisation model.

NOMENCLATURE

Roman Symbols

SYMBOL	DEFINITION
a_n	finite difference coefficient
A	area, pre-exponential factor, empirical constant
b	remaining part of the source term after subtracting the pressure gradient
C	empirical constant
C_b	correction constant for the k-ε in case of curvature
C_c	correction constant for the k-ε in case of curvature
C_D	drag coefficient
C_p	specific heat
C_1, C_2	turbulence model constants
C_μ	empirical constant for the turbulent viscosity
d	diameter
D_o	binary diffusion coefficient
D_{ij}	diffusion term
E	activation energy
$E_{v,p}$	emission rate per unit path length and solid angle
f	scattering factor
f	weighing factor for discretisation
F	interphase friction coefficient
F_R	radiation flux
g	gravitational accelaration
G	generation of turbulent energy
G_x	axial thrust

G_ϕ	tangential momentum
h_m	mass transfer coefficient
H_c	heat of reaction of char
I	radiative intensity
k	turbulent energy
k_e	equivalent absorption coefficient
k_g	thermal conductivity of the combustion gas
l_m	length scale
Lv	latent heat of volatiles
m	mass
M	molecular weight
n	unit in the direction perpendicular to curvature
n_v	spectral index of reflection
N	number of particles
Nu	Nusselt number
P	pressure
P_r	Prandtl number
r	radial distance
R	universal gas constant
R_c	radius of curvaturez
Re	Reynolds number
Ri	Richardson number
s	distance travelled by radiative ray
S	stichiometric oxygen
S_p	particulate phase source
t	time
T	temperature

u	fluctuated component of the axial velocity
U	Axial/x component of velocity
U_s	stream line velocity
U_τ	friction velocity
x	axial distance
v	fluctuated component of the radial velocity
V	radial component of velocity
V	concentration of volatiles at time t
V	volume
w	fluctuated component of tangential velocity
W	tangential velocity
X_{UB}	fraction of char remaining in the particle
X_v	remaining volatile content on the particle
y	vertical distance
$y+$	normal distance Reynold number

Greek Symbols

α_1, α_2	devolatilisation constants for the two competing scheme model
ε	dissipation energy
Γ	diffusion
Φ	general scaler entity
η_v	emission coefficient
ρ	density
κ	von Karman constant
μ	molecular viscosity

μ_t	turbulent viscosity
σ	Stefan Boltzman constant
σ_{iv}	scattering coefficient
τ_d	particle relax time
τ_l	lagrangian time scale
Ω	solid angle

Subscribts

c	char
d	diffusive
D	drag
e, E	east
eff	effective
g	gas
p	particle
n,N	north
s,S	south
w,W	west
v	volatile

Key Words

CCRL	Canadian Combustion Research Laboratory
ERZ	Externa Recirculation Zone
ICSTM	Imperial College for Science, Technology and Medicine

IFRF	International Flame Research Foundation
IRZ	Internal Recirculation Zone
NBR	Near Burner Region
PF	Pulverised Fuel

CHAPTER 1

INTRODUCTION

1.1 PREAMBLE

The use of mathematical models to explore the details of pulverised coal flames as characterised by such quantities as mean temperature, the compositions of various chemical species and other properties of interest to the combustion application should be of increasing assistance to burner designers as well as furnace operators. Early combustion models were predominantly zero- or one-dimensional. The present day multi-dimensional mathematical modelling of pulverised coal flames dates from about the mid 1970's but continues to remain a pursuit which is practiced by relatively few groups. One reason for this is that the number of relevant physical phenomena are so large that, even if the mathematical and numerical ingredients are ignored, it is still a highly multidisciplinary topic. Another reason is an apparent reluctance to accept that the models are developed to the point where they can predict accurately the complex coal combustion processes in real furnaces.

The power generation industry remains the principal user of coal, almost exclusively in the form of a powder which is frequently fired by swirl type burners. There remains considerable scope for optimising the design of these burners, particularly in terms of: improved tolerance to coal types, enhanced flame stability performance, reduced NO emissions and augmented char burnout. Improved designs can be evolved empirically, but the process can be accelerated by the intelligent use of a mathematical model. It would be foolish to claim that any existing or foreseeable model can, or will, substitute entirely for the need for experimentation. However, an achievable model can, if it is correct in essentials, serve to elucidate relevant features of the many participating physical phenomena enabling the enlightened engineer to achieve goals faster and with greater success.

Knowledge of the details of the NBR becomes more critical since this region controls most of the pollutant emissions. This fact along with the importance of that region for flame stability and knowledge of the flame structure have not been specifically addressed by the last generation of mathematical models.The early prediction efforts that did not empathise this region were quite encouraging. However, subsequent studies have revealed that improvements are very hard won. The predictive failings have become particularly apparent in the face of new data for the NBR. Nonetheless the amount of data is still far smaller than is required to pinpoint confidently the sources of model failure. For example, reliable measurements of the velocities of both phases for combustion conditions are totally absent. It is clearly very difficult to validate higher level modelled physics if the fluid mechanical basis cannot be verified. Laser doppler anemometry was at one point heralded as the practicable saviour. There are however serious practical impediments associated mainly with beam obscuration and the irregular geometries of the particles.

In spite of many shortcomings which will be identified in this thesis the PF mathematical model is able to guide engineers in a useful manner provided that the user is sufficiently experienced to be fully aware of the strengths and limitations of his complex tool. Some of this experience can be extracted from the literature, but personal involvement and hands on effort are the hallmarks of the successful user.

1.2 BACKGROUND OF PHYSICAL MODELLING IN PULVERISED COAL FURNACES

Comprehensive models of the type presented in this study are time-consuming to develop, require significant computer time to operate and their reliability is still difficult to determine. In the past, they have been restricted by lack of computer speed and capacity and by the technical difficulties of describing essential model elements, Smoot [1981]. Most of the present comprehensive multi-dimensional mathematical models for pulverised coal furnaces owe their origins to the general computer program for two-dimensional, turbulent flows, known as the TEACH code devised at the Imperial College by Gosman and Ideriah [1976].

Gibson and Morgan [1970] presented the earliest known comprehensive attempt to mathematical model pulverised coal diffusion flames in two dimensional steady state swirling flow. They applied a stream function-vorticity formulation. The techniques of finite differencing were successfully introduced for solving the set of differential equations. An algebraic equation was used for modelling the turbulence. The volatiles were assumed to be emitted separately in gaseous form and burn instantaneously when mixed with the oxidant. The carbon particles were represented by discrete sizes and coal reaction rate was based on experimental measurements.

The study presented by Lockwood et al [1980] was amongst the earliest to introduce sophisticated computational methods for PF combustors. Many of the components of the model discussed there are still the main features of most PF mathematical models today. They introduced the treatment of the particulate phase in a Lagrangian frame, encouraged by the ease with which it accounts for slip velocity between gas and particles, the minimal computer storage it requires for the increased particle size groups and by the more ready application of the drag, heat transfer, devolatilisation and other laws that govern the particle behaviour. The interaction of the particulate phase with the gas phase was included in what is known as particle source in cell (PSIC) method suggested by Migdal and Agosta [1967]. They extended the application of the eddy break-up model by Magnussen and Hjertager [1976], originally formulated to be applied to gaseous diffusion flames, to regulate the combustion of volatiles released from the coal particles. A flux model was used for modelling the radiation transfer. Since at that time the experimental data for PF combustors were scarce, a situation that did not improve much over a decade, they presented a parametric study on a hypothetical cylindrical furnace where they drew some interesting conclusions as the unimportance of the angle of injection, decreasing the primary to secondary velocity ratio increases the total heat transfer as well as lengthening the flame; coarse grinds flatten the heat transfer distribution; and the need for a very accurate volatile release law was probably unnecessary.

Lockwood et al [1984] used a faster particle tracking procedure compared with the one presented in Lockwood et al [1980]. They examined the performance of different devolatilisation schemes, namely the constant evaporation rate model proposed by Baum and Street [1967], the single reaction, the two competing reaction and the multiple reaction models, of features detailed latter in chapter 2. They applied the model to predict two swirling pulverised coal flames in the canadian CCRL cylindrical furnace. The experimental data in common with most of those available at the time did not include details of the all important NBR. Nevertheless, the comparison of the predictions with the experimental data showed promising predictive performance. They also performed a numerical exercise for optimising the constants for the char chemical reaction rates which compared well with the available experimental data.

Rizvi [1985] evaluated the predictive capabilities of the solution procedure in a hypothetical cylindrical furnace and three swirling flames from the Canada Centre for Mineral and Energy Technology, Canada. It was concluded from the study of the hypothetical case that higher ash content results in a decrease of the flame temperature that counters the effect of the increased absorptivity and leads to less radiative heat transfer. The strong dependence between the control of the air/coal ratio and the exit burnout was emphasized. The validation studies for the three experimental flames were used to optimise the model constants. However, the fairly good agreement between the predictions and the measurements provided encouragement for the reliability of the model and that precise knowledge of the complex chemistry and diffusion processes were not a pre-requiste for good computation, a conclusion that can be justified by the scarcity of detailed NBR measurements in the complicated pulverised coal combustors at the time.

Lockwood et al [1988 b] outlined the features of the three dimensional model which incorporated a Lagrangian frame for the particulate phase following the procedure of the two dimensional model given by Lockwood et al [1980]. They emphasized their method in treating the collision and rebouncing of the particles with the furnace walls. The radiation was treated by the discrete transfer method proposed by Lockwood and Shah [1981]. The velocity comparisons for the isothermal case were remarkably good and considered in excess of engineering heat transfer needs. However, no validation test was presented for a combustion case. Instead, the performance of the model was demonstrated for a full-scale combustor for gas-firing at an input rate of 660 MW.

Levy [1991] emphasized the application of the mathematical model to simulate coal fired cement kilns. The aerodynamic performance of the model was assessed through comparing the predicted flow pattern with flow visualisation results for a 1/20th scale water model of a cement kiln obtained using a laser sheet technique. The model was also validated against combustion data obtained for the IFRF furnace reported by Bortz [1983] for a three inlets burner which was fed simultaneously by natural gas and pulverised coal. The isothermal comparison between the predictions and the flow visualisation demonstrated the ability of the model to simulate the qualitative features of the flow pattern. The combustion cases predicted gave acceptable agreement with the measurement for three out of the four flames studied. The discrepancies in the fourth flame were attributed to the defects in the particle dispersion model used and/or the lack of symmetry on the measurements.

The model presented by Truelove [1984] was similar to that described by Lockwood et al [1980] but differed in the treatment of the radiation and the volatiles combustion. For the former, a discrete ordinate method was incorporated in contrast with the flux model and the latter differed in the use of the probability density function for obtaining the mixture fraction f and its variance g. The model performance was examined through comparison with the limited data obtained by Hein and Leuckel [1969] at the IFRF furnace. The model's ability to elucidate the interactions between the different combustion parameters such as the aerodynamic flow pattern, the volatile release and combustion, radiation and char combustion was demonstrated.

Truelove [1986] validated his mathematical model against data obtained for a high and a medium volatile bituminous-coal flames measured in the IFRF furnace by Phelan and Bortz [1985]. The model was equiped with the computationally expensive stochastic method by Crowe et al [1977] for the particle dispersion. A satisfactory qualitative agreement was obtained for the aerodynamic features. The effect of the particle dispersion was more sound in the medium volatile coal since sufficient large particles failed to penetrate the IRZ as a result only of their inertia and in the absence of dispersion, did not release enough volatiles to stabilise the flame. Both the single and two competing reaction models yielded almost identical predictions. This was due to the effect of the blowing correction that reduced the particles heat transfer with the volatile release rates experienced in the latter model restricting the particles temperature below 1000 °C while the lower volatile release rates experienced in the former resulted in less effect on the blowing correction allowing particles temperature in the order of 1500 °C resulting in overall similar behaviour.

Truelove and Holcombe [1990] compared the performance of three bituminous coals of volatile contents ranging between 19% and 41% in a pilot-scale combustor. Their study involved both experimental measurements and simulations. The measurements taken were for flames fired in a 150 kw furnace of dimensions close to that of the ICSTM furnace. The three coals showed similar stability features suggesting that the stability criterion is dictated by aerodynamic effects rather than volatile content, a phenomenon that has also been confirmed experimentally by Costa et al [1991b]. The higher combustion efficiency experienced for the high volatile coal was shown to be the result of rapid burnout in the near burner zone. The exit burnout for all the cases studied was over-predicted even when using a measured char reactivity. Detailed in-flame measurements of the flow, temperature and gas composition were used to validate the mathematical model. The prediction showed some discrepancies for the oxygen concentration and gas temperature in the internal recirculation zone (IRZ). Remedies were sought by exchanging the standard k-ε model used for modelling the turbulence by an algebraic stress model but this produced marginally worse predictions. The implementation of the multiple parallel reaction model for devolatilisation instead of the single-reaction model yielded no improvement. The only sensible improvement was brought by the unjustified increase of the swirl level from 0.27 to 0.6. The alteration of the volatile combustion constant that relates the turbulence time scale to the rate of combustion of volatiles improved the agreement with the oxygen measurements within the NBR but caused a gross oxygen over-prediction downstream.

Wennerberg [1988] compared his mathematical simulation to data obtained for pulverised coal and peat, characterised by its high volatile content and oxygen as compared with coal. The data used in this study involved two non-swirling flames and consisted of measurements away from the ignition region. The agreement obtained for the pulverised coal flame was reasonably good. However, the quality of agreement obtained for the peat flame where the only reported parameter was the gas temperature was not as good. This was thought to be due to the simplicity of the devolatilisation model, the inadequacies of the eddy-breakup model and the lack of sound particle turbulent dispersion model.

Visser et al [1990] of the IFRF presented an interesting study that included the quarl zone properties of swirling pulverised coal flames. This zone together with the region in its proximity controls the stability of and the pollution mechanisms in pulverised coal combustion. Their study may be considered unique for the availability of data inside the quarl, other experminters usually avoid inserting a probe in that region in order not to cause perturbation of the flow, see for example Costa et al [1991.a]. They validated the mathematical model against two sets of data distinguished by the axial position of the burner pipe. The agreement obtained was reasonable for the first case though there were sensible discrepancies in the CO predictions. When the burner pipe was inserted into the quarl, a technique aiming to reduce the exit NO, poorer agreement was experienced. A somewhat surprising phenomenon was mentioned concerning the possibility of obtaining two different solutions for the same inlet conditions according to the setting of the initial conditions. This might be attributed to the use of the less than developed algebraic stress model to simulate the turbulence which relies on the solution of a quadratic equation.

Further simulation details from IFRF were included in the study by Visser [1991]. The isothermal cases studied revealed that the use of the algebraic stress model to simulate the turbulence gave better results than those brought by the use of the standard k-ε model. As for the combustion cases studied, it was shown that the agreement between the model predictions and the experimental data was good only at axial distances more than half a quarl diameter downstream from the burner exit. The discrepancies experienced in the flow around the IRZ for the gas temperature and chemical composition were not very serious.

In their 1988 study Gorner and Zinser demonstrated the features of their three dimensional model. It was distinguished from the majority of its type by employing an eulerian technique for the particulate phase as well as the the gas phase. This was facilitated by neglecting the slip velocities between the two phases and reducing the problem into a one phase flow. They also incorporated an elegant chemical model that considered CO as the intermediate product for both volatile and char combustion. This might be the reason for the over-prediction of oxygen in the comparison case that they showed for measurements obtained in the IFRF furnace by Michel and Payne [1980] for a long pulverised coal flame. However, the simulation obtained for an isothermal case represented fairly well the main flow situation. They also presented a demonstration for the model's performance in predicting a 300 MW electrical power brown coal fired utility boiler furnace.

Smoot [1981] examined from the perspective of the modeler, the state of understanding of the behaviour of pulverised coal flames. The study gave an outline of the effort that had been made to develop detailed codes for pulverised coal reaction processes which integrate the various code elements. It was reported that most of the multidimensional codes were not well advanced and that the analysis of the sensitivity of numerical and physical parameters was also greatly lacking.

Slaon et al [1987] conducted a review of the experimental and theoretical parametric studies in which the effect of incremental adjustments in the swirl level, flow rate,velocity ratios and geometrical designs were analysed. Many of the theoretical computations that were rigourously compared with experimental data reported discouraging disparities. The performance of the k-ε turbulence model was held responsible for the poor predictions in the vicinity of the central toroidal recirculation zone. The dissipation equation was sensitized to the local swirl level through the incorporation of different forms of the so-called Richardson number. This practice was not found to be sufficiently general and the magnitude of the corrections required to be monitored and limited appropriately. The algebraic stress models did not increase prediction accuracy to the desired degree. The pulverised coal flame studies presented under-predicted the oxygen concentration at the reactor centreline and over-predicted the oxygen concentration near the wall, particularly in the upstream regions. It was suggested that the factors which contribute to prediction discrepancies in the fuel-rich core include kinetic or equilibrium considerations, limitations of the particle dispersion model, and perturbations imposed by the penetrated recirculation zone.

Smith et al [1990] presented a new approach for using comprehensive coal combustion models in conjunction with a statistical response surface methodology in furnace design applications. The technique was demonstrated on two gasification injectors and on one pulverised coal combustion burner design. For the gasification injectors, maps were obtained for the highest cold gas efficiency obtained when varying the pressure, oxygen/coal ratio and steam/coal ratio. In the case of the pulverised coal combustion burner, maps were obtained giving the maximum exit burnout combined with adequate NO exit levels when changing the secondary swirl, the primary/secondary momentum ratio and the particle size distribution. The calculations emphasized the uniqueness of each injector or burner; consequently, operating conditions from one system cannot be imposed on different injector swirl burners.

Fiveland et al [1984] developed the combustion model, COMO, which involved the major processes for pulverised coal combustion. The standard k-ϵ model was used to model the turbulence. The gas phase chemistry was modelled using the fuel mixture fraction, f, and its variance, g, assuming a probability density function to account for the fuel-oxidant unmixedness. A lagrangian formulation was used for the particulate phase but the particle turbulent dispersion was totally ignored. The particle energy equation accounted only for the radiative and convective effects ignoring the latent and devolatilisation heats. The devolatilisation was simulated using the two competing reaction scheme. The discrete-ordinate method was used for modelling the radiation transport equation. The performance of the model was demonstrated by comparing its predictions with those obtained by experimental measurements when predicting a gaseous flame, the agreement was good. The model was also validated for a non-swirling pulverised coal flame measured in the Brigham Young University furnace by Thurgood [1979]. Qualitative agreement between the measurements and the predictions was obtained. In common with most of studies of its time, predictions were compared with measurements along the centreline. Radial profiles comparisons were restricted to the combustor exit.

1.3 OBJECTIVES AND PRESENT CONTRIBUTION

The main objective of this work is the development, demonstration, and evaluation of a numerically efficient and user friendly computer procedure to simulate within an acceptable precision the performance of pulverised coal furnaces in two dimensional frame.

The performance of this computer procedure will be particularly assessed in the NBR to ensure its reliability for predicting the pollution emissions and stability limits and to locate the deficiencies in the used physical models.

The two-dimensional axi-symmetric computer code developed for and during this study in collaboration with Levy [1991], bears the name of FAFNIR and is designed to provide most of the aims required for the combustion community. Its ease of use is extended by the pre- and post-processors. The pre-processor is designed to run interactively giving the user the possibility of introducing the data into the program in a set of alternate simple ways. The post-processor enables the output to be displayed in various forms including the graphical representation of contours, axial and radial profiles and vector plots of the velocities with the particle trajectories. Fig. (1.1) presents a diagram of the structure of the code. More details can be obtained from Lockwood et al [1991]. The ease of use of the FAFNIR code has been demonstrated by users of various backgrounds from both the industry and education communities.

The present validation study of FAFNIR has been carried out in four steps. Firstly, the model has been validated against isothermal measurements to ensure the ability of the model to predict the basic isothermal fluid dynamics features. The data used were obtained from the Canadian Combustion Research Laboratory (CCRL). Secondly, it is validated against combustion measurements taken at the same laboratory. Thirdly, it is validated against near burner measurements that are obtained in the International Flame Research Foundation (IFRF) and the Imperial College for Science, Technology and Medicine (ICSTM) with a burner with central bluff body. The last step involved the validation with measurements obtained at the ICSTM furnace with a burner of single central orifice. The different geometries used acertained the independence of the evaluation study from the geometrical configurations involved. A sensitivity study is also performed to identify the inadequacies in the model and to set a priority list for future developments in the field.

1.4 LAYOUT OF THE THESIS

Chapter 2 presents the physical basis for the model components incorporated: the turbulence fluid mechanics and radiation models are given. It also presents the particulate governing equations for motion and energy on the used lagrangian frame. The devolatilisation process, heterogeneous char combustion and the gas phase combustion are also outlined. Comparisons between alternative models are mentioned where possible.

In chapter 3 the details of the numerical solution are presented. The computational grid and the methods followed for the discretisation of the general differential equations are given. Some of the available methods for decoupling pressure and velocity equations are demonstrated. The methods followed in imposing the boundary conditions are explained. Finally, the numerical methods used for the particulate phase are summarised.

As the experimental cases involved in this study are numerous and obtained from several research institutions, a separate chapter is devoted to the presentation of the relevant details of these cases, the furnaces geometries, the analyses of the coals used and the inlet conditions. This task is accomplished by chapter 4, in which the various cases considered are subdivided into the four stages of the validation program.

Chapter 5 presents the results and discussion for all of the cases considered. The validation of the mathematical model for the four stages is presented together with a brief description of the features of the flame as demonstrated by the model. The description of the validation studies is followed by that of the sensitivity tests on the separate components of the mathematical model.

Finally, the conclusions of the present study along with suggestions for future work are given in chapter 6.

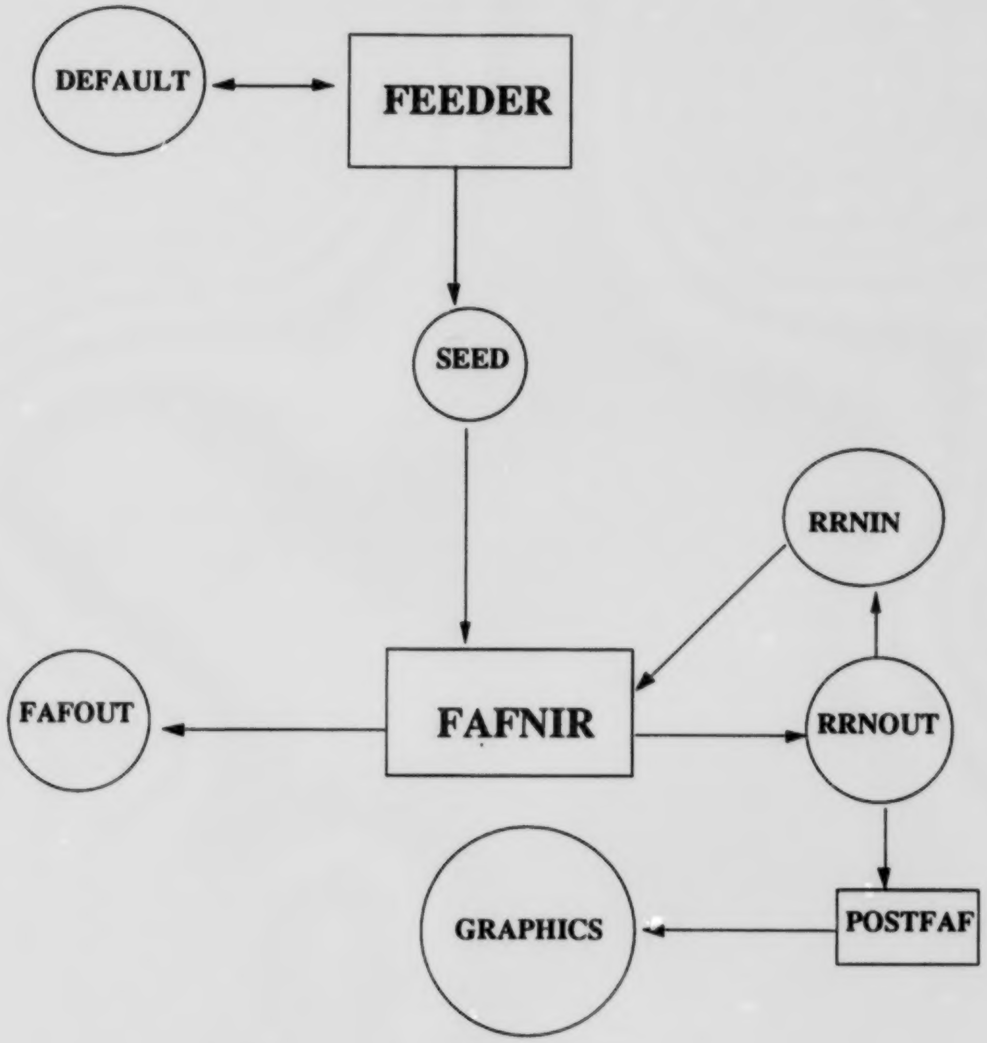
DEFAULT
FEEDER
SEED
RRNIN
FAFOUT
FAFNIR
RRNOUT
GRAPHICS
POSTFAF

Programs are shown in rectangles and files are shown in circles/ovals

Figure 1.1 Layout of the FAFNIR program

CHAPTER 2

PHYSICAL MODELLING

2.1 INTRODUCTION

This chapter describes briefly the physical models upon which the mathematical algorithm used in this study is based. These deal mainly with three different areas: gas flow aerodynamics, radiation and the particulate phase motion, heat transfer and chemical changes.

The calculations of the gas flow aerodynamics involve the use of a model to account for the stresses arising from the turbulence fluctuations. A summary of the available models and the recent developments is given and comparison is set between the models which are commonly used in similar applications therby justifying the use of the k-ε model. The deficiencies of this model are outlined with their possible remedies.

The inclusion of radiation heat transfer treatment has an influence in the accuracy of the calculation of local properties in the furnaces that is proportional with the size of the geometry under consideration, Bhattacharjee and Grosshandler [1989]. An exact solution for the radiation component may add an unbearable load on the computational economic necessity. The models available are numerous and offering different combinations of accuracy and simplicity. A flux model formulated by Gibb [1973] has been selected for its suitability to the problems addressed.

The Lagrangian frame applied to the particulate phase after Lockwood et al [1980] offers the ability to use more elaborate models. Nevertheless, the momentum equations controlling the particles motion still only crudely account for some of the important aspects like the turbulence interaction due to the complexity expected in modelling it, Lockwood and Papadopoulos [1989]. The particles heat balance involve different theories concerning the order of reactions and whether these reactions are taking place inside the porous of the particle, in its proximity or outside its boundary in the potential of the gas phase. The devolatilisation process is a very complicated one where the scientific probes are limited to the weight and temperature histories only.

Attempts to model this phenomenon in a way that lie within permissible limits are compromising and giving great concessions from what is actually taking place physically. The char burns either after the termination of the volatile release or simultaneously according to rates limited by mass transfer of oxygen at high temperatures and by chemical rate approximated in the form of Arrhenius type equation. The oxidation rate of the light hydrocarbons evolved from the particles is decided by mixing rather than chemical constraints regarding the level of turbulence experienced in pulverised fuel combustors. The accuracy of these limits depends largely on the degree of success achieved in determining the turbulence quantities.

2.2 TURBULENCE MODEL

In solving the Navier-Stokes equations for turbulent flows an approximate technique has to be employed in order to avoid formidable obstacles. Amongst these is the nature of fluctuations due to turbulence in all parameters that would require a mesh size that defines the length scales of eddies and time steps that handle the turbulence time scales. Fortunately engineering interests can for the most part be met through solving the time-averaged values rather than the time-dependent random turbulence parameters defined as follows:

$$\overline{U} = U - u' \qquad (2.1)$$

$$\overline{\Phi} = \Phi - \phi' \qquad (2.2)$$

where U is the axial velocity and Φ is a general scaler entity which may stand for a velocity component, enthalpy, concentration, turbulence energy, etc..

Two types of averaging are available for variable density flows, Gibson et al [1989], The first is the Reynolds averaging where:

$$\overline{\Phi} = \frac{1}{\Delta t} \int \Phi\,(t)\,\partial t \qquad (2.3)$$

and the second is the Favre-averaging:

$$\overline{\Phi} = \frac{1}{\rho}\frac{1}{\Delta t} \int \rho(t)\,\Phi\,(t)\,\partial t \qquad (2.4)$$

In the present study the Favre averaging is favoured since the resulting equations are simpler for combusting flows and identical to the equations obtained for the time-averaged properties when the flow is incompressible, see Jones and Whitelaw [1984]. The substitution of mean values in the Navier-Stokes equations necessitates the use of a turbulence model to account for the effects of stresses due to fluctuations. Note that the notation in this study will omit the '¯' from the mean values for sake of simplicity. The conservation equations yield:

Continuity:

$$\frac{\partial}{\partial x}(\rho U) + \frac{1}{r}\frac{\partial}{\partial r}(\rho r V) = S_p \tag{2.5}$$

Momentum:

Axial direction

$$\frac{\partial}{\partial x}\left(\rho U^2\right) + \frac{1}{r}\frac{\partial}{\partial r}(\rho r U V) = -\frac{\partial P}{\partial x} + \frac{\partial}{\partial x}\left[2\mu\frac{\partial U}{\partial x} - \rho u u\right] +$$

$$\frac{1}{r}\frac{\partial}{\partial r}\left[r\mu\left(\frac{\partial U}{\partial r} + \frac{\partial V}{\partial x}\right) - \rho r u v\right] - \frac{\partial}{\partial x}\left[\frac{2}{3}\mu\left(\frac{\partial U}{\partial x} + \frac{\partial V}{\partial r}\right)\right] + S_p \tag{2.6}$$

Radial direction

$$\frac{\partial}{\partial x}(\rho U V) + \frac{1}{r}\frac{\partial}{\partial r}\left(\rho r V^2\right) = -\frac{\partial P}{\partial r} + \frac{\partial}{\partial x}\left[\mu\left(\frac{\partial U}{\partial r} + \frac{\partial V}{\partial x}\right) - \rho u v\right] +$$

$$\frac{1}{r}\frac{\partial}{\partial r}\left[2r\mu\frac{\partial V}{\partial r} - \rho r v v\right] - 2\mu\frac{V}{r^2} + \frac{\rho W^2}{r} + \rho\frac{ww}{r} + \frac{1}{r}\frac{\partial}{\partial r}\left[\frac{2}{3}r\mu\left(\frac{\partial U}{\partial x} + \frac{\partial V}{\partial r}\right)\right]$$

$$+ \frac{2}{3}\frac{1}{r}\mu\left(\frac{\partial U}{\partial x} + \frac{\partial V}{\partial r}\right) + S_p \tag{2.7}$$

Angular direction

$$\frac{\partial}{\partial x}(\rho U W) + \frac{1}{r}\frac{\partial}{\partial r}\left(\rho r W V\right) = \frac{\partial}{\partial x}\left[\mu\frac{\partial W}{\partial x} - \rho u w\right] +$$

$$\frac{1}{r}\frac{\partial}{\partial r}\left[r\mu\frac{\partial W}{\partial r} - \rho r v w\right] - \left(\frac{\mu}{r} + \frac{\partial \mu}{\partial r}\right)\frac{W}{r} - \rho\frac{VW}{r} - \rho\frac{vw}{r} + S_p \tag{2.8}$$

where U, V and W are the axial, radial and tangential velocities respectively, ρ is the density, r the radial distance, P the pressure, μ the molecular viscosity, u, v and w the fluctuating components of the velocities and S_p is the particulate phase source.

The correlations involving fluctuated quantities in the mean flow equations remove the condition of closed set of equations. The unknown terms usually termed as Reynolds stresses represent the transfer by turbulent motion. The methods used to find these unknowns are termed "turbulence models".

A wide range of "turbulence models" have been proposed in literature, see for example Launder and Spalding [1974] and Gibson et al [1989]. They can be briefly classified in the manner described below.

2.2.1. Eddy Viscosity Models

These are based on the hypothesis of eddy viscosity first proposed by Boussinesq [1877]. This hypothesis assumes an analogy with the laminar flow of Newtonian fluids where the laminar viscosity represents the constant of proportionality between the stress and the rate of strain. In case of turbulence, the suggested eddy viscosity, μ_t, is no more a function of the fluid but instead it is calculated from the flow conditions. Thus the gradients of Reynolds stresses may be approximated in the following relation:

$$\rho \frac{\partial}{\partial x_i} u_i u_i = \mu_{eff} \left(\frac{\partial}{\partial x_i} \left(\frac{\partial U_i}{\partial x_i} + \frac{\partial U_j}{\partial x_i} \right) \right) \qquad (2.9)$$

2.2.1.1 Zero-equation Models

Prandtl [1925] expressed μ_t in terms of l_m,the mixing length, a length scale characteristic of the local turbulent flow. Since such turbulence models use an algebraic expression to define turbulent viscosity and involve no differential equations they are called zero-equation models. These models contain very specific experimental data as essential ingredients. Accordingly, they lack universality and more elaborate models have been developed to provide more generality and to reduce the need for extensive experimental work.

2.2.1.2 One-equation Models

These models are based on defining the eddy viscosity as:

$$\mu_t = C_\mu l_m k^{\frac{1}{2}} \tag{2.10}$$

where C_μ is an empirical constant, l_m is a length scale defined on basis of the flow geometry and k the turbulence kinetic energy a characteristic of the flow. A transport equation is solved for k and thus such models are called one equation models. The k-equation is in the form of:

$$U\frac{\partial k}{\partial x} + V\frac{\partial k}{\partial y} = \frac{\partial}{\partial x}\left(\frac{\mu_{eff}}{\rho\sigma_k}\frac{\partial k}{\partial x}\right) + \frac{1}{y_j}\frac{\partial}{\partial y}\left(y_j\frac{\gamma_{eff}}{\sigma_k}\frac{\partial k}{\partial y}\right) + G - \varepsilon \tag{2.11}$$

where

$$\gamma_{eff} = \gamma_l + \gamma_t$$

$$G = \gamma_{eff}\ \{2[(\frac{\partial U}{\partial x})^2 + (\frac{\partial V}{\partial y})^2 + (\frac{V}{yj})^2] + (\frac{\partial U}{\partial y} + \frac{\partial V}{\partial x})^2 + (\frac{\partial W}{\partial x}^2 + (r\frac{\partial}{\partial y}(\frac{W}{y}))^2\}$$

represents the generation of turbulence energy by the interaction of mean velocity gradients and turbulent stresses

2.2.1.3 Two-equation Models

These include in addition to the transport equation for k another transport equation for a length-scale related variable. Amongst the various two-equation models are those introduced by Harlow and Nakayama [1968], Rodi and Spalding [1970], and

Jones and Launder [1972]. The most popular is the k-ε model. It is favoured because the dissipation rate, ε appears as an unknown in the k-equation and because of the ease of deriving its exact equation. ε can be defined as:

$$\varepsilon = \nu_t \left[\frac{\partial u_i}{\partial x_j} \frac{\partial u_i}{\partial x_j} \right] \tag{2.12}$$

Both the eddy viscosity and the length scale are directly related to the k through the following relations:

$$\mu_t = \rho \, C_\mu \frac{k^2}{\varepsilon} \tag{2.13}$$

$$l_m = \frac{k^{\frac{3}{2}}}{\varepsilon} \tag{2.14}$$

In eq.(2.12) the turbulence energy k characterizes the intensity of the turbulent fluctuations ($\frac{1}{2}\,\overline{u_i u_i}$ which is assumed to be isotropic, one of the drawbacks of the model). The distribution of k and ε are determined from the solution of the semi-empirical transport equations which, in the standard k-ε model are as follows:

$$U \frac{\partial \varepsilon}{\partial x} + V \frac{\partial \varepsilon}{\partial y} = \frac{\partial}{\partial x} \left(\frac{\mu_{eff}}{\rho \sigma_\varepsilon} \frac{d\varepsilon}{dx} \right) + \frac{1}{y_j} \frac{\partial}{\partial y} \left(y_j \frac{\gamma_{eff}}{\sigma_\varepsilon} \frac{\partial \varepsilon}{\partial y} \right) + \frac{c_1 \varepsilon}{k} G - \frac{c_2 \varepsilon^2}{k} \tag{2.15}$$

The constants appearing in (2.11) to (2.15) take the values shown in table (2.1) as given by Launder and Spalding [1974].

Table (2.1)
The K-ε model constants

C_μ	C_1	C_2	σ_k	σ_ε
0.09	1.44	1.92	0.9	1.3

2.2.2.Reynolds Stress Models

The implied isotropic nature of eddy viscosity models neglects the transport of the individual stresses. More complicated models are formulated in which the equations of the stress components are solved. When forming these equations higher order correlations appear as extra unknowns. If equations were formed for these correlations higher order correlations would appear. The procedure may be continued yet further that the equation set never closes. The available Reynolds stress models (RSM) thus approximate these correlations in terms of the calculated parameters. Samples of these models can be found in Launder et al [1975], Reece [1977], Rodi [1980], Gibson and Launder [1978], Jones [1980] and Fu et al [1987]. The Reynolds stress transport equation may be written as:

$$\frac{D\overline{u_iu_j}}{Dt} = G_{ij} + Y_{ij} - \frac{2}{3}\varepsilon\, d_{ij} + D_{ij} \qquad (2.16)$$

The pressure-strain correlation, Y_{ij} is calculated according to

$$Y_{ij} = - C_1\frac{\varepsilon}{k}\left(\overline{u_iu_j} - \frac{2}{3}k\, d_{ij}\right) - C_2\left(G_{ij} - \frac{2}{3}G\, d_{ij}\right) \qquad (2.17)$$

where $G = \frac{1}{2}G_{ij}$ and G_{ij} is given by

$$G_{ij} = -\overline{u_ju_k}\frac{\partial U_i}{\partial x_k} - \overline{u_iu_k}\frac{\partial U_j}{\partial x_k} \qquad (2.18)$$

and the diffusion term D_{ij} is given by

$$D_{ij} = \frac{\partial}{\partial x_k}\ \mu_t\frac{\partial\overline{u_iu_j}}{\partial x_k} \qquad (2.19)$$

For axisymmetric swirling flow configurations, five transport equations for the following stresses or their combination are solved: $\overline{uv}$, $\overline{uw}$,$\overline{vw}$,$\overline{v^2}$,-$\overline{u^2}$,$\overline{v^2}$-$\overline{w^2}$ together with the transport equations for the kinetic energy k, and its dissipation rate, ε. The model constants can be found in Sturger and Syed [1985].

2.2.3 Algebraic Stress Models

The algebraic stress models (ASM) aim to retain the degree of physical realism attained by the Reynolds stress models while achieving computational times comparable to those required for solving the two-equation eddy viscosity models. This is achieved through approximating the differential transport equations for the stress components into algebraic relations that are obtained through solving the two-equations and using simple pressure strain model. Details of such models may be found in Rodi [1972] and Launder [1982]

2.2.4 Comparison Between k-ε Model, ASM and RSM

The three models have been the issue of comparative studies. The RSM was here avoided in order to save both CPU time and memory space. It does not appear to have reached a stage where they can be profitably used in combusting flows for practical configurations, Jones and Whitelaw [1984]. The ASM which appears to retain greater physical realism while achieving computational times comparable to that of an eddy viscosity model has proved to be seriously misrepresenting the stress components. Lockwood and Stolakis [1983] assessed the k-ε and the ASM models through comparing with an axisymmetric gaseous jet diffusion flame. The comparison showed that the k-ε model gives better agreement with the measurements than the ASM. A buoyancy source term correction was added to the k-equation in the k-ε but its effect was found to be small.

The algebraic and differential second-moment closures were compared by Fu et al [1988] for axisymmetric turbulent shear flows with and without swirl. They analysed the different terms of both the ASM and the RSM and showed that in both the convection and diffusion terms the components that account for swirl in RSM are missing in the ASM leading to differences in results that would be proportional to the magnitude of the swirl. They demonstrated their analysis through comparing the performance of both models against several sets of experimental data where the ASM showed poorer performance than that obtained for the RSM. They concluded that the ASM ought not to be used in axisymmetric swirling flows where circumferential stress-transport processes give rise to significant terms in the overall Reynolds stress budget. They recommended that in the absence of a full second-moment closure, a simple eddy-viscosity model should be employed.

On the other hand Weber et al [1986] compared the performance of the k-ε with that of the RSM for two isothermal cases. The two models were able to identify the important aerodynamic features for one of the cases while only the RSM succeeded in identifying the other. A similar study by Weber et al [1990] showed the performance of the three models for several isothermal swirling cases where the ASM gave results close to those of the RSM in the burner quarl while the k-ε failed to produce satisfactory performance. They concluded that neither the (anisotropic) generation of turbulence nor the distribution of tangential momentum in the downstream flow were correctly predicted by the k-ε effective viscosity model. Speziale et al [1989] showed that the quantitative superiority of the RSM over the k-ε and other two equation models is limited to a narrow range of rotation rates. For rotation rates outside this range, there is an exchange of stabilities with a solution whose kinetic energy and dissipation rate decay with time.

From the above discussion, it may be concluded that the comparison between the ASM and k-ε models depend on the case under consideration and it cannot be stated that either of the two models provides better results than the other for all cases. Because of the high computational price and the time required to incorporate the RSM, the k-ε model was used throughout this study.

2.2.5 Dificiencies of Standard k-ε Model and their Possible Remedies

2.2.5.1 Streamline curvature

Bradshaw [1973, 1979] indicated that the turbulence of a fluid subject to centrifugal force is suppressed when the angular momentum increases towards the centre of curvature. The standard k-ε model fails to reproduce the full effects of curvature, Sloan et al [1986].

In an attempt to avoid the need for recourse to Reynolds stress models, several attempts have been made to modify the k-ε model to take account of the curvature effects. Leschziner and Rodi [1981] obtained improvements in their predictions of annular and twin parallel jets by making C_μ a function of a curvature dependent parameter. They proposed that it should take the form of:

$$C_\mu = \frac{0.09}{\left[1 + 8K_1^2 \frac{k^2}{\varepsilon^2}\left(\frac{\partial U_s}{\partial n} + \frac{U_s}{R_c}\right)\frac{U_s}{R_c}\right]} \tag{2.20}$$

where U_s is the stream line average velocity, R_c is the radius of curvature, n coordinate normal to the stream line and K_1 is a constant given the value of 0.6. Sloan et al. [1986] obtained the following formula for swirling flows:

$$C_\mu = \frac{0.09}{1 + C_a\left(\frac{k}{\varepsilon}\right)^2\left[\left(\frac{w}{r}\right)^2 + C_b\left(\frac{w}{r}\right)\left(\frac{\partial w}{\partial r}\right) + \left(\frac{\partial w}{\partial r}\right)^2\right]} \tag{2.21}$$

Bradshaw [1969] demonstrated the analogy between the effects of streamline curvature and buoyancy effects on turbulence: this led him to propose a dimensionless parameter, the Richardson number (Ri) defined as:

$$\mathrm{Ri} = \frac{\text{typical body force}}{\text{typical inertial force}}$$

The body force for curved flows can be taken as the centrifugal force. The Richardson number can then be written in the form:

$$Ri = \frac{k^2}{\varepsilon^2}\left(\frac{\partial w}{\partial r} + \frac{w}{r}\right) \tag{2.22}$$

Following this analogy, and the fact that the ε equation is the more heavily modelled one (with less physical indication), Launder et al [1977] chose to leave the k-equation intact and replaced the coefficient C_2 of the ε equation by the expression:

$$C_2(1 - C_c Ri) \tag{2.23}$$

where C_c is a constant whose recommended value is 0.2. In the turbulence transport equations the term which explicitly contains the extra rate of strain is the generation hence Rodi [1979] corrected the coefficient C_1 rather than C_2 by the formula:

$$C_1(1 + C_c Ri) \tag{2.24}$$

2.2.5.2 Interaction of particles

The standard k-ε model was initially formed assuming a single phase flow. However, it has been used without any modification in the presence of the particulate phase. Mostafa and Mongia [1988] studied the interaction of particles and turbulent fluid flow and proposed that the damping effect caused by the particles can be accounted for through the insertion of source terms to both the k and ε equations. The source term proposed for the k equation is:

$$-\sum_k 2KF^K\phi^K\left(1 - \frac{\tau_l}{\tau_l + \tau_d}\right) \tag{2.25}$$

where F, the interphase friction coefficient is given by:

$$F^k = \frac{3\rho}{4d_p} C_D \left|U_g - U_p\right| \tag{2.26}$$

and ϕ, the volume fraction of the particles is given by:

$$\phi^k = N\frac{\pi d_p^3}{6\Delta V} \tag{2.27}$$

τ_l is the carrier phase Lagrangian time scale given by:

$$\tau_l = 0.35\frac{k}{\varepsilon} \tag{2.28}$$

τ_d is the particle relaxation time and is defined in Sec (2.8)

The source term proposed for the ε equation is:

$$-C_3\frac{\varepsilon}{k}\sum_k 2KF^K\phi^K\left(1-\frac{\tau_l}{\tau_l+\tau_d}\right) \tag{2.29}$$

where C_3 is a constant taken as unity.

All of the suggested remedies given in 2.2.5.1 and 2.2.5.2 were attempted in the course of the present study without success. The main difficulty is that the algorithms fail to converge due to the lower calculated values of k and ε.

2.3 Radiation Heat Transfer Modelling

An adequate treatment of thermal radiation is essential to a mathematical model of combustion systems of practical sizes. The fraction of the total heat transfer due to radiation grows with combustor size, attaining prominence for a characteristic combustion length of about 1 m. Bhattacharjee and Grosshandler [1989] studied the effect of radiative heat transfer in two-dimensional axisymmetric furnaces and found that neglecting radiation can cause over-prediction of the mean velocities and temperatures by more than a factor of 2 and of the wall heat flux by a factor of 5 for a furnace of 2 m diameter and 50 m length.

Unfortunately, radiation heat transfer is governed by a complex integro-differential equation which is time consuming to solve. Thus, the decision to incorporate the exact solution in the elaborated computational domain is not always the most likely choice. A comprehensive review of the available methods of solving the radiative component of heat transfer in combustors was given by Viskanta and Mengue [1987].

2.3.1 Radiation Transfer Equation

The radiation transfer equation (RTE) forms the basis for quantitative study of the transfer of radiant energy in a participating medium. The equation is a mathematical statement of the conservation principle applied to a monochromatic pencil of rays. The RTE is based on application of an energy balance on an elementary volume taken along the direction of a pencil of rays and confined within an elementary solid angle.

Equating the change of energy in the cylindrical volume element shown in Fig. 2.1 to the net gain or loss of energy along the traversal path of the cylinder in terms of the processes of attenuation, emission and in-scattering yields:

$$
\begin{aligned}
dI_{\nu} dA d\Omega d\nu dt = (\kappa_{\nu} + \sigma_{\nu}) I_{\nu} ds dA \; d\Omega \; d\nu \; dt \qquad & (1) \\
+ \eta_{\nu} dV \; d\Omega \; d\nu \; dt \qquad & (2) \\
\sigma_{\nu} ds \left[\frac{1}{4\pi} \int_{\Delta\nu'} \int_{\Omega' = 4\pi} \Phi_{\nu}(\vec{s}' \rightarrow \vec{s}; \nu' \rightarrow \nu) \times I_{\nu'}(\vec{s}') d\Omega' d\nu' \right] dA \; d\Omega \; d\nu \; dt \qquad & (3)
\end{aligned}
\tag{2.30}
$$

where the left hand side is the net gain of radiant energy. (1) is the loss of energy from the pencil of rays due to absorption and scattering in the cylinder. (2) is the emission of matter inside the cylindrical volume dV, in time interval dt, in the frequency range $d\nu'$, confined in the solid angle $d\Omega$ about the direction s. If Kirchhoff's law is valid the emission coefficient η_{ν} can be expressed as:

$$\eta_{\nu} = \kappa_{\nu} n_{\nu}^{2} I_{b\nu} \tag{2.31}$$

where $I_{b\nu}$ is Plank's spectral black-body intensity of radiation and n_{ν} is the spectral index of reflection of the medium.

(3) is the increase in energy of the pencil of matter into the elementary of cylindrical volume from all possible directions s'. In this expression the phase function $\phi_{\nu} (\vec{s}' \rightarrow \vec{s}; \nu' \rightarrow \nu) \dfrac{d\Omega' d\nu}{4\pi}$ represents the probability that radiation of frequency ν' propagating in the $\vec{s}'$ and confined within the solid angle $d\Omega'$ is scattered through the angle $(\vec{s}' \rightarrow \vec{s})$ into the solid angle $d\Omega$ and the frequency interval $d\nu$. This probability is determined by the scattering mechanism.

Dividing equation (2.30) by dA $d\Omega$ $d\nu$ dt ds yields:

$$\frac{dI_{\nu}}{ds} = - (\kappa_{\nu} + \sigma_{\nu}) I_{\nu} + \eta_{\nu} + \frac{\sigma_{\nu}}{4\pi} \int_{\Delta\nu'} \int_{\Omega' = 4\pi} \Phi_{\nu}(\vec{s}' \rightarrow \vec{s}; \nu' \rightarrow \nu) + I_{\nu'}(\vec{s}') d\Omega' d\nu' \tag{2.32}$$

Equation (2.32) is a statement of the conservation of energy principle for a monochromatic pencil radiation and is generally called the RTE.

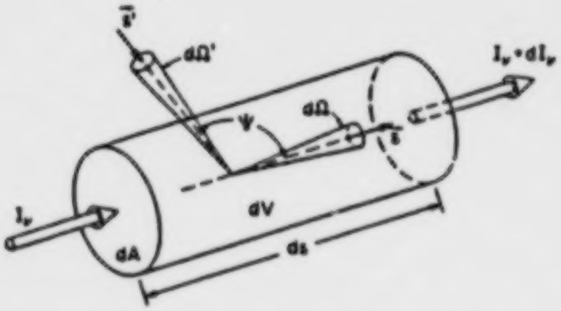

Figure 2.1 Cylindrical volume element showing the change of radiative energy.

2.3.2 Radiation Solution Methods

The RTE is an integro-differential equation, and its exact solution is quite difficult. Therefore, it is usual to introduce some simplifying assumptions before attempting to solve it in general form.

2.3.2.1 Statistical Methods

The purely statistical solution methods, such as Monte Carlo method are suitable for complex geometries and spectral effects can be accounted for without much difficulty. Stewart and Cannon [1971] and Taniguchi et al [1984] successfully employed this method to solve radiative transfer problems in furnaces. In its simplest form the method consists of simulating a finite number of photon histories through the use of a random generator. For each photon random numbers are generated and used to sample appropriate probability distributions for scattering angles and path lengths between collisions. Since the directions of photons are obtained from a random generator, the method is always subject to statistical errors. Monte Carlo calculations, thus yield answers that fluctuate around the real answer.

2.3.2.2 Zonal Method

Hottel and Cohen [1958] introduced one of the most widely used methods for calculating radiation heat transfer in practical engineering systems. It involves dividing the volume of the enclosure into zones, each assumed to have uniform temperature distribution and radiative properties. Then the direct exchange ratios (view factors) between the surface and the volume elements are determined using matrix inversion techniques. The zonal method reduces the radiative transfer problem to the solution of a set of non-linear algebraic equations. It is difficult to couple the zonal method with the flow field and energy equations which are solved using finite difference techniques. This is mainly because of the different size of the control volumes required: the zonal method can be computationally prohibitive if the same grid used by the finite difference equations is adopted. Another problem is the need to calculate the complicated view factors.

2.3.2.3 Flux Methods

Flux methods are based on separating the directional dependence of the intensity from its spatial dependence in order to simplify the governing equation. Assuming that the intensity is uniform over given intervals of the solid angle allows reducing the integro-differential equations into a series of coupled linear second order differential equations in terms of average radiation intensities or fluxes. Viskanta and Mengu [1989] classified the available flux models into multi-flux models, moment methods, spherical harmonic approximation, discrete-ordinate approximation and hybrid methods.

Abramzon et al [1984] presented a general analysis for flux models in a three-dimensional rectangular enclosure and showed that most of the models reported in the literature can be obtained from this general formulation.

The discrete transfer method proposed by Lockwood and Shah [1981] ignores the scattering term (term 3 in Eq. 2.30). This assumption allows for reducing the problem to a linear differential equation. A recurrence relation for the radiative intensity is thus derived. Representative rays are tracked along their travel between the boundaries across finite difference cells which are assumed to be at uniform temperature and absorption coefficient. The accuracy of this methos is controlled by the number of representative rays tracked. There is a technical difficulty in applying this model to the two-dimensional axi-symmetric frame and the inclusion of the effect of the particulate phase requires essential modifications.

A non-equilibrium diffusion model proposed by Gibb [1973] which can be considered as a moment flux model was incorporated for this study on basis of its simplicity, ease of application and computational economy. This method reduces to what is essentially an integral equation describing a non-local field to a local field problem described by a diffusion type second order differential equation. Through approximation, this method is capable of generating satisfactory solution for a permitted degree of engineering accuracy. Lockwood et al [1984] reported prediction of the incident radiation wall fluxes and successfully compared the results with measurements in pulverised coal combustors. A brief description of the method is given below.

2.3.3 Mathematical Formulation of the Non-Equilibrium Diffusion Model

Separating radiation effects of the gas and particles eq. 2.32 can be rewritten in the form:

$$\frac{dI_v}{ds} = K_{v,g}(I_{bv}(T_g) - I_v) + E_{v,p} - A_{v,p} - s_v^o + s_v^i \tag{2.33}$$

where the first term in the right hand side is the change in intensity by the combined effects of emission and absorption of the gas medium at temperature T_g. The rest of the terms in the equation relate to the particulate phase as follows:

i. Total emission rate per unit path length and solid angle:

$$E_{v,p} = \int_0^\infty dr \int_0^\infty n(r,T_p) k_{v,p}(r,T_p) I_{Bv}(T_p)\, dT_p \tag{2.34}$$

ii. Total absorption rate per unit path length and solid angle:

$$A_{v,p} = I_v \int_0^\infty dr \int_0^\infty n(r,T_p) k_{v,p}(r,T_p)\, dT_p \tag{2.35}$$

iii. Total out-scattering rate per unit path length and solid angle:

$$s_v^o = I_v \int_0^\infty dr \int_0^\infty n(r,T_p) k_{vs,p}(r,T_p)\, dT_p \tag{2.36}$$

iv. Total in-scattering rate per unit path length and solid angle:

$$s_v^i = \frac{1}{4\pi} \int_0^\infty dr \int_0^\infty n(r,T_p) k_{vs,p}(r,T_p)\, dT_p \int_{4\pi} P_v(\Omega,\Omega') I_v(\Omega')\, dw' \tag{2.37}$$

where $n(r,T_p).dr\, dT_p$ is the number of particles of radius between r and r+dr and of temperature between T_p and T_p+dT_p in a unit volume.

The complexity of eq.(2.33) can be reduced to the following form by assuming all materials to be grey:

$$\Omega.\nabla I = \kappa_g\left(\frac{\sigma}{\pi}T_g^4 - I\right) + \varepsilon_p\left(\frac{\sigma}{\pi}T_p^4 - I\right) + \tau_p\left\{\frac{1}{4\pi}\int_{4\pi} P(\Omega,\Omega') I(\Omega')\, dw' - I\right\} \tag{2.38}$$

The boundary condition for a grey Lambert surface is expressed as:

$$I(\Omega) = \frac{1}{\pi}\left\{\varepsilon_w T_w^4 + r_w F_R^+ . n\right\} \qquad (2.39)$$

where

$$F_R^+ . n = \int_{2\pi} I(\Omega^+)\Omega^+ . n dw$$

is the flux incident on the wall, n is the outward normal to the wall, Ω^- and Ω^+ are respectively the directions of the reflected and incident radiation at the surface. The subscript w denote the conditions at the wall. (+) denotes the incident direction.

The radiation field variable F_R the radiation flux at any point within the gas and T_R the radiation temperature are defined as follows:

$$F_R = \int_0^\infty dv \int_0^{4\pi} I_v \Omega dw \qquad (2.40)$$

$$T_R^4 = \frac{1}{4\sigma}\int_{4\pi} I dw \qquad (2.41)$$

Gibb [1973] employed the truncated moment expansion technique for reducing the dimensionality of the problem by eliminating the directional dependence Ω from eq.(2.38) thus allowing the derivation of the following two equations:

$$\nabla . F_R = 4\sigma k_g\left(T_g^4 - T_R^4\right) + 4\sigma\varepsilon_p\left(T_p^4 - T_R^4\right) \qquad (2.42)$$

$$F_R = -\frac{4}{3}\frac{\sigma}{k_e}\nabla T_R^4 \qquad (2.43)$$

where k_e is the equivalent absorption coefficient and is defined as:

$$k_e = k_g + \left(\varepsilon_p + r_p(1 - f)\right) \qquad (2.44)$$

where f is a scattering factor given by

$$f = \frac{1}{(4\pi)^2}\int_0^{4\pi} dw \int_0^{4\pi} P(\Omega.\Omega')\Omega.\Omega' dw' \tag{2.45}$$

The boundary condition can be expressed as:

$$-\frac{1}{3k_e}\frac{\partial T_R^4}{\partial n} = \frac{1}{2}\frac{\left\{(1-r_w)T_R^4 - \varepsilon_w T_w^4\right\}}{1+r_w} \tag{2.46}$$

The non-equilibrium diffusion radiation model for a small volume in the combustion space, a single order elliptic equation can be obtained from eq.(2.42) and (2.43):

$$\nabla.\left(\frac{1}{3k_e}\nabla T_R^4\right) = \left(k_g + \varepsilon_p\right)T_R^4 - k_g T_g^4 - \varepsilon_p T_p^4 \tag{2.47}$$

where k_g is the gas absorption coefficient, T_p is the particle mean temperature and ε_p is the total absorption coefficient for the particle phase.

The net gas and particle absorption rates can be expressed as:

$$S_{g,h} = 4\sigma k_g\left(T_R^4 - T_g^4\right) \tag{2.48}$$

and

$$S_{p,h} = 4\sigma\varepsilon_p\left(T_R^4 - T_p^4\right) \tag{2.49}$$

2.4 PARTICLE MOTION EQUATION

In large-scale coal-fired furnaces and boilers, the coal is pulverised into fine particles before injection into the combustion region, and particle sizes typically range from 20 to 200 μm. The small mass of these particles allow them to flow at nearly the speed of gas. The Reynolds number based on the slip velocity is on the order of 0.1.

The particle motion can be described by the momentum equation. The particles are assumed to be spherical in shape and the forces taken into consideration are the drag, centrifugal force due to swirl, the gravitational force and turbulence dispersion. The particle to particle interaction is ignored. The three components of the momentum equation for particle motion in a cylindrical geometry are:

$$\begin{aligned}
\frac{dU_p}{dt} &= \frac{1}{\tau_d}[U_g - (U_p + U_{diff})] + g_u \\
\frac{dV_p}{dt} &= \frac{1}{\tau_d}[V_g - (V_p + V_{diff})] - \frac{W_p^2}{r} + g_v \\
\frac{dW_p}{dt} &= \frac{1}{\tau_d}[W_g - (W_p + W_{diff})] - \frac{V_p W_p}{r}
\end{aligned} \qquad (2.50)$$

where τ_d is the particle relaxation time and is obtained from the relation:

$$\tau_d = \frac{\rho_p d_p^2}{18 \mu C_D \frac{Re_p}{24}} \qquad (2.51)$$

where C_D the drag coefficient. It was obtained by employing the drag law due to Wallis [1969] as:

$$C_D = \frac{1 + 0.15\, Re_p^{0.687}}{\frac{Re_p}{24}} \qquad (2.52)$$

r is the distance of the particle from the centreline. The particle diffusion terms included in eq. (2.50) are calculated according to Lockwood and Syed [1977] as follows:

$$U_{diff} = C\sqrt{|u^2|} \tag{2.53}$$

$$V_{diff} = C\sqrt{|v^2|} \tag{2.54}$$

where C is an empirical constant with a sign obtained by a random function. Note that u^2 and v^2 are calculated according to Boussinesq relationship:

$$u^2 = -2\frac{\mu_t}{\rho}\left(\frac{\partial U}{\partial x}\right) + \frac{2}{3}k \tag{2.55}$$

and

$$v^2 = -2\frac{\mu_t}{\rho}\left(\frac{\partial V}{\partial r}\right) + \frac{2}{3}k \tag{2.56}$$

Unfortunately these calculations do not give the sign of the diffusion velocities. As the direction taken by the drift is random, there is no deterministic way to calculate it.

Integration of the momentum conservation equations yields the particle velocity and trajectory in the gas flow field.

2.5 PARTICLE ENERGY BALANCE EQUATION

The description of the combustion behaviour of single particles of pulverised coal has been the research subject of numerous authors, see for example Baum and Street [1971], Choi and Kruger [1985] and Musarra et al [1986]. The energy conservation equation for a particle under simultaneous devolatilisation and combustion can be expressed as:

$$\begin{aligned}\frac{d}{dt}\left(\dot{m}_p C_p \frac{\partial(T_p)}{\partial t}\right) = \\ \pi d_p^2 Nu \frac{k_g}{d_p}(T_g - T_p) + \sigma\varepsilon_p d_p^2 \pi\left(T_R^4 - T_p^4\right) + \mu H_c\left(-\frac{dm_{pc}}{dt}\right) \\ - C_p T_{p_c}\left(-\frac{dm_{pc}}{dt}\right) - L_v \frac{dm_{pv}}{dt}\end{aligned} \qquad (2.57)$$

The specific heat for the coal of variable volatile content was calculated and expressed as a function of burnout following Baum and Street [1971] as:

$$C_p = 1214.0 + 209.3X_v - 544.2X_{UB} \qquad (2.58)$$

where X_v is the total volatile content in the particle and X_{UB} is the fraction of original char mass remaining unburnt.

The first term in the right hand side represents the convective transfer between the particle and the gas, where the Nusselt number Nu is obtained from the conventional expression:

$$Nu = 2.0 + 0.6\, Re_p^{0.5}\, Pr^{0.33} \qquad (2.59)$$

and the thermal conductivity of the combustion gas is obtained through the relation:

$$k_g = 6.739 * 10^{-5} T_g + 6.446 * 10^{-3} \qquad (2.60)$$

The second term represents the radiation heat exchange between the particle and the surrounding where T_R is the radiation temperature (see section 2.3), σ is the Stefan

Boltzman constant and ε_p is the particle emissivity which was shown to vary between 1 and 0.6 , see Street and Twamley [1971] and is allowed to follow the approximate relationship suggested by Gibb and Joyner [1974]:

$$\varepsilon_p = X_{UB} + 0.6(1 - X_{UB}) \tag{2.61}$$

The third term represents the heat of reaction of char combustion, the value of μ depends on the assumption of the product of the reaction wether is CO or CO_2. In the present study it is assumed that the product is CO_2 and thus μ equals unity, H_c is the calorific value of carbon. The last term represents the heat of evaporation of volatiles. L_v, is a distinct heat of vaporisation which has to be supplied in order for volatiles to escape. The value cited in the work of Baum and Street [1971] is 627.9 J/g of coal, and is based upon the authors' experiments. The latent heat of devolatilisation is set to zero after devolatilisation is complete.

2.6 DEVOLATILISATION MODEL

Prior to ignition, the cold coal particles introduced into the hot gas would heat up to the point where the volatiles would start evolving from the surface of the particle. It has been suggested by Howard and Essenhigh [1967.a] and [1967 b] and more recently Essenhigh et al [1989] that for particle sizes greater than 65 μm, homogenous ignition is expected to take place as the surface flux of the volatiles would be large enough to prevent the oxygen from reaching the coal surface. Tsai and Scaroni [1987] observed the unchanged microscopic structure of char for particles of 90 μm diameter that had been through intial stages of combustion which strengthen the above mentioned suggestion. For particles of smaller sizes,however, Howard and Essenhigh [1967 a] and [1967 b], Essenhigh et al [1989] and Gupta et al [1990] pointed out that ignition may take place heterogenously for certain combination of particle size and heating rates. The ignition temperature was found to be less for high volatile coals and bigger size particles, Gupta et al [1990]. Gas devolatilisation mechanism is thus a main factor in flame performance. Up to 70 % of the ash and moisture free coal matter can be devolatilised, mainly depending on the coal type, heating rate and final temperature, Kollrack and Edelman [1987].

The modelling of devolatilisation rate mechanism is based on measurements in entrained-flow type or heated-grid type. In the former, the coal particles are injected into a reactor chamber and entrained in a preheated secondary gas. The residence time of the particle is adjusted by changing the distance between the probe and the injector port. The time-temperature history is thus determined. In the latter, a small sample of coal is placed betwen folded wire-cloth screen suspended horizontally between two electrodes. The time-temperature history of the coal is assumed to be the same as that recorded by a thermocouple attached to the screen or placed within the folds.

A typical study by Suuberg et al [1979] suggests that pyrolysis behaviour of bituminous coal is distinct by four general phases:

(i) Low temperature removal of surface moisture.

(ii) Evolution of pyrolytically formed water (300 - 400 °C).

(iii) A broad phase involving softening of the coal, accompanied by tar and hydrocarbon evolution (400 - 900°C).

(iv) Evolution of CO and H_2 (above 900 °C).

The main distinction between the various available devolatilisation models is the number or type of reaction steps incorporated into the model. It is important to note that even the most sophisticated models are still not totally adequate to represent the process since they do not account for some important effects like pressure and particle size. Some of the devolatilisation models are introduced below.

2.6.1 Single Reacting Model

The model incorporated assumes that the rate of volatile evolution can be described by a first order equation:

$$\frac{dV}{dt} = k(V^{*} - V) \qquad (2.62)$$

where V = Concentration of volatiles at time t.

V^{*} = Maximum concentration of volatile obtained in infinite time

k = Rate constant (s^{-1})

Single reacting model implies that the rate $\frac{dV}{dt}$ is proportional to the concentration of available volatiles in the coal.

The rate constant is given in Arrhenius form:

$$k = k_v \exp\left(\frac{-E_v}{RT_p}\right) \qquad (2.63)$$

where k_v = pre-exponential factor,(s^{-1})

E_v = Activation energy, J/kg mol

R = Universal gas constant

T_p = particle temperature,(K)

It should be noted that V^* can be related to the proximate volatile content as follows:

V^* = Proximate volatile content x Q-factor

Typical values for the Q-factor in the heating rates experienced in pulverised coal furnaces range between 1.2 to 2.2 according to the coal type and burner design.

k_v and E_v are empirical constants that are determined experimentally. A collection of constants reported has been compiled by Solomon et al [1986] and Badzioch and Hawksley [1970]. The cause of variation in effective devolatilisation rates has been largely attributed to coal type variation, limitations of the one step model and incorrect temperature measurements.

2.6.2 Two Competing Reaction Model

The two competing reaction model was proposed by Kobayashi et al [1976]. This model aimed at accommodating the different release rate at low and high temperature regions. It offers an explanation of the effects on yield of both temperature and heating rate. The model can be explained as shown in Figure 2.2 below.

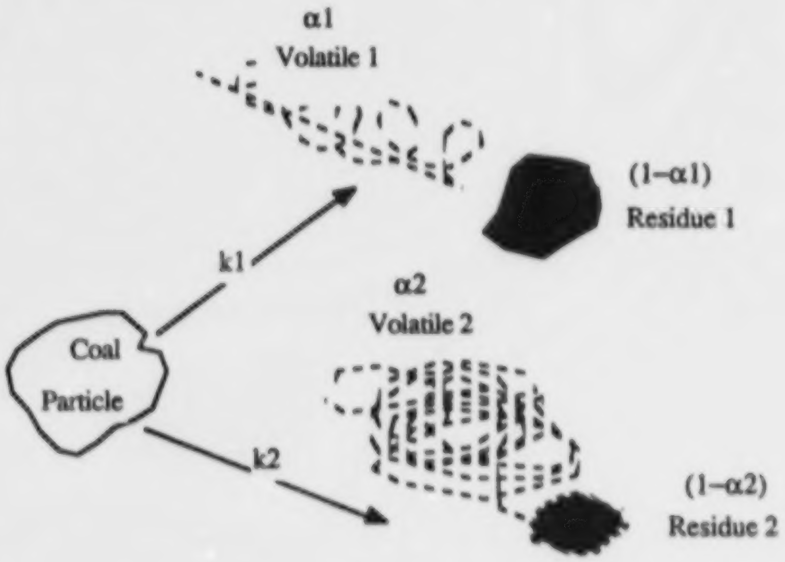
α1
Volatile 1
(1−α1)
Residue 1
k1
α2
Volatile 2
Coal
Particle
k2
(1−α2)
Residue 2

Fig.2.2 Schematic diagram illustrating the two competing reactions model

The rate of devolatilisation is:

$$\frac{dV}{dt} = (\alpha_1 k_1 + \alpha_2 k_2)(V^* - V) \tag{2.64}$$

where k_1 and k_2 are determined from the expression:

$$k_1 = k_{v_1} \exp\left(\frac{-E_{v_1}}{RT_p}\right)$$
$$k_2 = k_{v_2} \exp\left(\frac{-E_{v_2}}{RT_p}\right) \tag{2.65}$$

The model contains six adjustable constants. However the constants adjusted by Kobyashi et al [1976] performed poorly for the cases studied by Wall et al [1986]. Another set of data has been reported by Ubhayakar et al [1976].

2.6.3 Multiple Parallel Reaction Model

The multiple-parallel reaction model is an extension of the two-competing reactions model. It proposes a Gaussian distributoin of the activarion energies, Anthony et al [1975]. The rate of volatile loss for the i-th parallel reacion is:

$$\frac{dV_i}{dt} = k\left(V_i^* - V_i \right) \tag{2.66}$$

where V_i is:

$$V_i = V^* \frac{1}{\sigma\sqrt{2\pi}} \int e^{-\frac{(E_a - E_o)^2}{2\sigma^2}} dE \tag{2.67}$$

σ is the standard Gaussian deviation (kmole)

Anthony et al [1975] presented two sets of rate constats and standard deviations.

1. $k_0 = 1.647 \times 10^{13}\ s^{-1}$; $E_0 = 212$ kJ/mole; $\sigma = 29.4$ kJ/mole

2. $k_0 = 2.91 \times 10^{9}\ s^{-1}$; $E_0 = 154.5$ kJ/mole; $\sigma = 17.5$ kJ/mole

2.6.4 Advanced Devolatilisation Models

Experimental evidence shows that the light hydro-carbons are not the immediate product of the devolatilising particle. As the particle temperature is elevated, it starts releasing heavy tars of molecular weights larger than that of C_6. The latter undergoes secondary reactions namely cracking and deposition.

2.6.4.1 Wen and Chen Model [1979]

This model assumes that three simultaneous reactions occur during pyrolysis: devolatilisation, cracking and deposition. During pyrolysis, all of the chemical reactions are assumed to be first-order with respect to the concentration of the reactants. The temperature effect on the rate constants is expressed by an Arrhenius form. The chemical reactions and the rate expressions for the pyrolysis of a coal particle are summarized as follows:

Devolatilisation

$$\text{Coal} \xrightarrow{k_1} X_1\ \text{tar} + (1-X_1)\ \text{char}$$

Rate $k_1 = k_{10}.\exp(-E_1/RT).\ C_{coal}$

Cracking

$$\text{Tar} \xrightarrow{k_2} \text{Product gas}$$

Rate $k_2 = k_{20}.\exp(-E_2/RT).\ C_{tar}$

Deposition

$$\text{Tar} \xrightarrow{k_3} \text{char}$$

Rate $k_3 = k_{30}.\exp(-E_3/RT).\ C_{tar}$

2.6.4.2 Suuberg et al Model [1979]

The model suggests that heavy tar is formed from coal structure by a pyrolysis reaction having rate constant k_1, and then either converted to coke and light hydrocarbons by a secondary reaction having rate constant k_2 or evolved from the particle by a diffusion process having the effective rate constant k_T. The rate constants k_1 and k_2 are assumed to be of the Arrhenius form with pre-exponentials of $10^{13}\ s^{-1}$, typical of many unimolecular decomposition reactions. The activation energy for tar formation, assumed to be first-order in the amount of tar yet to be formed, is estimated to be roughly 40 kcal / mole. Tar cracking becomes apparent at around 800°C. Assuming tar cracking to be a first order process, an activation energy of 27.2×10^7 J / kg-mol is implied.The evaporation-diffusion model for the vapour-liquid tar interface is approximated as the outer surface of the coal particle. Assuming that the enthalpies of vaporisation of the tar components have the empirical molecular weight dependence the vapour pressure of a component having molecular weight M is approximated as $(1.23 \times 10^5\ \text{atm}) \exp(-236M^{0.654} / T)$, where M and T are expressed in g/mole and K, respectively. The range of molecular weights is assumed to be 400 - 1200 g / mole. The vapour diffusion coefficient of tar molecules is assumed to be $(O.1\text{cm}^2/\text{s}) \times (T/273K)^{1.5} \times (1\text{atm}/P)$, where P is the total pressure.

2.6.5 Choice of Devolatilisation Model

A sensitivity study was carried out for the single, two-competing and multiple parallel reaction models and showed that they yielded similar performance. It was thus decided to use the single reacting model for the simplicity of optimising its constants for different types of coals. However, a scheme based on Suuberg's proposals was developed during the course of this study to account for the effects of secondary cracking. This scheme and its implication on the predictions are included in the parametric study given in chapter 5.

2.7 VOLATILE COMBUSTION

Treatment of volatiles combustion cannot neglect the effect of fluctuations in the turbulent mixing based on time scale considerations. Time scales for these reactions are as fast as the time scale of turbulence; effects of turbulence must therefore be incorporated when calculating mean reaction rates or mean composition fields, Smith and Fletcher [1988]. Khalil et al [1975] studied a gaseous flame and suggested that the simplest approach to volatile combustion in diffusion flame is to assume that the chemical reaction is so fast that the process is entirely mixing controlled. This conforms with the earlier suggestion by Hubbard [1958] that in high temperature turbulent diffusion flames it is the physical processes of mixing which govern the combustion length. Magnussen and Hjertager [1979] presented a model for the rate of combustion which relates the rate of dissipation of eddies and expresses the rate of reaction by the mean concentration of a reacting specie, the turbulent kinetic energy and the rate of dissipation of this energy. The combustion rate can thus be expressed as follows:

$$R_v = A\rho\left(\frac{\varepsilon}{k}\right)\min\left\{C_v, \frac{C_{O_2}}{S}, B\frac{C_{Pr}}{1+S}\right\} \tag{2.68}$$

where C_v, C_{O_2} and C_{Pr} are the concentrations of the volatiles, oxygen and product species respectively, S is the stoichmetric oxygen requirement to burn 1 kg. volatiles. A and B are constants that depend on the structure of the flame and the rate of reaction between volatiles and oxygen.

The cases that were studied by Magnussen and Hjertager [1979] suggest the values of 4 and 0.5 for the constants respectively. However, the universality and simplicity of these values are questionable. This is discussed latter in Chapter 5.

The above mentioned model which was originally formulated to model gaseous premixed and diffusion flames was first extended to model the combustion of volatiles in pulverised coal flames by Lockwood et al [1980].

An alternative method to model the turbulence effects on the volatile combustion is the statistical coal gas mixture fraction model which is based on an extension of the conserved scaler approach in gaseous flames, Pratt [1976]. This model involves the solution of the transport equation for the local mean value of the coal mass fraction which is defined as the mass of gas originating from the coal particle or fuel droplet divided by the total local gas mass. It is thus a progress variable measuring evolution and mixing of the volatile products in the turbulent transporting fluid. The solution of this variable is accompanied by the solution of the conservation equation for the variance of the coal-gas mixture fraction where a shape for the statistical probability distribution function is chosen. Local instantaneous equilibrium is assumed and the mean value for the chemical properties is computed by integrating the local instantaneous properties over the probability distribution function.

Smith and Fletcher [1988] compared the performance of the two models together with another approach that ignores the effect of turbulence fluctuations. The approach that ignores turbulence fluctuations resulted in a misreprestation of the flame structure. Both of the former models were able to predict the smoothing or averaging due to the turbulence. However, the statistical model required twice as much computational time to solve the same problem as the eddy-break up model. Therefore, the latter was chosen for application throughout the present study.

2.8 HETEROGENEOUS CHAR COMBUSTION

The accurate physical description of char oxidation is complicated by evolving pore structures, internal temperature gradients, mass and heat transfer effects both inside and outside the particle. Catalytic effects of the inorganic matter and the history of the coal also play roles in its oxidation behaviour. Complete reviews of the many issues involved are offered by Laurendeau [1978], and Smith [1982].

The experimental techniques used to determine the coal reactivity as given by, for example, Smith [1971] or Hamor et al [1973] involve metered supplies of the sized particles and preheated O_2 - N_2 mixtures which pass through a laminar-flow reactor contained in a high electrically heated furnace. Measurements of the O_2 and CO_2 contents of the gas samples withdrawn at successive intervals along the reactor, measurements of gas velocities and deducing the particle temperature from measurements or calculatiing from the energy equation determine the char oxygen reactivity.

The reported data of intrinsic reactivity which is defined by Smith [1978] as the reaction rate per unit area of pore surface in the absence of any mass transfer restrictions show a wide range of reactivities towards oxygen. Similar intrinsic reactivities for different carbons were obtained only when heated to at least 2973 K, and after several of the carbons had been exposed to chlorine at high temperature.

However, because of the many complications, global oxidation rates based on external surface area and simple Arrhenius expressions for reaction rate coefficients are the most common descriptions of oxidation processes by both furnace designers and coal kinetisits.

The overall reaction rate R_c of the heterogeneous reaction between carbon and oxygen is affected by both the mass transfer and the chemical constraints. However, recent evidences tend to restrict the importance of the mass transfer between char and oxygen. For example, Solomon et al [1990] suggested that the char combustion involves the reduction of the surrounding CO_2. At low temperature, external diffusion is often ignored because chemical reactions rate are so low. On the other-hand, the diffusion controls the burning rates at high temperatures. This phenomenon stimulated the concept of three regimes where the chemical rate dominates the first and the diffusion rate dominates the third and the second is determined by both rates, see for example Prado el al [1987].

The order of reaction for the oxygen partial pressure which is determined experimentally varies between 0 to 1 though its physical implication is unclear and often doubted if it has much more than experimental validity, Smith [1978]. Young and smith [1981] developed statistical technique for determining the order of reaction and found that the chemical reaction rate coefficient is dependent on oxygen pressure for a value close to 0.5. However, in the present study it is assumed to be of first order for simplicity.

The overall reaction rate is expressed as:

$$R_c = P_{ox}\left(\frac{1}{K_d} + \frac{1}{K_c}\right)^{-1} \tag{2.69}$$

where
$$k_c = A_c \exp\left(\frac{-E_c}{RT_p}\right) \tag{2.70}$$

where P_{ox} is the oxygen partial pressure and k_d is the diffusional rate coefficient, T_p is particle temperature. The rate of reaction refers to the external surface of the particle, but because of their porous structure, eventual internal combustion is occuring. All effects of internal combustion on the reaction rate are included in the factors A_c and the apparent activation energy E_c. These factors are known to be coal specific, Smith [1978]. K_d, the diffusion rate assuming that the particle is of spherical shape, is given by Field et al [1967] and Hamor et al [1973]:

$$k_d = \frac{D_c M_c \Phi}{\left\{R \frac{d_p}{2}\left(\frac{(T_p + T_g)}{2}\right)\right\}} \tag{2.71}$$

where D_c is the diffusion coefficient and it changes with pressure and temperature according to the relation:

$$D_c = D_o\left(\frac{P_o}{P}\right)\left(\frac{T_g}{T_o}\right)^{1.75} \tag{2.72}$$

D_o is taken to be $3.13 {*} 10^{-4}$ m^2/s at the reference temperature of 1500 ^{o}k and the reference pressure of $1.013 {*} 10^5$ N/m^2. M_c is the atomic weight of carbon, ϕ is a mechanism factor and its value is 2 if CO is the main product and 1 if CO_2 is the main product being driven away from the particle boundary layer.

Wall and Gurarajan [1986] suggest that the chemical reaction rate is not constant through the burning of the coal particles. Slower rates are experienced at the later stages of combustion due to the increasing of the percentage of impurities in the coal particles. This phenomenon leads to the over-estimation of calculated exit burnout in PF combustors.

CHAPTER 3

NUMERICAL SOLUTION

3.1 INTRODUCTION

The complexity of the partial differential equations presented in the previous chapter for the conservation of mass, momentum, species and energy along with those for the modelled turbulence quantities (k and ε), radiation etc. place them well out of the reach of any possible analytical treatment. The numerical options available are either the finite element or finite difference method. Finite element techniques for fluid flow calculations have not been so extensively developed as finite difference methods which have received great deal of attention during the past two decades, see Jones and Whitelaw [1984] and Gosman and Issa [1989]. The latter has been employed in the present study.

This chapter describes the numerical methods incorporated in the employed code. The geometries considerated are represented by a computational grid over which the differential equations are discretised into algebraic forms which are solved with the aid of an iterative procedure.

The aim of validating the physical models presented in the previous chapter highlights the problem of the numerical accuracy of the prediction. The pressure-velocity decoupling methods are outlined .The treatment of the boundary conditions is explained, and finally a description of the numerical methods implemented in the calculation of the particulate phase is given.

3.2 THE COMPUTATIONAL GRID

A staggered orthogonal grid arranged such that the velocity nodes are located in between the scalar ones in backwards form as shown in Fig. (3.1) is used. The grid spacing may be non-uniform with grid nodes concentrated in areas of steep gradients or complex boundary configurations.

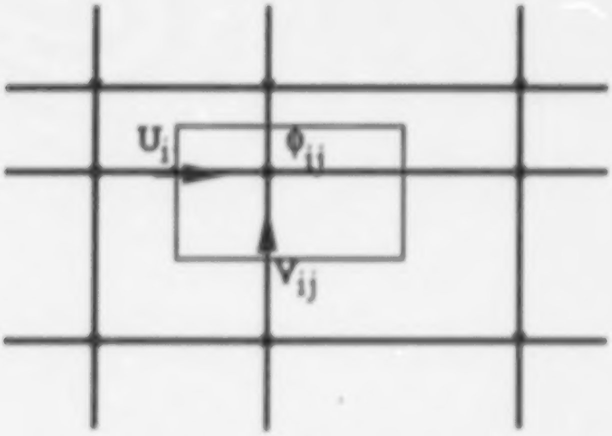
U_i
ϕ_{ij}
V_{ij}

Fig. 3.1 The Staggered Grid

The boundaries of the scalar, U-velocity and V-velocity cells are located midway between the two node points as shown in Fig. (3.2).

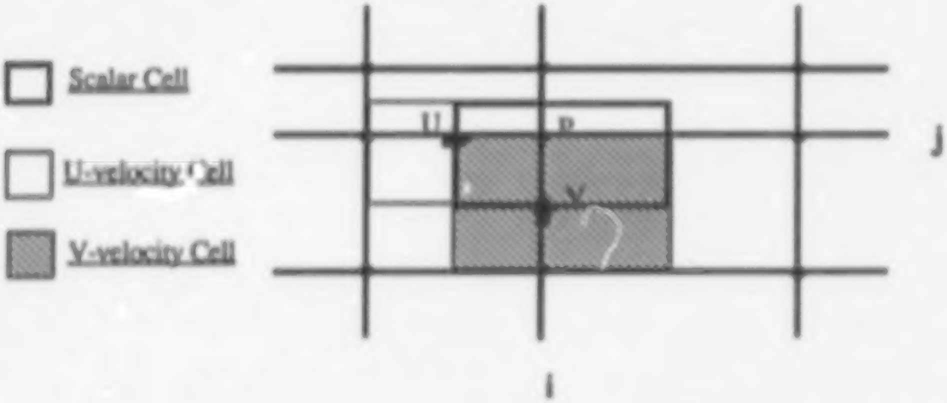
Scalar Cell
U-velocity Cell
V-velocity Cell
U
P
V
j
i

Fig. 3.2 The control volumes for scalar, U-velocity and V-velocity cells

3.3 DISCRETISATION OF THE GENERAL DIFFERENTIAL EQUATION

The general differential equation for a conserved quantity ϕ under steady state condition can be written as:

$$\frac{\partial}{\partial x_j}(\rho U_j \phi) - \frac{\partial}{\partial x_j}\left(\Gamma \frac{\partial \phi}{\partial x_j}\right) = S \tag{3.1}$$

The first term on the L.H.S. represents the convective flux while the second term represents the diffusion with Γ being the diffusive exchange coefficient. The R.H.S. represents the source term.

Rewriting Eq.(3.1) in cylindrical coordinates for the case of two dimensional axi-symmetric flow and integrating over the control volume shown in Fig. (3.3) gives:

$$\int_w^e \int_s^n \int_0^1 \left[\frac{\partial}{\partial x}(\rho U r \phi) + \frac{\partial}{\partial r}(\rho V r \phi) - \frac{\partial}{\partial x}\left(r\Gamma \frac{\partial \phi}{\partial x}\right) - \frac{\partial}{\partial r}\left(r\Gamma \frac{\partial \phi}{\partial r}\right) - rS\right] dx \quad dr \quad d\zeta = 0 \tag{3.2}$$

where, because of the assumed symmetry, the third integrand ζ has the integration limits of 0 to 1 radians instead of 0 to 2π.

3.3.1 The Convection Terms

Integration of the first term of Eq.(3.2) gives:

$$\left[(\rho U \phi)_e - (\rho U \phi)_w\right] \int_w^e \int_s^n \int_0^1 r \quad dx \quad dr \quad d\zeta$$

$$= \left[(\rho U \phi)_e - (\rho U \phi)_w\right] \frac{R_n^2 - R_s^2}{2}$$

$$= \left[(\rho U \phi)_e - (\rho U \phi)_w\right] (R_n - R_s) \left(\frac{R_n + R_s}{2}\right) \tag{3.3}$$

where R_n and R_s are the radii of the north and south faces of the control volume respectively.

Taking the scalar cell shown in Fig.3.3 as an example Eq.(3.3) may be reduced to:

$$\left[(\rho U \phi)_e - (\rho U \phi)_w\right] \quad A_{ew} \tag{3.4}$$

Convection coefficients are defined as:

$$C_E = \rho_e U_E A_{ew}$$
$$C_W = \rho_w U_P A_{ew} \qquad (3.5)$$

where density ρ is defined at the scalar grid nodes and is obtained at the boundaries by simple averaging, thus:

$$\rho_e = \frac{\rho_P + \rho_E}{2}$$
$$\rho_w = \frac{\rho_W + \rho_P}{2} \qquad (3.6)$$

Similarly, the second convection term in Eq.(3.2) can be written as:

$$C_n = \frac{\rho_N + \rho_P}{2} V_N A_n$$
$$C_s = \frac{\rho_S + \rho_P}{2} V_S A_s \qquad (3.7)$$

As the conserved variable ϕ is defined at the grid nodes and not at all boundaries, an interpolation technique is required for velocity. Its main requirements are the assurance of numerical accuracy and stability. Any degree of accuracy can be achieved through decreasing the distance between the nodes, a condition that cannot always be met because of the computational storage/run times limits. This constraint thus allows for the approximation errors referred at as numerical diffusion, Roach [1976]. The simpler interpolation techniques are obtained using the five point molecule shown in Fig. 3.3. A more accurate scheme is obtained by incorporating more points, by way of example a nine point molecule is shown in Fig. 3.4. A brief description of these schemes is given below.

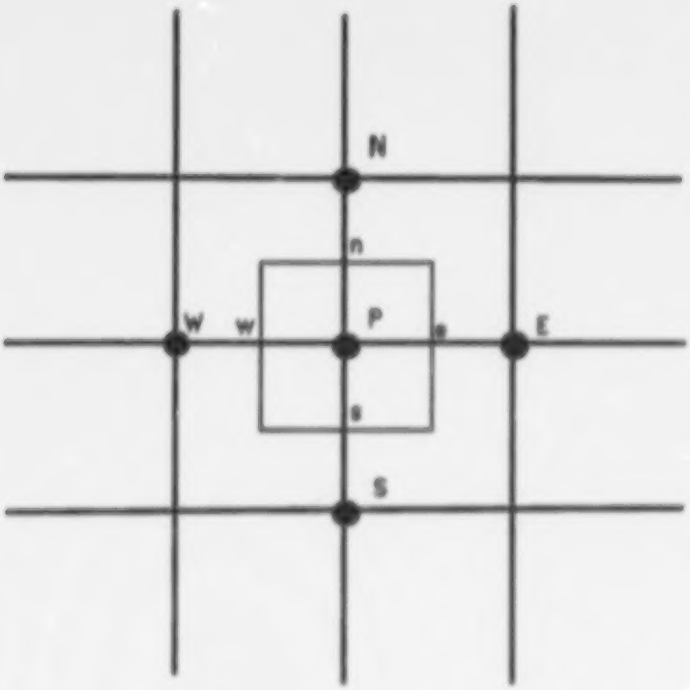

Fig 3.3 Standard five point molecule

3.3.1.1. The Central Differencing Scheme

This scheme assumes a linear first order profile for the distribution of ϕ between the nodes in the form of:

$$\phi_e = \frac{\phi_E + \phi_P}{2} \tag{3.8}$$

It involves a second order truncation error, Syed et al [1985]. Its main drawback is that when substituted in Eq.(3.3), ϕ_P will be eliminated from the final form, thus causing potential for instabilities for Pe > 2, where Pe, the Peclet number is defined as:

$$Pe = \frac{\rho U}{\Gamma} \tag{3.9}$$

3.3.1.2.The Upwind Scheme

This scheme was formulated to avoid the central differencing drawback. Again taking ϕ_e as an example, it is approximated by:

$$\phi_e = \begin{cases} \phi_P & \text{for} \quad Pe \geq 0 \\ \\ \phi_E & \text{for} \quad Pe \leq 0 \end{cases} \tag{3.10}$$

The upwind scheme is stable but less accurate than the central differencing scheme. It can be named zeroth order since the profile of the assumed distribution of ϕ between two consecutive nodes is flat.

3.3.1.3 The Hybrid Scheme

This scheme is aimed to combine the advantages of the two preceding schemes. It approximates the variables in the form:

$$\phi_e = \begin{cases} \phi_P & \text{for} \quad Pe \geq 2 \\ \\ \dfrac{\phi_E + \phi_P}{2} & \text{for} \quad Pe \ < |2| \\ \\ \phi_E & \text{for} \quad Pe \leq -2 \qquad -2 < Pe < 2 \end{cases} \tag{3.11}$$

The hybrid scheme has been widely used since it is inherently stable and provides a reasonable degree of numerical accuracy that can be enhanced through refining the grids. However, it is subjected to numerical error termed false diffusion, Roach [1976] whenever the flow streamlines cross the grid lines at an oblique angle.

3.3.1.4.The QUICK scheme

The problem of false numerical diffusion has been addressed in various papers including those of Raithby [1976], McDonald [1979], Leonard [1979], McGuirk et al [1982], and Sturgess and Syed [1985]. Higher order differencing schemes have been proposed to improve the accuracy of the predicted flow field. Amongst these are the quadratic upstream interpolation for convective kinematics, referred to as QUICK proposed by Leonard [1979], the skew-upwind differencing scheme proposed by

Raithby [1976], the Agrawal differencing scheme proposed by Agrawal [1981] and the Hermetian scheme proposed by Glass and Rodi [1982].

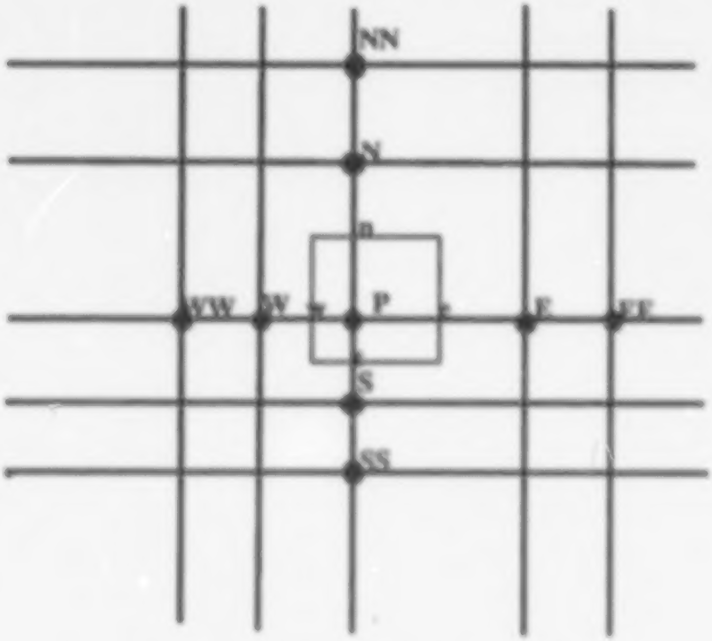

Fig. 3.4 Extended nine point molecule

The QUICK scheme provides good accuracy. This is achieved through considering an extended nine point molecule as shown in Fig. 3.4. It uses the upstream based quadratic interpolation to approximate the convective operator. For example, the term ϕ_e for uniform grids is evaluated as follows:

$$\phi_e = \begin{cases} \phi_P + \frac{1}{8}(3\phi_E - 2\phi_P - \phi_W) & \text{for} \quad Pe \geq 0 \\ \\ \phi_E + \frac{1}{8}(3\phi_P - 2\phi_E - \phi_{EE}) & \text{for} \quad Pe \leq 0 \end{cases} \qquad (3.12)$$

In the present study the discretisation coefficients used for Eq.(3.12) when using the QUICK scheme, are those obtained for the UPWIND scheme to satisfy the Scarborough criterion, Patankar [1980]. The differences in coefficients are summed and inserted into a source term. The coefficients calculated in the literature are usually obtained for uniform grids, which is not the situation of the present study. These coefficients are herein calculated using a modified form as Eq. (3.12) yields to:

$$\phi_e = \begin{cases} \phi_P + g_1e_1\phi_E - (g_1e_1 - g_2e_1)\phi_P - g_2e_1\phi_W & \text{for} \quad Pe \geq 0 \\ \phi_E + g_1e_2\phi_P - (g_1e_2 - g_2e_2)\phi_E - g_2e_2\phi_{EE} & \text{for} \quad Pe \leq 0 \end{cases} \tag{3.13}$$

where

$$\begin{aligned} g_1e_1 &= \frac{b+2a}{4(a+b)} \\ g_2e_1 &= \frac{b^2}{4a\,(a+b)} \\ g_1e_2 &= \frac{b+2c}{4(c+b)} \\ g_2e_2 &= \frac{b^2}{4c\,(c+b)} \end{aligned} \tag{3.14}$$

where a, b and c are the distances between the cell nodes as shown in Fig. 3.5

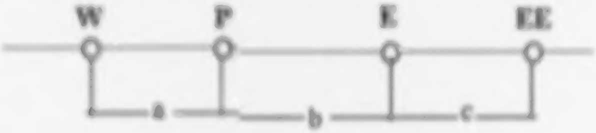

Fig. 3.5 Schematic diagram for the grid clusters in one dimensional notation

The QUICK scheme was introduced on the momentum equations only. It was not incorporated in the scalar equations as these are mainly source dominated and the effects of numerical diffusion should not be large and in any case debilitating overshoots can result.

3.3.1.5 Choice of discretisation scheme

The hybrid differencing scheme has been used for the majority of previous studies, see Rizvi [1987], Lockwood and Rizvi [1988] and Levy [1991]. This scheme has also been used in the early parts of this present study.

Syed et al [1985] assessed a number of candidate numerical schemes for accuracy, ease of solution and overall cost effectiveness. A companion study, Syed and Chiapetta [1985] compared their performance by computing flows that are representative of those found in a combustor in two and three dimensions. They concluded that both the QUICK and Skew Upwind schemes are more efficient than the lower order schemes. Leschziner and Rodi [1981] observed the superiority of the QUICK scheme as compared to Hybrid.

3.3.1.6 Final form of the convection terms

From the above discussion, the following expression can be defined:

$$\phi_e = f_E\phi_E + (1-f_E)\phi_P$$
$$\phi_w = f_W\phi_P + (1-f_W)\phi_W$$
$$\phi_n = f_N\phi_N + (1-f_N)\phi_P$$
$$\phi_s = f_S\phi_P + (1-f_S)\phi_S \tag{3.15}$$

where the values of f's depend upon the discretisation scheme involved. As for the QUICK scheme, the Upwind coefficients are used for the convection term and the rest of the interpolation components are dumped into the source term. Thus the convection terms of Eq. (3.2) can be expressed as:

$$C_E f_E\phi_E - C_W(1-f_W)\phi_W + C_N f_N\phi_N - C_S(1-f_S)\phi_S$$
$$+ [C_E(1-f_E) - C_W f_W + C_N(1-f_N) - C_S f_S]\phi_P \tag{3.16}$$

3.3.2 The Diffusion Terms

Integrating the diffusion terms in an analogue manner to the convection terms gives:

$$-\Gamma_e\left(\frac{\partial\phi}{\partial x}\right)_e A_{ew} + \Gamma_w\left(\frac{\partial\phi}{\partial x}\right)_w A_{ew} - \Gamma_n\left(\frac{\partial\phi}{\partial r}\right)_n A_n + \Gamma_s\left(\frac{\partial\phi}{\partial x}\right)_s A_s \tag{3.17}$$

where the derivatives are evaluated using the values at the main nodes, for example:

$$\left(\frac{\partial \phi}{\partial x}\right)_e = \frac{\phi_E - \phi_P}{\Delta x_{PE}} \tag{3.18}$$

where ∂x_{PE} is the co-ordinate distance between the node points P and E.

Defining the diffusion coefficients as:

$$\begin{aligned}
D_E &= \Gamma_e \frac{A_{ew}}{\partial x_{PE}} = \left(\frac{\Gamma_P + \Gamma_E}{2}\right)\left(\frac{A_{ew}}{\partial x_{PE}}\right)\\
D_W &= \Gamma_w \frac{A_{ew}}{\partial x_{PW}} = \left(\frac{\Gamma_P + \Gamma_W}{2}\right)\left(\frac{A_{ew}}{\partial x_{PW}}\right)\\
D_N &= \Gamma_n \frac{A_n}{\partial x_{NP}} = \left(\frac{\Gamma_P + \Gamma_N}{2}\right)\left(\frac{A_n}{\partial x_{NP}}\right)\\
D_S &= \Gamma_s \frac{A_s}{\partial x_{PS}} = \left(\frac{\Gamma_P + \Gamma_S}{2}\right)\left(\frac{A_s}{\partial x_{PS}}\right)
\end{aligned} \tag{3.19}$$

One can write the diffusion terms in the form:

$$-D_E(\phi_E - \phi_P) + D_W(\phi_P - \phi_W) - D_N(\phi_N - \phi_P) + D_S(\phi_P - \phi_S) \tag{3.20}$$

3.3.3 The Source Terms

The source terms are integrated in a linearised form following the TEACH formulation, Gosman and Ideriah [1976], to give:

$$S_\phi = S_u + S_P \phi_P \tag{3.21}$$

The exact values for the source terms for various equations are given in table (3.1).

At steady state the continuity equation displayed below in Eq.(3.25) should be satisfied in a converged solution. During the course of iterating to obtain a converged solution, the quantity $C_E - C_W + C_N - C_S - S_P^M(\Delta V)$ will not in general vanish. In addition, a situation may arise where all of the total coefficients are zero, thus causing singularities, Patankar [1980]. It was thus recommended that the commulative mass flow rate multiplied by the corresponding function be added to both components of the source term as:

$$
\begin{aligned}
S'_{u} &= S_{u} + \max\left(C_{E} - C_{W} + C_{N} - C_{S} - S_{P}^{M}(\Delta V) , 0\right)\phi_{P} ,\\
S'_{P} &= S_{P} + \max\left(C_{E} - C_{W} + C_{N} - C_{S} - S_{P}^{M}(\Delta V) , 0\right) \qquad (3.22)
\end{aligned}
$$

Note that the ϕ_P in the expression of S'_u is that calculated from the previous iteration while S'_P is going to be multiplied by the newly calculated ϕ_P as shown in Eq.(3.21) thus ensuring that the finite difference equation will behave reasonably when the mass flow rates for the control volume do not satisfy the continuity.

3.3.4. The Final Form of the Discretised Equation

Substituting the coefficients defined by the expressions (3.16), (3.20) and (3.22) into Eq.(3.2), the general ϕ-equation becomes:

$$
\begin{aligned}
&[C_{E}(1-f_{E}) + D_{E} - C_{W}f_{W} + D_{W} + C_{N}(1-f_{N}) + D_{N} - C_{S}f_{S} + D_{S}]\phi_{P}\\
&= [C_{E}f_{E} - D_{E}]\phi_{E} - [C_{W}(1-f_{W}) + D_{W}]\phi_{W} +\\
&[C_{N}f_{N} - D_{N}]\phi_{N} - [C_{S}(1-f_{S}) + D_{S}]\phi_{S} + S'_{U} + S'_{P}\phi_{P} \qquad (3.23)
\end{aligned}
$$

Now, to simplify the handling of Eq.(3.23) the following coefficients are defined:

$$
\begin{aligned}
a_{E} &= D_{E} - f_{E}C_{E},\\
a_{W} &= D_{W} + (1-f_{W})C_{W},\\
a_{N} &= D_{N} - f_{N}C_{N},\\
a_{S} &= D_{S} + (1-f_{S})C_{S}
\end{aligned}
$$

and

$$
a_{P} = a_{E} + a_{W} + a_{N} + a_{S} - S'_{P} + S_{P}^{M} \qquad (3.24)
$$

Substituting for the continuity equation for two phase flow which is:

$$
C_{E} - C_{W} + C_{N} - C_{S} = S_{P}^{M} \qquad (3.25)
$$

thus the final form of the discretisation equation may be written as:

$$a_P\phi_P = a_E\phi_E + a_W\phi_W + a_N\phi_N + a_S\phi_S + S'_U \qquad (3.26)$$

3.4 PRESSURE VELOCITY DECOUPLING

The pressure gradient is included as one of the constituents of the source term in the momentum equations, see Table (3.1). Pressure fields for enclosed flows are generally unknown. An algorithm is required to transform the continuity equation into a pressure correction equation. The pressure correction equation is formed by substituting the momentum equations for the guessed velocities into the continuity equation.

The momentum equation over a U-cell can be written as:

$$a_w U_w = \sum a_{nb} U_{nb} + A_{ew}(P_W - P_P) + b \qquad (3.27)$$

where $b = S'_c - A_{ew}(P_W - P_P)$ (3.28)

3.4.1 The SIMPLE Algorithm

The simplest algorithm is the iterative and sequential Semi-Implicit Method for Pressure-Linked equations,SIMPLE,proposed by Patankar and Spalding [1972]. This algorithm presumes a guessed pressure and velocity fields P^*, U^* and V^* which when substituted in the discretised momentum equation, Eq.(3.27) yields:

$$a_w U^*_w = \sum a_{nb} U^*_{nb} + A_{ew}(P^*_W - P^*_P) + b \qquad (3.29)$$

If Eq.(3.29) is subtracted from Eq. (3.28) and neglecting $\Sigma a_{nb} U_{nb} - \Sigma a_{nb} U^*_{nb}$ for simplicity, a velocity correction equation is obtained:

$$U_w = U^*_w + d_w(P'_W - P'_P) \qquad (3.30)$$

where

$$d_w = \frac{A_{ew}}{a_w}$$
$$P'_P = P_P - P^*_P$$
$$P'_W = P_W - P^*_W \qquad (3.31)$$

Similarly for the radial velocity:

$$V_s = V^*_s + d_s\left(P'_S - P'_P\right) \tag{3.32}$$

Substituting the continuity equation for the scalar cell:

$$(\rho UA)_e - (\rho UA)_w + (\rho VA)_n - (\rho VA)_s = S_P^M \tag{3.33}$$

Now if the velocities are substituted from the velocity correction expressions given in Eq.(3.30) and Eq.(3.32) into Eq.(3.33), the pressure correction equation is obtained:

$$a_P P'_P = a_E P'_E + a_W P'_W + a_N P'_N + a_S P'_S + b \tag{3.34}$$

Solving Eq.(3.34), the pressure correction may be deduced and thus the pressure can be obtained with the aid of under-relaxation factor λ, as follow:

$$P = P^* + \lambda P' \tag{3.35}$$

The velocities can then be updated using Eq.(3.27). The same steps are repeated until the pressure correction vanishes and thus convergence is obtained.

The SIMPLE algorithm consists of the following steps:

1. Guess the pressure field P^*.
2. Solve the momentum equations eq.(3.29) to obtain U^* and V^*.
3. Solve the P' equation , eq.(3.34), and update the pressure by eq. (3.35).
4. Update velocities U and V by the velocity correction equation (3.30) and (3.32).
5. Repeat steps 2 and 4 until convergence is reached each iteration.

3.4.2 The SIMPLER Algorithm

Another method, SIMPLER, was proposed by Patankar [1985]. The main difference between this method and the previous one is that it does not ignore the term $\sum a_{nb} U_{nb} - \sum a_{nb} U^*_{nb}$ which was assessed to be slowing the convergence process. This was achieved through defining pseudo-velocities as:

$$\hat{U}_w = \frac{\sum a_{nb} U_{nb} + b_w}{a_w}$$
$$\hat{V}_s = \frac{\sum a_{nb} V_{nb} + b_s}{a_s} \qquad (3.36)$$

The momentum equations shown in eq.(3.27) are re-expressed as:

$$U_w = \hat{U}_w + d_w(P_W - P_P)$$
$$V_s = \hat{V}_s + d_s(P_S - P_P) \qquad (3.37)$$

Substituting eq. (3.37) into eq.(3.33) gives the pressure equation:

$$a_P P_P = a_E P_E + a_W P_W + a_N P_N + a_S P_S + S'_U \qquad (3.38)$$

The SIMPLER algorithm can be described by the following sequence of operations:

1. Using the currently available velocity field, calculate $\hat{U}$, $\hat{V}$ from eq.(3.36).
2. Calculate coefficients of the pressure equation [eq.(3.38)] and solve for the updated pressure field.
3. Using this pressure field, solve the momentum equation to calculate U^* and V^*.
4. Solve the P' equation [eq.(3.34)].
5. Correct the velocity field by the velocity correction equation [eq.(3.30) and eq(3.32)].
6. Repeat steps 1-5 until converged solutions are obtained.

3.4.3 The PISO Algorithm

The PISO algorithm was proposed by Issa et al (1983). It involves two predictor levels. Eq.(3.29) can be expressed implicitly as:

$$a_w U_w^* = \sum a_{nb} U_{nb}^* + A_{ew}(P'_W - P'_P) + b_w^* \qquad (3.39)$$

where the superscript $'$ denotes values obtained from the previous iteration, the superscript * denotes values obtained in the first predictor and ** the second predictor and so on. So:

$$a_w U_w^{**} = \sum a_{nb} U_{nb}^* + A_{ew}(P^*_W - P^*_P) + b_w^* \qquad (3.40)$$

Subtracting Eq.(3.40) from Eq.(3.39) gives the increment :

$$U_w^{**} = \hat{U}_w + d_w(P_W^* - P_P^*) \tag{3.41}$$

where $\hat{U}_w = U_w^* - d_w(P_W^* - P_P^*)$ (3.42)

substituting Eq.(3.41) into the continuity equation (3.33) leads to the pressure equation which is the same form as Eq.(3.38) with the $\hat{U}$ and $\hat{V}$ as given by Eq.(3.42) instead of Eq.(3.37). This equation is the predictor equation for pressure. The second corrector equation for velocity is obtained as:

$$U_w^{***} = \hat{U}^*_w + d_w(P_W^{**} - P_P^{**}) \tag{3.43}$$

where

$$\hat{U}^*_w = U_w^{**} + \frac{\left[\sum a_{nb}(U_{nb}^{**} - U_{nb}^*)\right]}{a_w} - d_w(P_W^* - P_P^*) \tag{3.44}$$

These values can be substituted again in the discretised continuity equation to give the second corrector equation.

The PISO algorithm can be described by the following steps:

1. Using the previous iteration solution (U^*, V^*, P^*), calculate the coefficients of the momentum equations and solve this system of implicit equations. This represents the predictor step for velocity.
2. Using this predicted velocity, calculate the coefficients of pressure equation (3.38) and solve for the pressure field. This is the predictor step for the pressure.
3. Correct (first corrector step for velocity) the velocity field, using explicit type equations such as eq.(3.41).
4. Using the corrected velocities, calculate the coefficients of the pressure equation in the corrector step and solve the implicit system of equations to obtain an updated pressure field.
5. Using the corrected pressure field, re-evaluate the velocity field (second corrector step) using explicit-type equations such as eq.(3.43).
6. March to the next iteration.

3.4.4 Choice of Solution Algorithm

It can be anticipated that the speed of convergence will depend upon the solution algorithm used.

Rizvi [1985] compared the performance of SIMPLE and PISO algorithms for a combustion case in an axi-symmetric furnace. He found that the latter is substantially more cost effective than the former. The saving in the computational time for the case studied was more than the factor of two.

Jang et al [1986] compared the performance of SIMPLE, SIMPLER and PISO amongst other algorithms for several cases. For the case relevant to the present study, a swirling reacting flow in an axi-symmetric furnace, PISO showed the clear superiority over both SIMPLE and SIMPLER when using secondary swirl of 0.2. However, when the swirl was highly increased to 20.0, the PISO algorithm lost its robust behaviour. It required greater computing effort to obtain a converged solution than the SIMPLER algorithm. This is due to the larger value of b, given by eq.(3.28) which is a function of the W-velocity..

For the present study the cases under consideration are of relatively low swirl as compared to that used by Jang. It was decided, thus, to use the PISO algorithm in light of its time/CPU saving merits. However, it was observed that the speed of convergence is inversely proportional with the degree of swirl of the examined flow.

3.5 SOLUTION OF THE FINITE DIFFERENCE EQUATIONS

The system of non linear algebraic equations of the form shown in Eq.(3.26) is too large to be solved by matrix inversion or other direct techniques. An iterative method is required. The *Tri-Diagonal Matrix Algorithm (TDMA)* is usually employed. The equations are in the form:

$$D_i\phi_i = A_i\phi_{i+1} + B_i\phi_{i-1} + C_i \tag{3.45}$$

where i = 2, N-1 and the values of the constant coefficients A_i, B_i, C_i and D_i are given for i = 2, N-1 together with the boundary values ϕ_1 and ϕ_N. The procedure calls for Eq.(3.45) to be rewritten as:

$$\phi_i = A'_i\phi_{i+1} + C'_i \tag{3.46}$$

The solution is obtained by successive substitution starting at i = N-1 and working backwards to i=2. The transformed coefficient A'_i and C'_i are given by the recurrence relations:

$$A'_i = \frac{A_i}{D_i - B_iA'_{i-1}}$$

$$C'_i = \frac{C_i + C'_{i-1}B_i}{D_i - B_iA'_{i-1}} \tag{3.47}$$

with the starting values of $A'_1 = 0$ and $C'_1 = \phi_1$. The TDMA is implemented to solve Eq.(3.26) by considering the equation for all the control volumes with the last estimates for the values of ϕ along the two neighbouring grid lines and hence constructing an equation set which can be solved by the TDMA. The grid lines are traversed in the x-direction then the solution is used over lines in the r-direction as:

$$A_P\phi'_P = A_N\phi'_N + A_S\phi'_S + (A_E\phi_E + A_W\phi_W + S_U) \tag{3.48}$$

The number of sweeps required to reach an accurate solution is arbitrary and problem dependent.

3.6 THE BOUNDARY CONDITIONS

The grids are arranged such that the boundaries coincide with the faces of the scalar cells to ensure the conservation of flux. The convective coefficients between the boundaries and the neighbouring cells are broken by setting them to zero. The correct value for the coefficient is provided from the prescribed boundary condition via the source term at the boundary. For the present code, the boundaries are defined in a user friendly way that permits the general use of the code in a relatively simple manner.

3.6.1 Inlet Boundary Conditions

At the inlets, the distributions of all the variables are defined either from measurements or based on estimates from operating conditions. The axial velocity distribution may be given or a constant profile can be deduced from the mass flow rate. The radial velocity distribution is required to be given. The tangential velocity distribution is either given or can be deduced from the swirl number, S, which is defined as:

$$S = \frac{G_\phi}{RG_x} \qquad (3.49)$$

where G_ϕ, the axial flux of tangential momentum, is defined as:

$$G_\phi = \int r^2 \rho (UW)\, dr \qquad (3.50)$$

R is equivalent nozzle or orifice radius and G_x, the axial thrust is defined as:

$$G_x = \int r \rho U^2 dr \qquad (3.51)$$

see for example Beer and Chigier [1974] and Mahmud et al [1987]. The temperature of the combustion air is specified at each inlet. The density is calculated from the equation of state and the enthalpy from the constitutive equation. The oxygen and product concentrations are also specified, to account for the specification of the air. Note that on some occasions the burners may use vitiated air as means of stabilizing the flame. The inlet volatile concentration is also given at each inlet. The inlet enthalpy is calculated knowing the enthalpy of the combustion air at the inlet section.

For the inlet turbulence quantities a uniform inlet kinetic energy of turbulence, k, is calculated from the relation using assumed turbulence intensity:

$$k_{inlet} = \frac{1}{2} I \left(U^2 + V^2 + W^2 \right) \qquad (3.52)$$

where I is the intensity which is assumed to be 0.1, following Rizvi [1985], Visser [1991] and Levy [1991]. The rate of dissipation of the kinetic energy, ε, is estimated as:

$$\varepsilon = \frac{k^{\frac{3}{2}}}{l} \qquad (3.53)$$

where l is a characteristic length scale.

Following Rizvi [1985], the initial velocities and temperature for the particles are taken to be those of the carrier stream as the predictions are found to be fairly insensitive to the particle inlet conditions. Sixteen representative particles are tracked, of four different sizes from four starting locations.

For the radiation calculations, the inlets are considered to be perfectly black sinks of temperature equal to those of the inlet gas temperature.

3.6.2 Exit Boundary Conditions

The variables at the exit plane are deduced assuming zero axial gradient at the exit, namely $\frac{\partial \phi}{\partial x} = 0$

The choice of the plane should be far enough downstream to ensure that these outlet values do not affect the computations due to the assumed parabolic nature of the flow in that plane. Rizvi [1985]. The axial velocity on the exit plane is estimated from the consideration of mass conservation.

3.6.3 Axis of Symmetry

At the centreline, the radial velocity is assigned the value zero. For all the other variables, the convective and diffusive fluxes are set to zero which implies zero gradient in the direction normal to the axis.

3.6.4 The Wall Boundary Condition

The flow in the near-wall regions exhibits levels of low turbulence Reynolds number that a quasi-laminar buffer region is experienced where the assumptions for the eddy viscosity concept no longer apply, Launder and Spalding [1972]. The molecular viscosity influences the production, dissipation and transport of turbulence energy rather than the turbulent viscosity in the modelled equations.

The details of the flow close to the walls are less influential on the overall performance than those close to the axis of symmetry in the applications considered in the present study. Thus the use of a wall function is preferred over the option of incorporating a special turbulence model suitable for the low turbulence levels experienced near the wall. The main assumptions made in the application of the former technique are:

i) the flow in the region near the wall behaves as a one dimensional Couette flow, Schlichting [1968],

ii) in the regions close to the wall the diffusion and convection are neglected, Hinze [1975], and the generation of turbulence is balanced by the dissipation rate.

Schlichting [1968] defined the normal-distance Reynolds number, y^+ as:

$$y^+ = \frac{\rho U_\tau y}{\mu} \tag{3.54}$$

where y is the normal distance from the wall, U_τ the friction velocity obtained from:

$$U_\tau = \frac{\sqrt{\tau_w}}{\rho} \tag{3.55}$$

Thus the velocity component U parallel to the wall at the first interior node close to the wall is obtained according to the value of the local normal-distance Reynolds number as follows:

$$\frac{U}{U_\tau} = U^+ = \begin{cases} y^+ & \text{for} \quad y^+ \le 11.63 \\ \frac{1}{\kappa}\ln(Ey^+) & \text{for} \quad y^+ > 11.63 \end{cases} \tag{3.56}$$

where $\kappa = 0.4187 \equiv$ Von Karman constant

$E = 9.793 \equiv$ f(roughness, shear stress variations)

The values of shear stress near the walls may be obtained from the Couette flow wall functions proposed by Launder and Spalding [1974]

$$\tau_w = \frac{\rho\kappa C_\mu^{\frac{1}{4}} k^{\frac{1}{2}} U}{\ln(Ey^+)} \tag{3.57}$$

The turbulence energy at the same node can be expressed as:

$$k = C_\mu^{-\frac{1}{2}} \frac{\tau_w}{\rho} \tag{3.58}$$

The rate of dissipation, ε, is obtained by balancing the generation and the dissipation of the turbulence energy, see Salooja [1978], Rizvi [1985] and Levy [1991.

$$\varepsilon = \frac{C_\mu^{\frac{3}{4}} k^{\frac{3}{2}}}{\kappa y} \tag{3.59}$$

Eqs. (3.58) and (3.59) are used to obtain source term expressions for the boundary cells for the solution of the equations for k and ε, see Gosman and Ideriah [1976].

The incorporation of wall boundary conditions for scalar variables like enthalpy can be expressed through representing the heat flux to the wall, q, in the form:

$$q = \frac{\rho U_\tau (h_p - h_w)}{\sigma_{h,t}(U^+ + P)} \tag{3.60}$$

where P_j is a parameter which depend on the ratio of the laminar to the turbulent Prandtl numbers, see Sahooja [1978].

3.6.5 The Quarl Boundary Condition

The quarl is represented by a sequence of steps, with vertical and horizontal segments, for the purposes of imposing boundary conditions within the framework of a rectilinear computational mesh.

3.7 THE PARTICULATE PHASE

The flow/particle interaction may be handled in either Eulerian or Lagrangian fashions. Abbas et al [1981] compared the performance of both methods and concluded that the latter is more economical in both memory space and computational time requirements. The authors also emphasised the ease of applying physical laws to the particulate phase in case of the Lagrangian method. The method used in the present study follows Lockwood et al [1980],Abbas et al [1981] and Lockwood et al [1986]. It involves the incorporation of the Particle Source In Cell technique originally proposed by Migdal and Agosta [1967]. In this method, representative particles are tracked through the same grid cells used for the gas phase conservation equations. At the inlet the representative particle sizes and starting locations are specified. The inlet velocity assigned to the particles is that of the carrier gas. The particle travels through the computational domain controlled by its momentum equation (2.50).

There are two possible options regarding the diameters of the particles. The first is to assume that they remain relatively constant,with the density varying until breakup or complete burnout of the fuel. Alternatively, the particle may be perceived to react mostly on the surface and thus burn out at a near constant density as a shrinking particle. The physical observations suggest that the particles undergo swelling during devolatilisation, Anthony and Howard [1976] and Jamaluddin et al [1986]. The swelling factor differs according to the rank of the coal. As char combustion proceeds, the visual observation of scanning electron micrograph of coal particle samples taken from combustors, Simons and Horton [1978] and Thurgood et al [1979] suggest that the particle diameter remains relatively constant. The average particle diameter increases during devolatilisation has been measured to be of the order of 10 % of the initial diameter for highly volatile bituminous coals, Smith and Simons [1980]. Xieu et al [1981] compared the performance of both models and concluded that the non-shrinking model was more suitable for high reacting chars found in bituminous coals.Thus this option is adopted in this study.

Summary of the particle tracking procedure:

- The clock is allowed to step for an arbitrary time step determined according to the following relationship:

$$\Delta t = \min\left[\frac{\Delta X}{U_p}, \frac{\Delta r}{V_p}\right] \tag{3.61}$$

where ΔX and Δr are the **axial and radial** lengths of the grid cell respectively and Up and Vp the axial and radial components of the particle velocity. As for some locations of interest the time step is reduced to 0.5 or 0.4 the calculated value to achieve better accuracy. The time step is ensured to fall in an arbitrary range ($10^{-7} < \Delta t < 2$).

- The particle velocity is then calculated at the end of the time step by means of integrating the momentum equations (2.37).

- Knowing the velocity components at the beginning and the end of the time step, the location of the particle at the end of the time step, *Z*, is deduced. Tests are made to detect wether the particle is departing from the computational domain via the walls or the inlets. If this is detected the particle is allowed to bounce back correcting both the position and velocity.

- The sectors' boundaries of the scalar, U and V-cells, a particle crosses between *A* and *Z* are identified in order to divide the sources according to the time sub-steps for every boundary intersection with the particle trajectory as shown in Fig. (3.5).

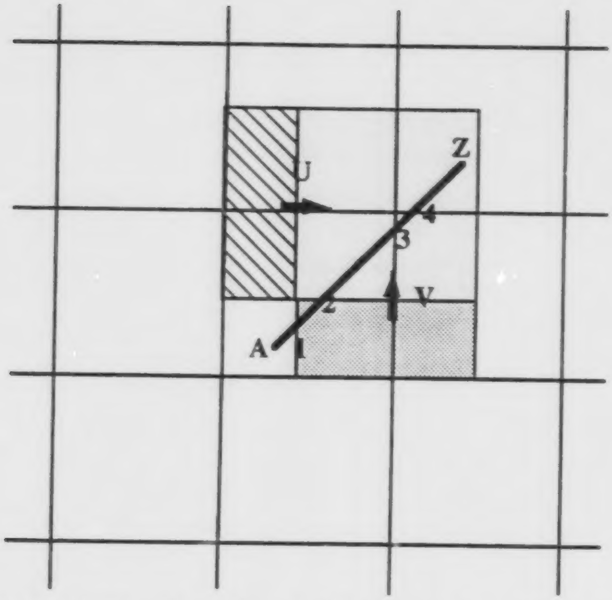

Fig.3.6 The particle trajectory for a time step between A and Z showing intersections with the boundaries of the cells

* The particle temperature is then calculated using Eq.(2.43) as permitting the devolatilisation and combustion and the sources generated during the time step to be calculated.

* The above steps are repeated from the entry of the particle to the computational domain until its exit or its full burnout.

* The above steps are repeated for all the starting locations and particle sizes.

* The commulative phase interaction source terms, $S_{P,\Phi}$ are evaluated and appended to the general finite volume equation (3.26).

Table 3.1

Gas and Particulate components of source terms for the solved equations

Equation	Gas Source	Particle Source
U-momentum	$\frac{1}{r}\frac{\partial}{\partial r}\left(r \cdot \mu_{eff}\frac{\partial V}{\partial x}\right) + \frac{\partial}{\partial x}\left(\mu_{eff}\frac{\partial U}{\partial x}\right) - \frac{\partial}{\partial x}\left(P + \frac{2}{3}\rho k\right)$	$\sum_N\sum_L\sum_M - \left\{\left\langle (\dot{m}_p U_p)_Z - (\dot{m}_p U_p)_A \right\rangle \frac{\delta t}{\Delta t}\right\}_M {}_{L,N}$
V-momentum	$\frac{1}{r}\frac{\partial}{\partial r}\left(r \cdot \mu_{eff}\frac{\partial V}{\partial r}\right) + \frac{\partial}{\partial x}\left(\mu_{eff}\frac{\partial U}{\partial r}\right) - \frac{\partial}{\partial r}\left(P + \frac{2}{3}\rho k\right)$ $- 2\mu_{eff}\frac{V}{r^2} + \frac{\rho W^2}{r}$	$\sum_N\sum_L\sum_M - \left\{\left\langle (\dot{m}_p V_p)_Z - (\dot{m}_p V_p)_A \right\rangle \frac{\delta t}{\Delta t}\right\}_M {}_{L,N}$
W-equation	$- W\left(\frac{\mu_{eff}}{r^2} + \frac{\rho V}{r} + \frac{1}{r}\frac{\partial \mu_{eff}}{\partial r}\right)$	$\sum_N\sum_L\sum_M - \left\{\left\langle (\dot{m}_p W_p)_Z - (\dot{m}_p W_p)_A \right\rangle \frac{\delta t}{\Delta t}\right\}_M {}_{L,N}$
k-equation	$G - \rho\,\varepsilon$	0
ε-equation	$(C_1 G - C_2 \rho\varepsilon)\frac{\varepsilon}{k}$	0
Enthalpy	$R_{fu} H_v + 4\sigma K_g\left(T_R^4 - T_g^4\right)$	$S_{p,h1} + S_{p,h2}$
Oxygen	$- R_{fu} S_v$	$- \frac{32}{12}\eta S_P^M$
Volatiles	$- R_{fu}$	$(1 - \eta) S_P^M$
Products	$- R_{fu} P_v$	$\frac{44}{12}\eta S_P^M$
Radiation	$- 4\sigma K_g\left(T_R^4 - T_g^4\right)$	$- \vartheta_P \sum_N\sum_L\sum_M \left\{\frac{n \cdot \pi \cdot d^2}{4\vartheta_P}\varepsilon_P\left(T_R^4 - T_P^4\right)\delta_{A,z}\right\}$

CHAPTER 4

EXPERIMENTAL FURNACES AND TEST CONDITIONS

4.1 INTRODUCTION

In this chapter the experimental furnaces and the test conditions used for the validation studies will be described. A considerable effort has been devoted to the selection of experimental data in order to ensure a systematic study. The presence of experimental facilities and ongoing programme in the same group was exploited in designing several experiments for specific purposes of the present study. The validation procedure was accomplished [illegible] stages.

The first stage was to assess the isothermal part of the model through comparison with velocity data for a non-reacting cold flow. The velocity measurements, Hughes [1987], for both the axial and tangential components, were obtained by means of a five hole Pitot probe in the CCRL tunnel furnace for different inlet conditions. Eleven different cases were predicted and compared with the data.

The second stage comprised an overall assessment of the code performance under firing conditions. The combustion data were obtained from the CCRL furnace and do not include near burner region (NBR) measurements. Seven combustion cases were predicted. This stage offered the advantage of isolating to an extent the interdependence of the momentum with the combustion models since the former is being assessed separtely in the previous stage giving a better opportunity to validate the latter.

In the third stage the model performance in the NBR, which is crucial for combustion efficiency, stability and pollutant emissions, was investigated. The validation of this stage was aimed at providing reasonably detailed assessment of the devolatilisation model and the ignition mechanism, a process which takes place very close to the burner for stabilised and so safe combustion. Such information was missing in the preceding stage where almost all the radial profiles for gas temperature and species were reported to indicate the termination of the flame. This stage dealt with data obtained for flow type 2 measurements, Roberts [1985], for a single annular orifice burner and swirling secondary air. This condition allows for the presence of an attached internal recirculation zone, (IRZ). This stage involved easy determination of the near burner aerodynamic features, thus obviating the complexity of explaining the source of discrepancies between measurements and predictions, whether they resulted from inaccurate aerodynamic features or difficiences in the combustion models. Two cases of this type were predicted, the first of which, related to measurements from the IFRF furnace reported in Phelan et al [1985] whilst the second used measurements from ICSTM furnace reported in Abbas et al [1991]. The use of data from the two different furnaces ensured that the model was free from any case dependency and the size difference between the two furnaces allowed for the detection of the effect of different particle residence times in the NBR.

The fourth stage was the validation of the performance of the model for the NBR using experimental data obtained for flow type 3 measurements, Roberts [1985] for a single central orifice burner with swirling secondary air. Although the third stage gave a closer simulation of industrial burners with the bluff body representing the burner gun used for ignition, it transpired that this stage was the most testing exercise for the model. The most prominent aerodynamic feature of this flow type is the presence of an IRZ partially penetrated by the primary flow. The accuracy with which the extent of the penetration is determined is a measure of the performance of the turbulence model under reacting conditions. Three cases from ICSTM reported by Costa et al [1990] and Abbas et al [1991] were used for comparison at this stage.

4.2 THE FURNACES

The following section provides a description of the configurations of the three furnaces, together with the relevant test conditions.

4.2.1 CCRL Furnace

The CCRL furnace is cylindrical and horizontally orientated, 1.0 m in diameter, and 5.0 m in length, fired along its axis by industry type swirl burners. The CCRL combustor geometry is sketched in Fig. (4.1). The initial 0.75 m of the furnace is lined with a refractory wall to allow for radiative exchange which enhances the devolatilisation of the coal. The remaining 4.22 m of the furnace is surrounded by a cooled wall to simulate the thermal loading.

The burner used has a moving block type swirl generator which is connected to a divergent quarl. The primary air carries the pulverised coal to the furnace through a central pipe of 0.0953 m. diameter. Three different burner geometries were used. The schematic diagrams are given in Fig (4.2).

4.2.2 The ICSTM Furnace

The ICSTM furnace is cylindrical and vertically orientated, 0.6 m in diameter and 3.0m in length and down-fired along its axis by industry type swirl burners. The burners used for the studied flames consist of two concentric nozzles, with and without a central bluff body, connected to a divergent refractory quarl. The furnace roof and the initial 1.5 m of the cylindrical walls are refractory lined. The remaining wall surfaces are water cooled only. The furnace details are shown in Fig. 4.3 and the two burners, namely the Single Central Orifice (SCO) and the Single Annular Orifice (SAO) are given in Fig. (4.4). Full details of the furnace and its instrumentation may be found in Mostafa [1989].

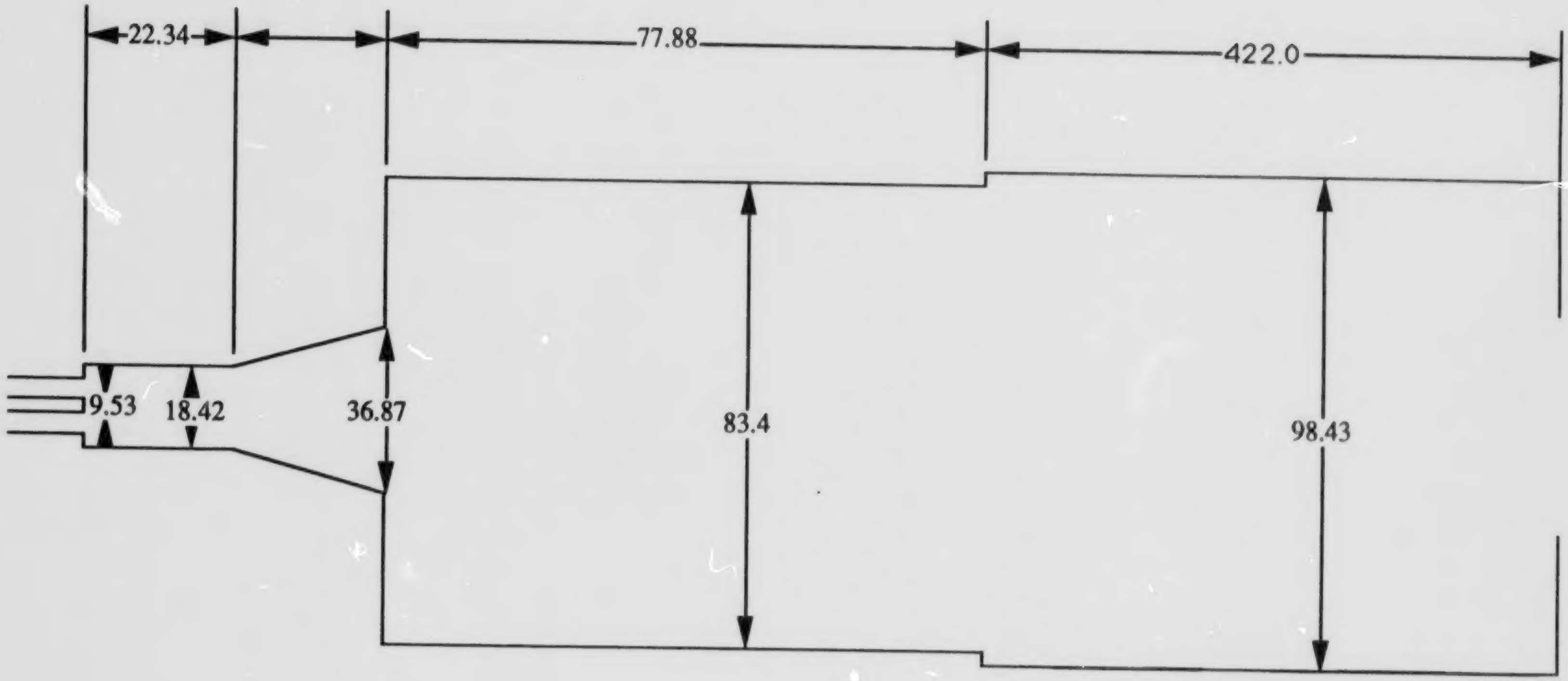
22.34
77.88
422.0
9.53
18.42
36.87
83.4
98.43

Figure 4.1 Schematic of the interior of the CANMETtunnel furnace, distances in cm.

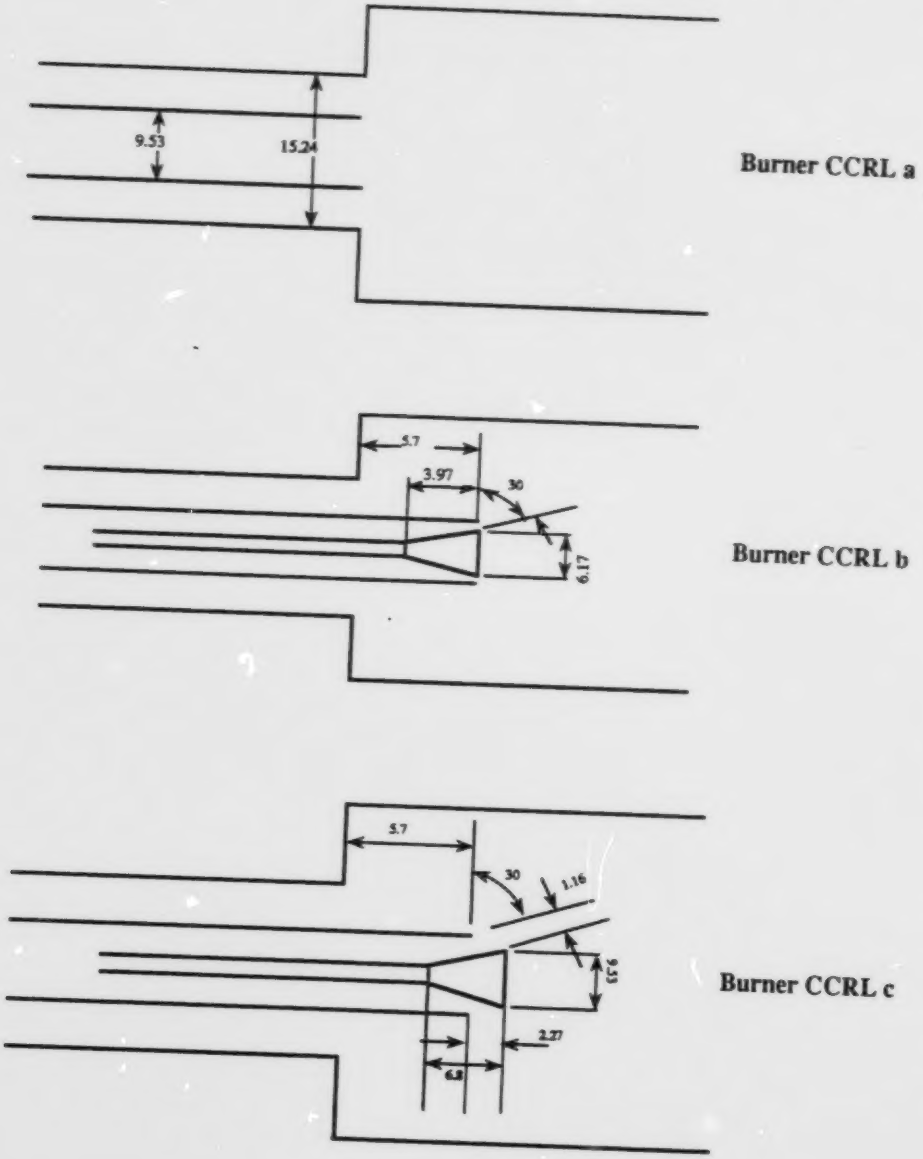
9.53
15.24
Burner CCRL a
5.7
3.97
30
6.17
Burner CCRL b
5.7
30
1.16
9.53
2.27
6.8
Burner CCRL c

Figure 4.2 Schematic diagram of the burner geometries used for the CCRL furnace, distances in cm.

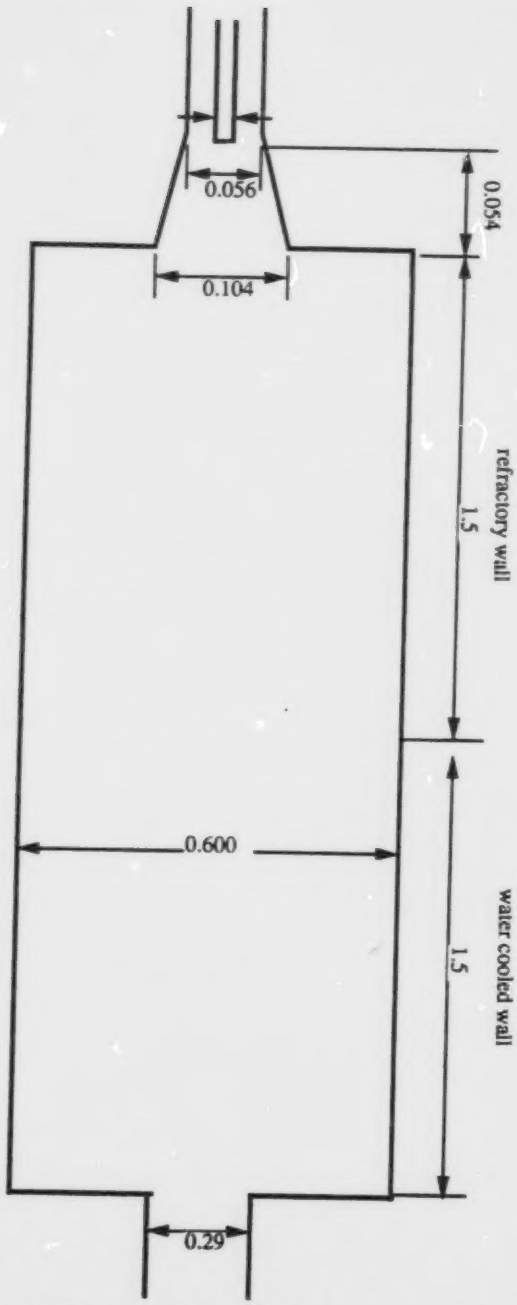
0.056
0.104
0.054
refractory wall
1.5
0.600
water cooled wall
1.5
0.29

Figure 4.3 Schematic of the interior of the ICSTM furnace, distances in mm.

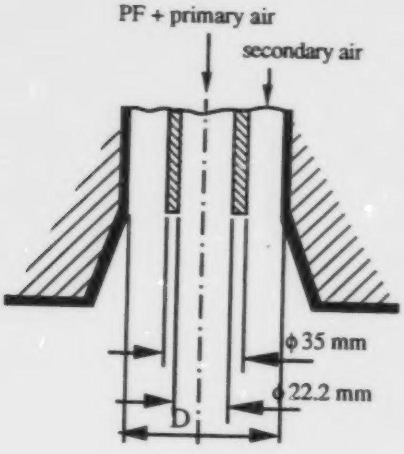
PF + primary air
secondary air
ϕ 35 mm
ϕ 22.2 mm
D

SCO Burner

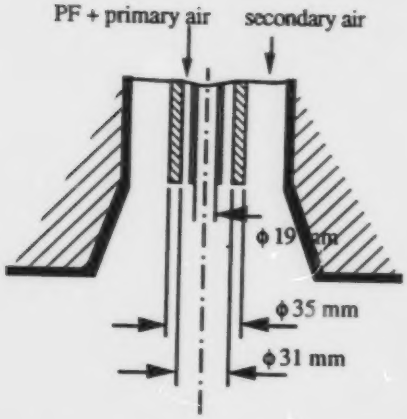
PF + primary air
secondary air
ϕ 19 mm
ϕ 35 mm
ϕ 31 mm

SAO Burner

Figure 4.4 Schematich diagram of the ICSTM Burners

4.2.3 The IFRF Furnace

The IFRF No. 1 furnace is a horizontal square section, 2x2 m and 6 m long, fired by the double concentric swirl burner, shown in Fig (4.5). It has a central bluff body and a divergent quarl. The furnace is refractory lined and fitted with a series of tubular cooling coils.

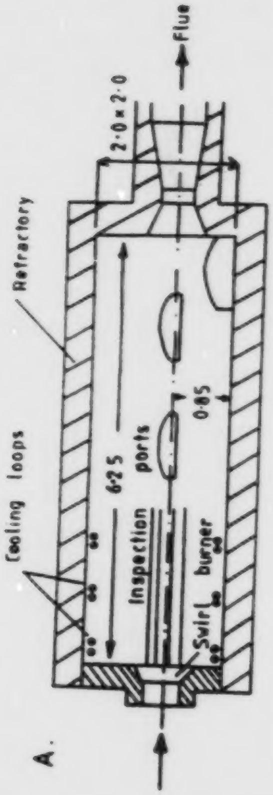

Figure 4.5 Schematic diagram of the IFRF furnace

4.3 TEST CONDITIONS

4.3.1 Isothermal Runs

Hughes [1987] measured the velocity in the CCRL furnace using a five hole pitot tube. The inlet velocity profile of the gases at the entrance of the furnace was measured. Two sets of inlet mass flow rates were used. The high flow rate case had 740 kg/hr and 2000 kg/hr for the primary and secondary inlets respectively. The low mass flow rates experiments which used 164.5 kg/hr and 444.6 kg/hr for primary and secondary streams, did not allow measurements to be taken after the quarl exit since they were below the measurable threshold of the pitot probe. Table 4.1 gives the inlet conditions for the Cases.i-1 to i-11. In this table the swirl is defined as a swirl setting. The inlet velocity profiles are given in Hughes [1987] where the swirl numbers are deduced. The swirl which was applied to the secondary stream was increased gradually for the seven cases that involved the high flow rates and the four cases that involved the low flow rates.

Table 4.1

Operating Conditions for Isothermal Cases in the CCRL Furnace

(Stage i)

CASE NO	m_p kg/hr	T_p (°C)	m_s kg/hr	T_s (°C)	swirl setting
i-1	740	45	2000	34	4.5
i-2	740	48	2000	37	4.0
i-3	740	48	2000	36	3.0
i-4	740	45	2000	30	2.0
i-5	740	46	2000	32	1.0
i-6	740	51	2000	39	0.5
i-7	740	50	2000	38	0.0
i-8	164.5	60	444.6	32	0.5
i-9	164.5	62	444.6	32	2.0
i-10	164.5	59	444.6	31	4.0
i-11	164.5	60	444.6	32	4.5

4.3.2 CCRL Combustion Runs

The seven combustion runs that were effected by Hughes [1987] in the CCRL furnace incorporated two types of coal having different volatile contents. The proximate and ultimate analyses of these coals are given in Table 4.2. For the runs using the high

Table 4.2

Coal Characteristics for the Combustion Cases in the CCRL Furnace (Stage ii)

Property	Coal No. 1	Coal No. 2
Proximate analysis (dry basis, %)		
Volatiles	34.59	21.32
Fixed Carbon	54.31	63.16
Ash	11.1	15.52
Ultimate analysis (%)		
Carbon	68.77	73.6
Hydrogen	3.79	3.92
Nitrogen	0.93	1.2
Sulphur	0.26	0.28
Oxygen	15.15	5.48
Calorific value, MJ/kg	26.7	29.12

volatile coal, namely Case ii-1, ii-2 and ii-3 the burner was a central pipe of diameter 0.0953 m in which the coal was transported by the stream of primary air (Burner CCRL a in Fig. (4.2)). The low volatile content of the other coal necessitated the use of a central bluff body for the purpose of enhancing the central recirculation zone and deflecting the coal particles into the swirling secondary air, (Burner CCRL b in Fig. (4.2)).These are Cases ii-4 and ii-5. The last two runs involved the usage of the high volatile coal and the bluff body burner (Burner CCRL c in Fig.(4.2)). The inlet primary and secondary flow rates and temperature, the swirl settings and the coal flow rates are given in Table 4.3. The inlet velocity profiles are deduced from cold flow

Table 4.3

Operating conditions for the CCRL combustion cases (stage ii)

Operating Conditions	Case						
	ii-1	ii-2	ii-3	ii-4	ii-5	ii-6	ii-7
Burner	CCRL a	CCRL a	CCRL a	CCRL b	CCRL b	CCRL c	CCRL c
Coal no.	1	1	1	2	2	1	1
Coal flow rate, kg/hr	50.64	50.50	53.80	61.60	57.0	59.7	61.2
Primary air flow rate, kg/hr	347.66	368.63	431.99	313.92	403.02	458.38	487.94
Secondary air flow rate, kg/hr	187.76	184.77	179.89	574.45	424.93	342.06	320.54
Primary air temperature, ^{o}C	99.99	89.7	84.0	96.0	94.0	98.0	88.0
Secondary air temperature, ^{o}C	122.53	116.5	122.0	136.0	153.0	138.0	135.0
Swirl setting	0.0	3.0	1.0	3.0	4.5	3.0	4.5

measurements for the corresponding swirl setting. No information was given for the inlet turbulence intensities and dissipation rates.

4.3.3 Near Burner Runs for Flow Type 2

Two cases were validated for this stage. The first was obtained in the No. 1 furnace of the IFRF. The properties of the high volatile coal (Scotts Branch) used are given in Table 4.4 while the operating conditions are given in Table 4.5. The velocity profiles and turbulence levels at the burner throat were estimated from the flow produced by the movable block swirl generator used at the IFRF. Turbulence intensities were typically 20%.

The data of the other case was obtained from the ICSTM furnace. The burner geometry is shown in Fig. 4.4. A very small amount of air (0.7% of the total air) was ejected through the centre to prevent recirculating particles from sticking at the burner wall. The properties of the Gedling coal used for this case are presented in Table 4.6 and the run conditions are given by Table 4.7.

4.3.4 Near Burner Runs for Flow Type 3

Three data sets have been obtained in the ICSTM furnace for the SCO burner shown in Fig. 4.4. Cases iv-1 and iv-2 used the Gedling coal while case iv-3 involved the low volatile Oakdale coal whose properties are given in Table 4.4. The conditions of the three runs are presented in Table 4.6.

Table 4.4

Coal Properties for the IFRF and ICSTM Cases

(Stages iii and iv)

	Coal		
Property	**Scotts Branch**	**Gedling**	**Oakdale**
Proximate analysis (dry basis, %)			
Volatiles	34.3	38.21	19.27
Fixed Carbon	59.7	57.31	71.45
Ash	6.0	4.48	9.28
Ultimate analysis (%)			
Carbon	81.9	72.6	81.9
Hydrogen	5.3	5.05	4.2
Nitrogen	1.6	1.29	1.32
Sulphur	0.7	1.55	0.57
Oxygen	10.5	15.31	2.81
Ash	6.0	4.48	9.28
Grind			
%under 25 μm	20	40	40
%under 75 μm	71.6	80	80
%under 100 μm	87.1	89	89
Calorific value, MJ/kg	32.7	29.29	33.34

Table 4.5

Operating Conditions for Type 2 Flame Cases

(Stage iii)

Operating Conditions	Case	
	iii-1	iii-2
Furnace	IFRF	ICSTM
Burner	SAO	SAO
Coal	Scotts Branch	Gedling
Coal flow rate, kg/hr	270	14.0
Primary air flow rate, kg/hr	360	31.3
Secondary air flow rate, kg/hr	2750	120.0
Excess air, %	16	15
Primary air temperature, ^{0}C	60	80
Secondary air temperature, ^{0}C	325	300
Secondary air swirl	0.95	1.03

Table 4.6

Operating Conditions for Type 3 Flame Cases

(Stage iv)

Operating Conditions	Case		
	iv-1	iv-2	iv-3
Furnace	ICSTM	ICSTM	ICSTM
Burner	SCO	SCO	SCO
Coal	Gedling	Gedling	Oakdale
Coal flow rate, kg/hr	14.4	16.0	14.4
Primary air flow rate, kg/hr	38.4	31.3	38.4
Secondary air flow rate, kg/hr	139.9	120.0	139.9
Excess air, %	15	15	15
Primary air temperature, ^{o}C	80	80	80
Secondary air temperature, ^{o}C	300	300	300
Secondary air swirl	1.45	1.03	1.45

4.4 PREDICTION PARAMETERS

The coal devolatilisation is simulated by the single reaction model. The heterogeneous char reaction is governed by the external diffusion rate of oxygen to the particle surface and by the chemical reaction presumed to be first order in oxygen partial pressure and to occur entirely at the particle surface.The values of the coal devolatilisation and char reaction kinetic parameters used to predict different cases of the present study are included in Table 4.7.

Table 4.7

Model Constants for the Standard Cases

Kinetic Parameters	*Devolatilisation*	*Char reaction*
Pre-exponential Factor:	8.36x10^{4} s^{-1}	0.86 kg/m^{2}.s.(N/m^{2})
Activation Energy:	7.4x10^{7} J/kg-mol	1.02x10^{8} J/kg-mol

The computations were carried out on a non-uniform 51 x 37 polar cylindrical mesh for the CCRL and ICSTM furnaces and on a mesh of 59 x 42 for the IFRF furnace with the highest concentrations of nodes being in the near burner regions. A first order hybrid differencing scheme was used in both the IFRF and the CCRL cases. In the ICSTM cases and for the solution of the momentum equatios, this was subsequently surplanted by the quadratic upwind scheme.

CHAPTER 5

RESULTS AND DISCUSSION

5.1 INTRODUCTION

The mathematical simulation of the experimental cases given in the previous chapter is presented here. Although the level of quantitative accuracy achieved is not constant across the predicted cases, the model has on the whole been successful in establishing the qualitative and conceptual behaviour. Thus the first part of this chapter will be devoted on giving the predicted features of the cases under consideration followed by the parametric studies performed to improve the quantitative agreement of the calculated values and to assess the relative importance of the physical models of different phenomena.

5.2 ISOTHERMAL CASES (STAGE i)

Isothermal cases have been considered (for the gas phase only) because of their relative simplicity compared to the ambiguities associated with kinetic reactions in combusting flows and the drag/dispersion empiricisms in particle flows. The set of equations to be solved consists of three momentum equations, a continuity equation and transport equations for k and ε.

The aerodynamic and mixing characteristics of the flows in the near burner region (NBR) play an important role in controlling all flame parameters. For example, the strength of the internal recirculation zone (IRZ) which is an entirely aerodynamic phenomenon, is crucial in determining the degree of stability of the flame, Costa et al [1991].

The eleven isothermal cases presented in section 4.3.1 (see Table 4.1) are predictions of the experimental data reported by Hughes [1987]. The computational grid used to represent the furnace geometry totals 51x37 cells with 25x25 cells in the quarl region. The hybrid scheme is adopted for the discretisation of the convective and diffusive terms

Figures 5.1 to 5.11 show the comparison between measurements and predictions for the radial profiles of the mean axial and tangential velocities at different axial locations. The features of the velocity profiles of all the cases are relatively similar owing to the fact that the inlet momentum ratio is maintained the same. The differences in profiles are attributed only to the effect of varying the secondary swirl number between 0 and 1. The overall agreement for the set of cases is believed to be satisfactory.

While setting the inlet conditions for these cases, the sensitivity of the calculations to the assumed inlet k and ε given by Eq. (3.51) and (3.52) was examined. It was observed that the calculations were insensitive to the inlet k while the upstream location of the IRZ was observed to be sensitive to the inlet ε. This is in conformity with the observation of Mahmud et al [1987]. The inlet ε used in the present predictions is three times higher than that given by Eq.(3.52). As for the effect of the inlet radial velocity, the use of zero radial velocity instead of the reported values resulted in shifting the near stagnation point on the axis further downstream while the far stagnation point was not affected.

The quality of the predictions obtained for the high mass flow rate cases is better than those of the low mass flow rate, suggesting that the discrepancies experienced in the latter may be due to higher experimental errors according to Hughes [1987] since pitot measurements are not reliable in regions where the mean velocities are close to zero and the turbulence fluctuations are high.

The main feature of the flow in all the cases consists of an external recirculation zone, ERZ due to the sudden expansion and an IRZ promoted by vortex breakdown. It is clear that the IRZ is induced by the secondary swirl, where the no-swirl cases do not show any IRZ and the aerodynamic features thus are similar to those of a free jet. The qualitative features are well predicted while showing better quantitative agreement for the ERZ implying that the grids are reasonably fine to minimise numerical diffusion brought about by the used hybrid scheme for interpolation. The predicted decay of both the axial and swirl velocities is in agreement with the measurements. The slight discrepancy in identifying the boundary of the IRZ might be due to deficiencies in the k-ε model. However, the degree of agreement achieved is good enough to justify avoiding the inclusion of the complicated and computationally expensive Reynolds stress model. This appears to be in conflict with the conclusions of Weber et al [1986] who demonstrated the inability of the k-ε model to simulate essential features of the IRZ but, of course, definitive conclusions are hindered by the significant differences in flow configuration; for instance Weber et al's [1986] geometry has no sudden expansion at the quarl exit, and hence the flow pattern is different from that studied here.

The deficiency of the k-ε model as discussed in section 2.5 would imply poorer agreement when the swirl number is increased as for example the case in Khalil et al [1975]. On the contrary, the figures show that relatively better agreement is achieved at the higher swirl runs. This is hard to interpret but may be due to experimental errors in the reported experimental results by Hughes [1987] particularly when one notices that the data indicate non-zero values for the tangential velocity at the axis indicative of some lack of symmetry in the experimental flow.

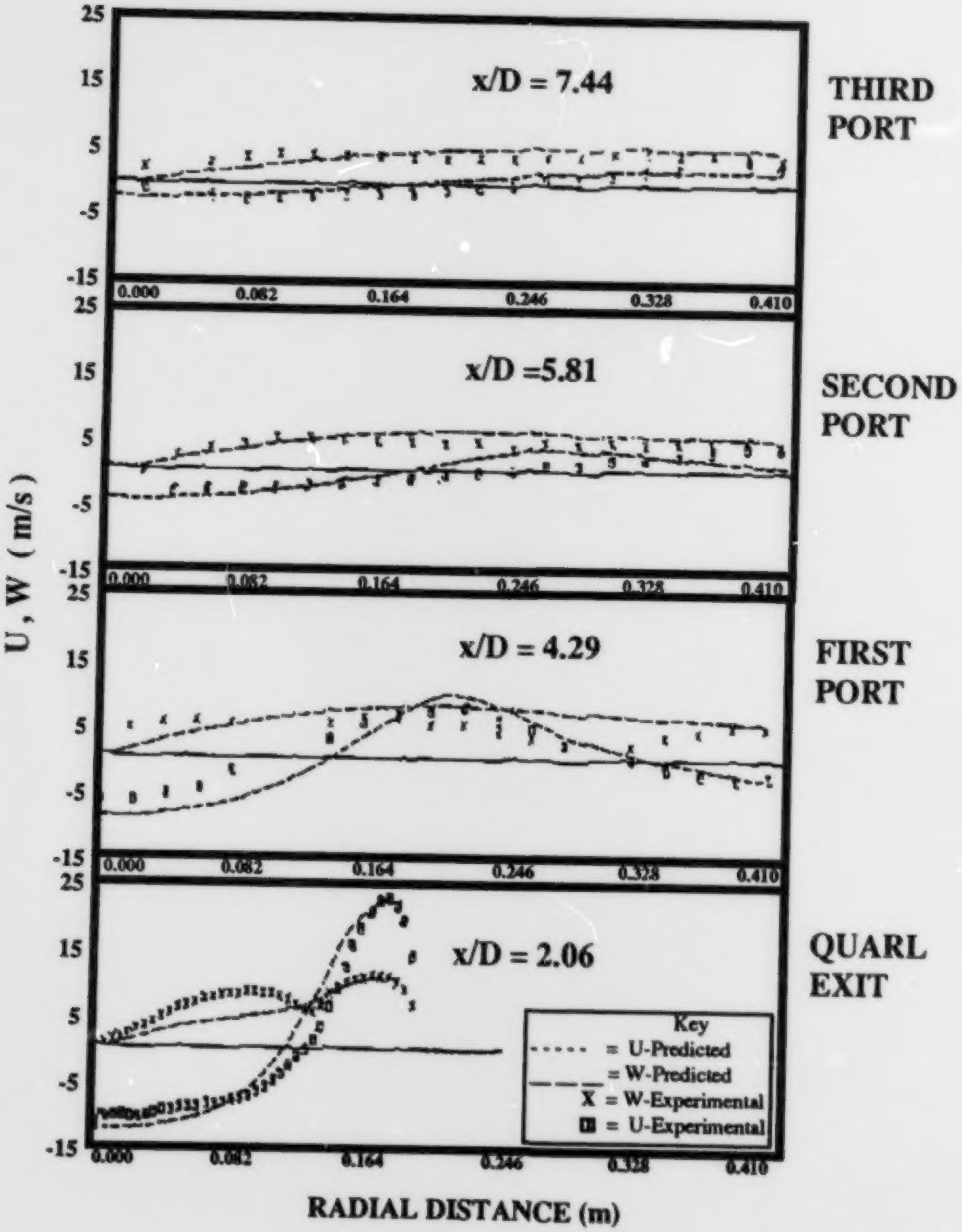

Figure 5.1 Comparison between measurements and predictions for the radial profiles of the mean axial and tangential velocities for Case i-1 at quarl exit (x/D = 2.06), first port (x/D = 4.29), second port (x/D = 5.81) and third port (x/D = 7.44).

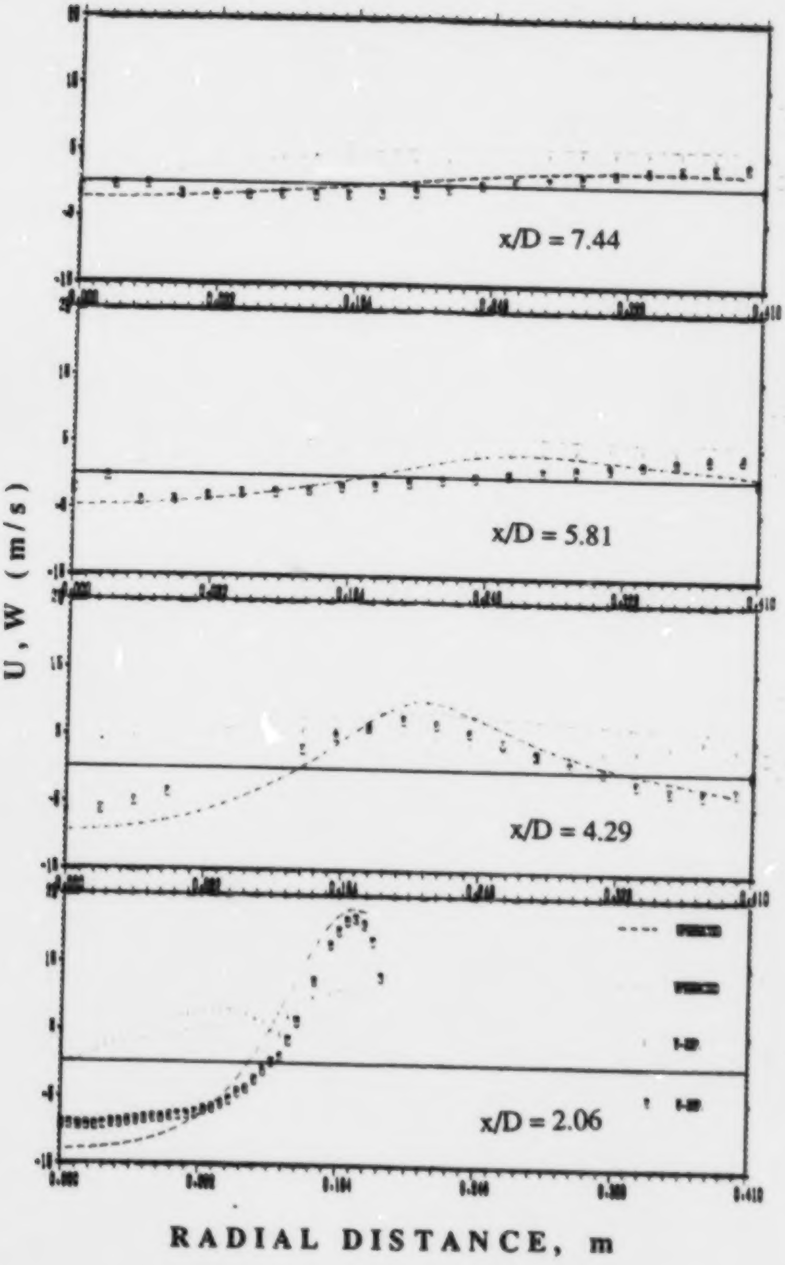

Figure 5.2 Comparison between measurements and predictions for the radial profiles of the mean axial and tangential velocities for case i-2 at quarl exit (x/D = 2.06), first port (x/D = 4.29), second port (x/D = 5.81) and third port (x/D = 7.44).

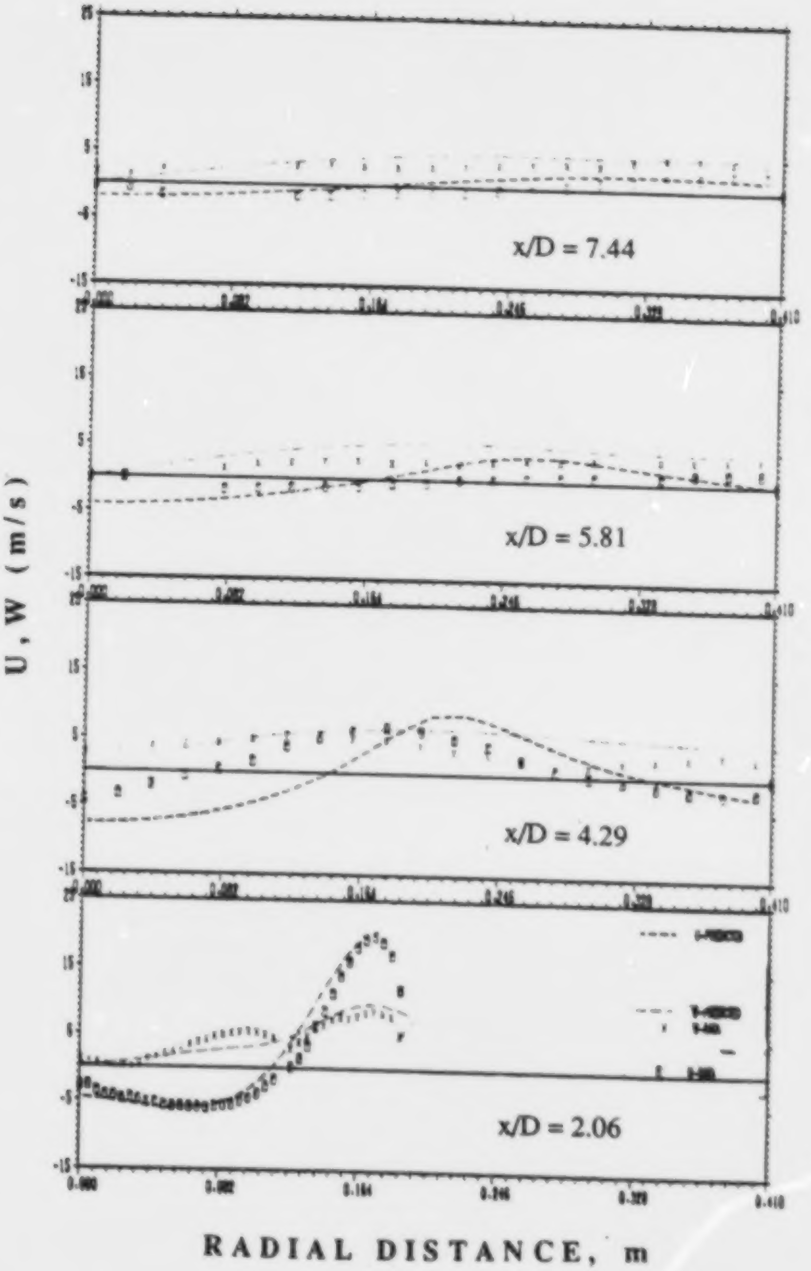

Figure 5.3 Comparison between measurements and predictions for the radial profiles of the mean axial and tangential velocities for case i-3 at quarl exit (x/D = 2.06), first port (x/D = 4.29), second port (x/D = 5.81) and third port (x/D = 7.44).

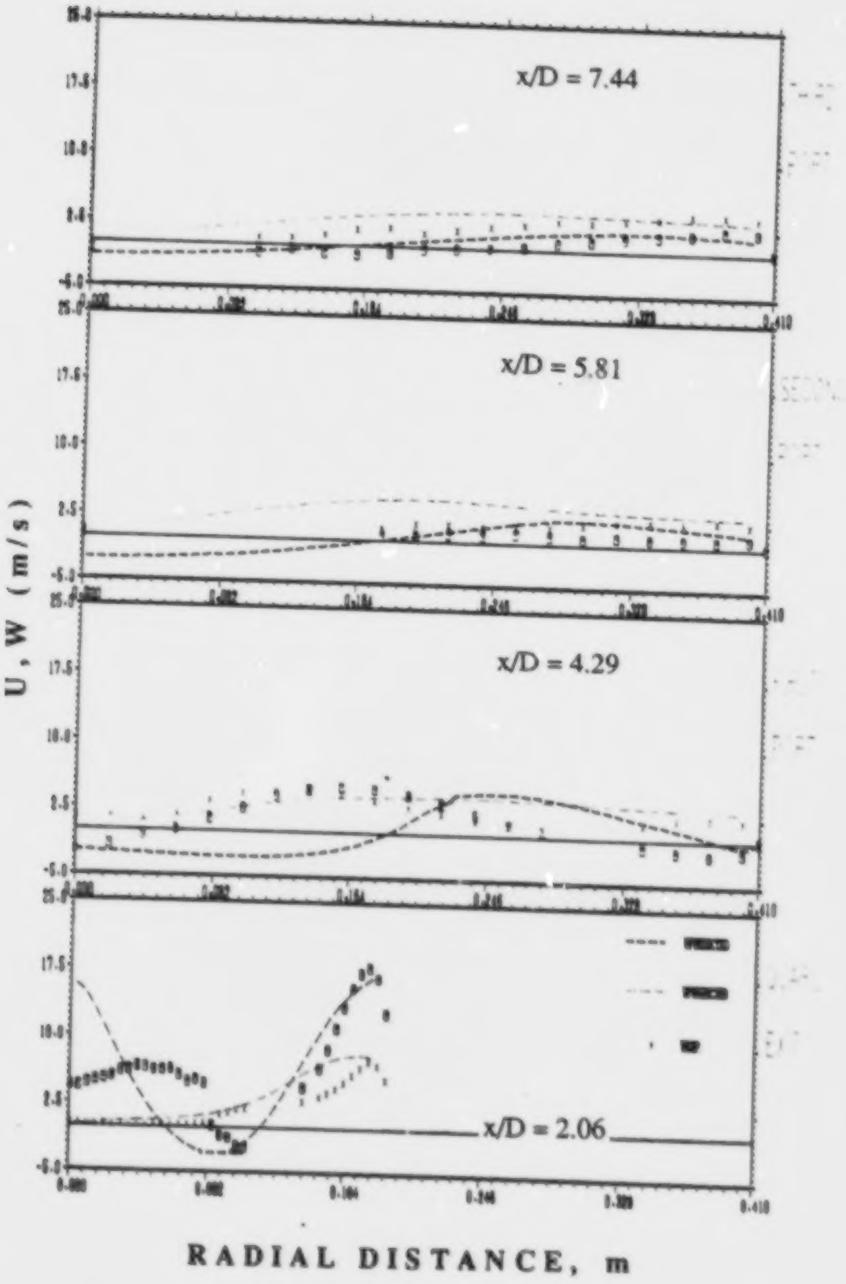

Figure 5.4 Comparison between measurements and predictions for the radial profiles of the mean axial and tangential velocities for case i-4 at quarl exit (x/D = 2 06), first port (x/D = 4.29), second port (x/D = 5.81) and third port (x/D = 7.44).

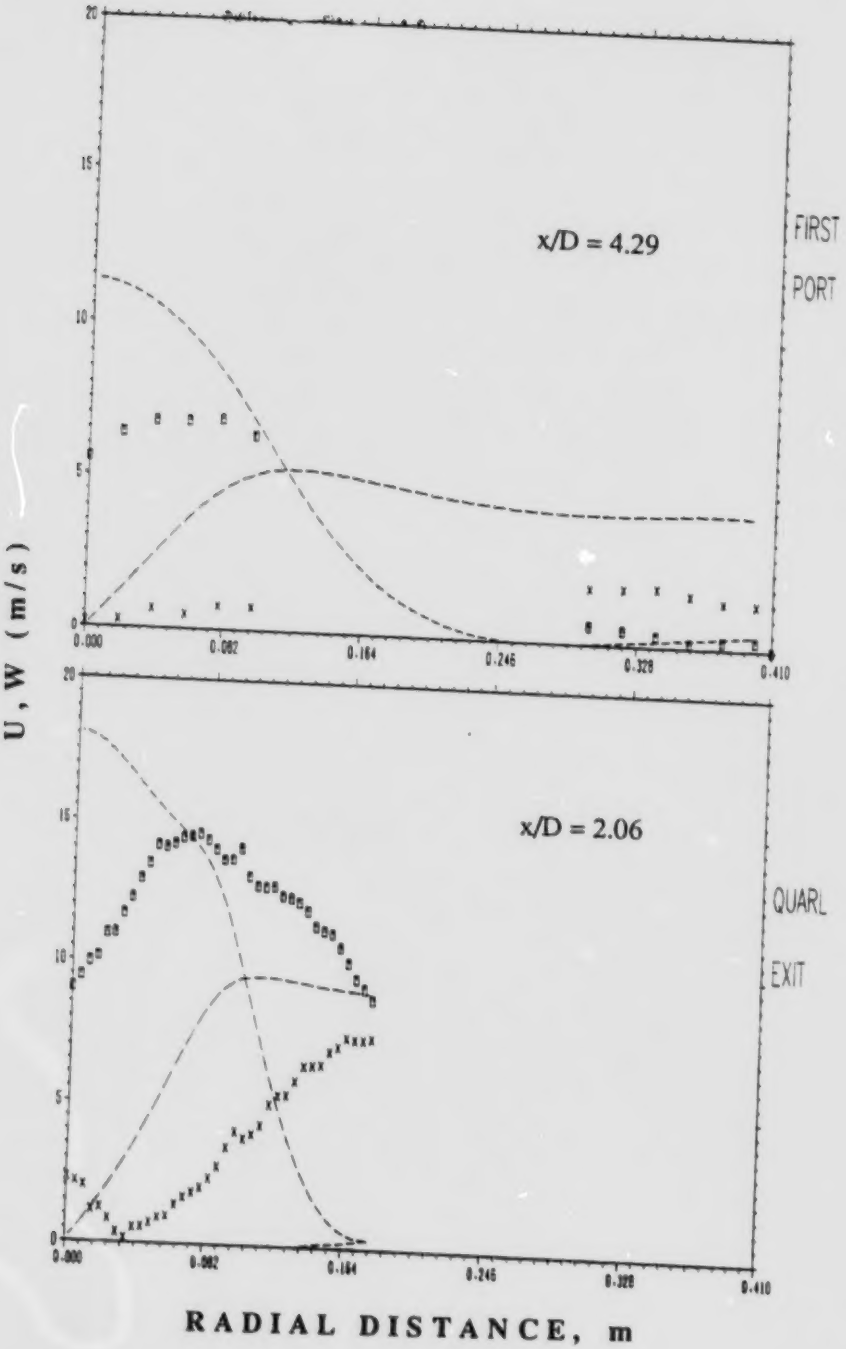

Figure 5.5 Comparison between measurements and predictions for the radial profiles of the mean axial and tangential velocities for case i-5 at quarl exit (x/D = 2.06), first port (x/D = 4.29).

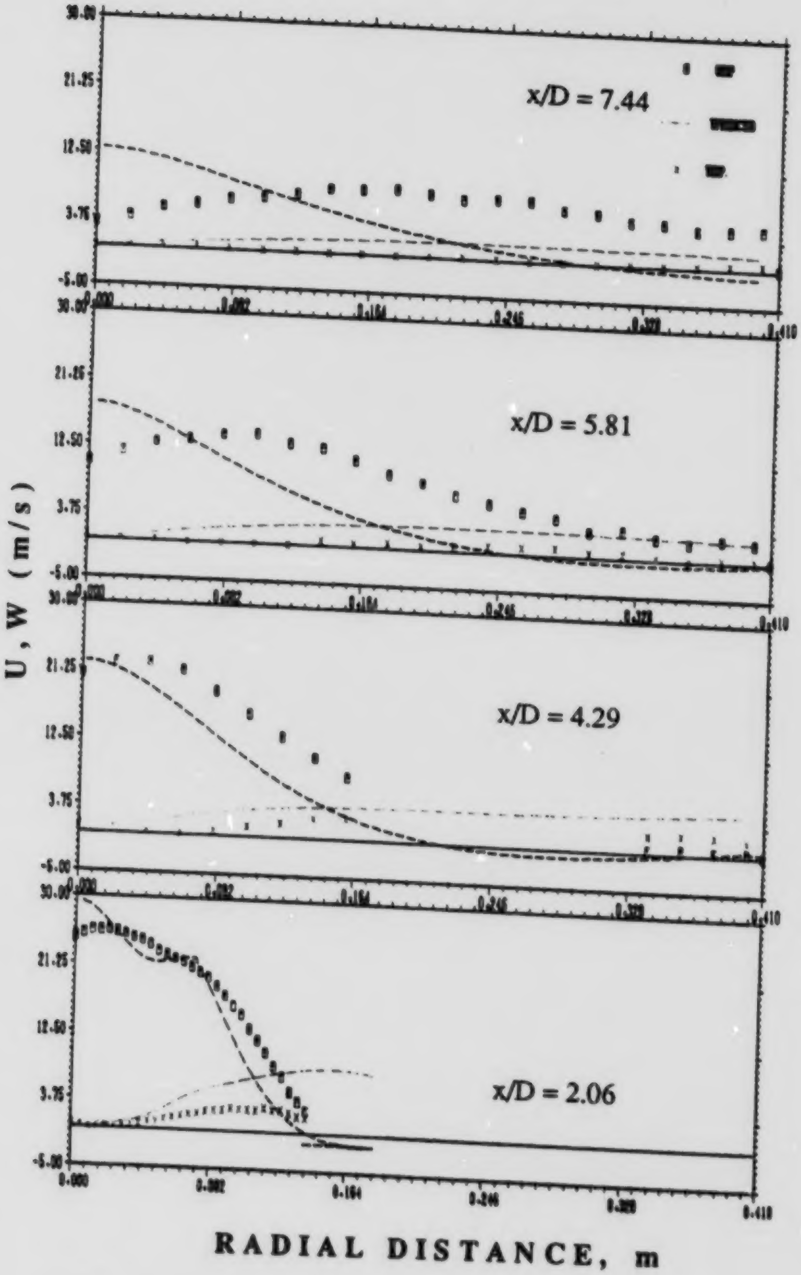

Figure 5.6 Comparison between measurements and predictions for the radial profiles of the mean axial and tangential velocities for case i-6 at quarl exit (x/D = 2.06), first port (x/D = 4.29), second port (x/D = 5.81) and third port (x/D = 7.44).

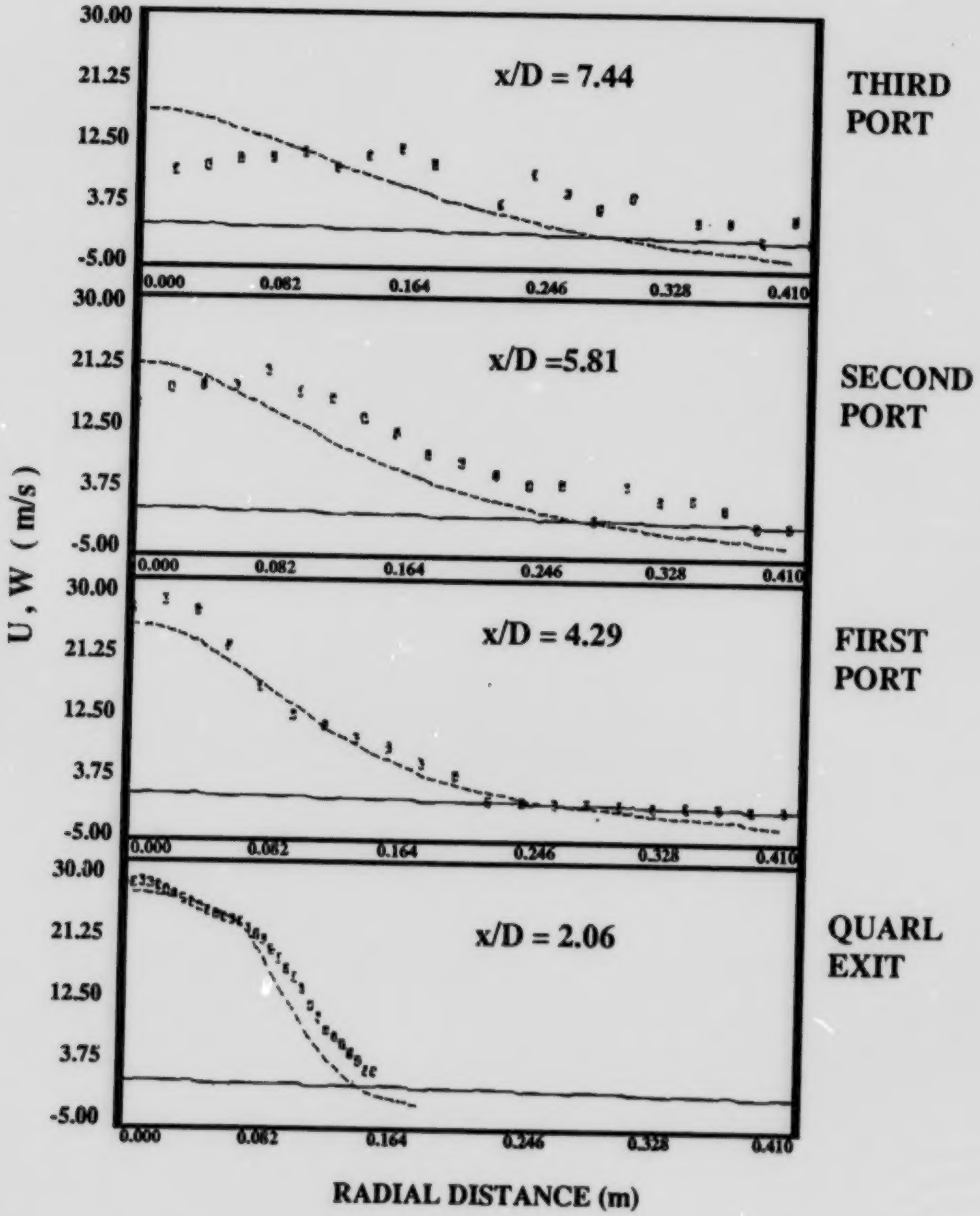

Figure 5.7 Comparison between measurements and predictions for the radial profiles of the mean axial and tangential velocities for Case i-7 at quarl exit (x/D = 2.06), first port (x/D = 4.29), second port (x/D = 5.81) and third port (x/D = 7.44).

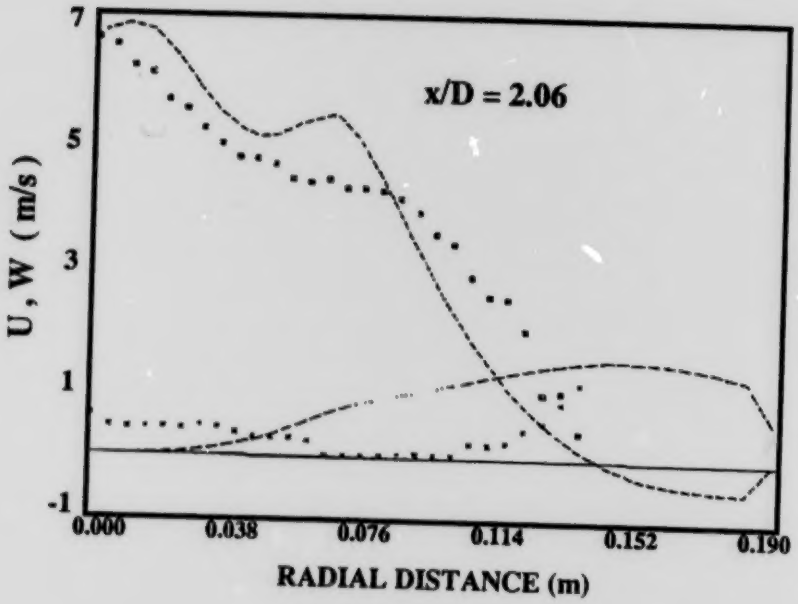

Figure 5.8 Comparison between measurements and predictions for the radial profiles of the mean axial and tangential velocities for Case i-8 at quarl exit (x/D = 2.06).

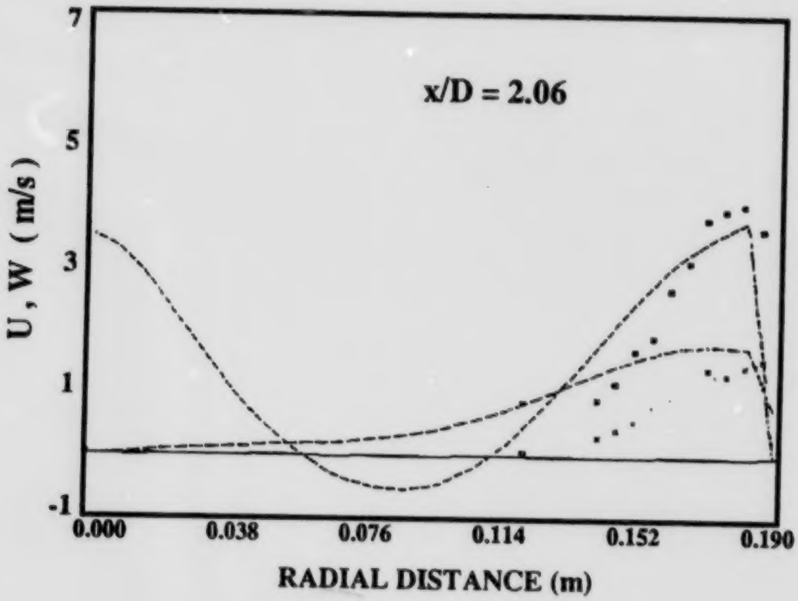

Figure 5.9 Comparison between measurements and predictions for the radial profiles of the mean axial and tangential velocities for Case i-9 at quarl exit (x/D = 2.06).

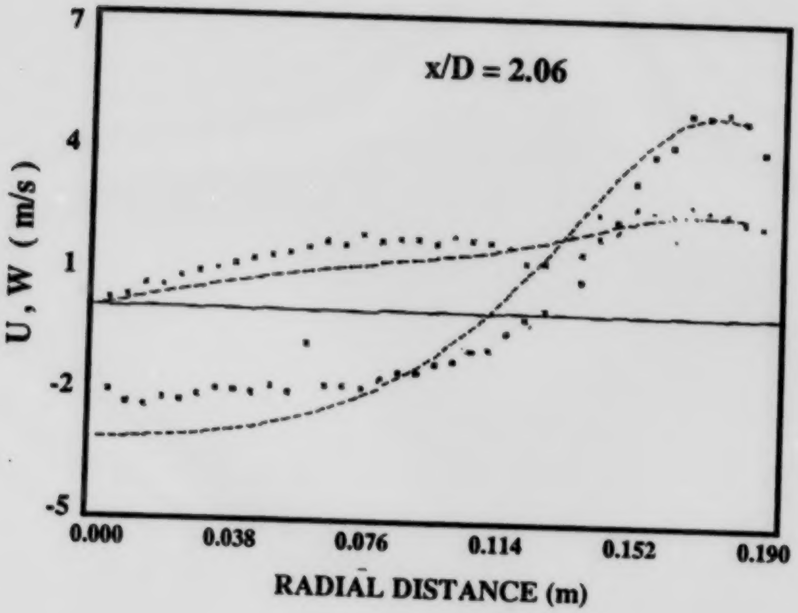

Figure 5.10 Comparison between measurements and predictions for the radial profiles of the mean axial and tangential velocities for Case i-10 at quarl exit (x/D = 2.06).

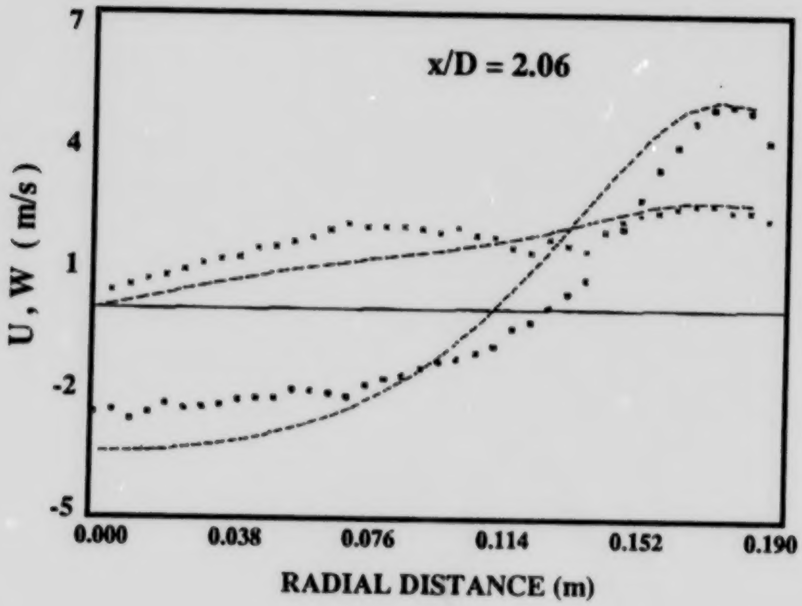

Figure 5.11 Comparison between measurements and predictions for the radial profiles of the mean axial and tangential velocities for Case i-11 at quarl exit (x/D = 2.06).

5.3 COMBUSTION CASES FOR CCRL FURNACE (STAGE ii)

The seven combustion cases for the CCRL furnace presented in section 4.3.2 were predicted using similar grid to that incorporated for the isothermal cases with necessary modifications in the radial direction for runs ii-4 to ii-7 to account for the presence of the bluff body. As the measurements were divided into two groups according to the burner design one case was selected of each, namely Case ii-2 and ii-4, for performing sensitivity tests to optomise the model constants. Both cases showed qualitative change in the predictions when a scaled down velocity profile from the isothermal flow measurements was used instead of a uniform profile. Thus a scaled down velocity profile was obtained from the isothermal data for the remaining cases at respective levels of swirl. The predictions for the cases presented in this stage are displayed in Figs. 5.12 to 5.18.

Figure 5.13.a shows the contours of the stream function, temperature and oxygen concentration for Case ii-2 while Fig. 5.13.b shows the axial distributions of temperature, oxygen concentration and burnout. It is evident from the stream function contours that the flow pattern does not exhibit an IRZ due to the large momentum ratio and only exhibits a large ERZ established downstream the quarl wall. As a consequence of the large momentum ratio the flame is lifted. The calculated gas temperature and oxygen concentration at the axis of symmetry undergo changes implying ignition only at a distance of about 0.5m ($x/D = 2.7$). Fig. 5.13.c shows a comparison between the predictions and measured values of the radial profiles for oxygen and temperature. The pairs of data points represent measurements either side of the axis and are indicative of the degree of flow symmetry. The measured profiles are already fairly uniform at the first two locations ($x/D = 3.31$ and 4.94) suggesting that this is already the post flame region. It can be seen that the quality of the predictions in this region is generally good. The predicted high gas temperature and low oxygen concentration near the furnace axis at x/D = 3.31 and 4.94 suggest that the NBR may not be especially well predicted.

The burner geometry and the inlet conditions of Cases ii-1 and ii-3 are very similar to those of Case ii-2 as shown in Table 4.3. The most evident difference is in the level of the secondary swirl but, because of the very high momenta of the primary streams, its net effect is negligible. Fig. 5.12.a and 5.14.a show similar features to those of Fig. 5.13.a. The flame structure as suggested by the temperature and oxygen contours is almost identical in the three cases. The difference in swirl level slightly affects the size and shape of the ERZ. The comparisons with radial profiles for both flames are shown in Fig. 5.12.b and 5.14.b. The agreement with predictions are as good as those obtained for Case ii-2.

It is noted in Fig. 4.2 that the primary inlet plane for Cases ii-4 to iiii-7 which is represented by the burner pipe exit is downstream that of the secondary pipe. It was not possible to handle such configuration with the original mathematical model. This problem was solved by dividing the computational domain into two. In the first domain the flow in the secondary pipe around the primary one was computed. A modified version of the mathematical model was designed to calculate those cases. It differed from the original one by the presence of treatment of south boundaries representing the primary pipe. It was assumed that no chemical reaction, mixing between the two jets or entrainment of particles took place in this domain and was calculated as if it were a one inlet flow. The calculated exit values were used as the inlet conditions of the secondary flow in the other domain which started at the plane of the burner exit. In the absence of near burner measurements, it was difficult to validate accurately the method used to assign the inlet conditions for the second computed domain.

Figure 5.15.a shows the predicted near burner aerodynamic flow pattern for Case ii-4. Three recirculation zones are exhibited. The upstream recirculation is due to the conical bluff body in the primary stream. The IRZ is the result of entrainment by the fast moving stream of the secondary flow. This is in contrast with the previous high momentum ratio cases. The ERZ which is not included in the figure merges with the separated flow in the quarl.

Figures 5.15.b and 5.15.c show comparisons of predictions of gas temperature and oxygen concentrations with the data.The good quality of the predictions reflects that of the previous cases obtained for different burner geometry and using a higher volatile coal. Fig. 5.16.a. and 5.16.b show similar trends obtained for Case ii-5 to those obtained for Case ii-4. The slightly higher momentum ratio for the primary to secondary stream is countered by the higher amount of swirl resulting in almost identical predictions and experimental data.

The same good quality of predictions was retained for the differing position of the bluff body used for Cases ii-6 and ii-7 as can be seen in Fig. 5.17 and Fig.5.18 respectively.

Inspite of the good predictions obtained for this stage, definite conclusion about the validity of the mathematical model is hindered by the fact that they lack comparisons for the more complicated near burner region.

Figure 5.12.a Predicted contours of stream function, oxygen and temperature for case ii-1

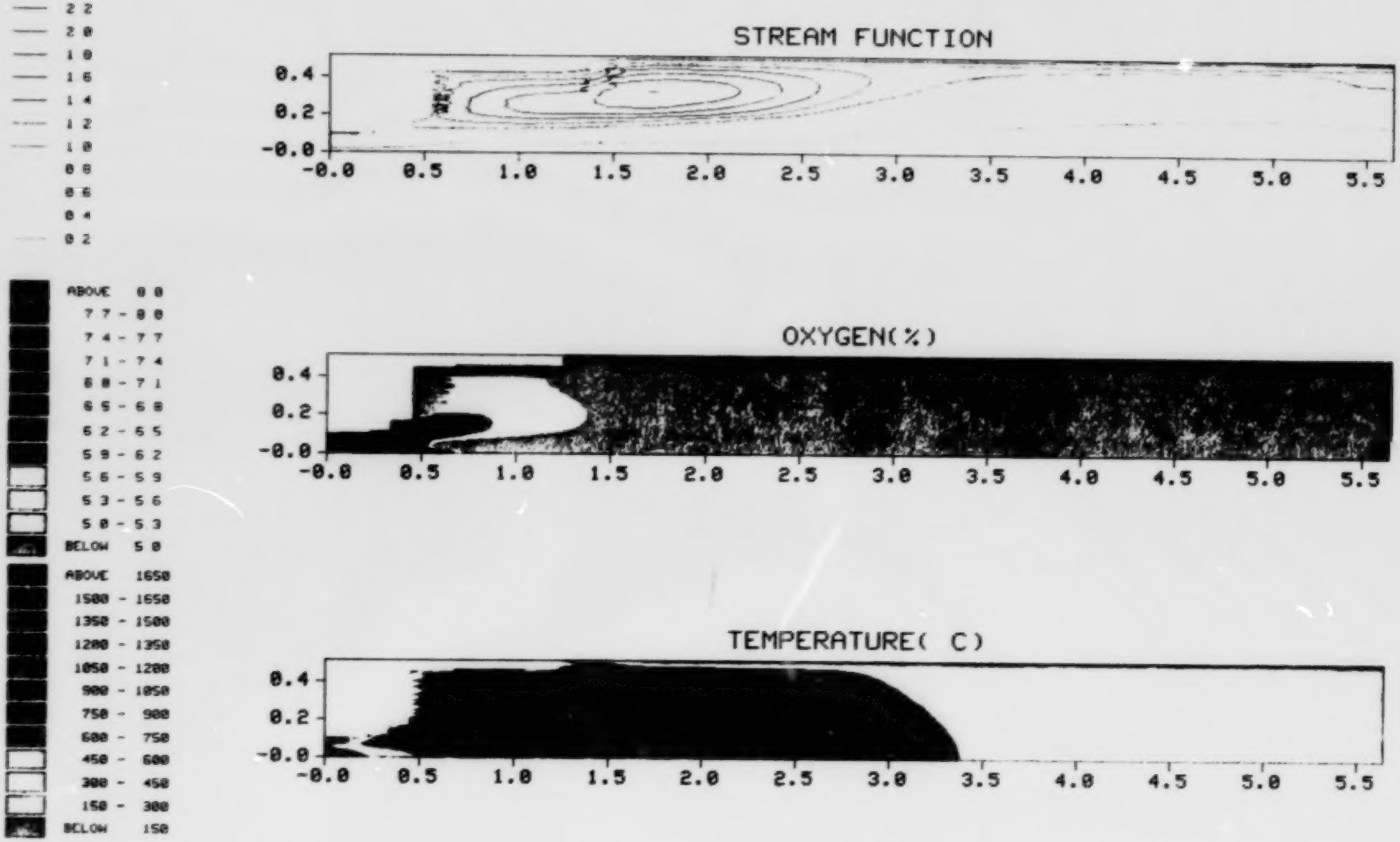

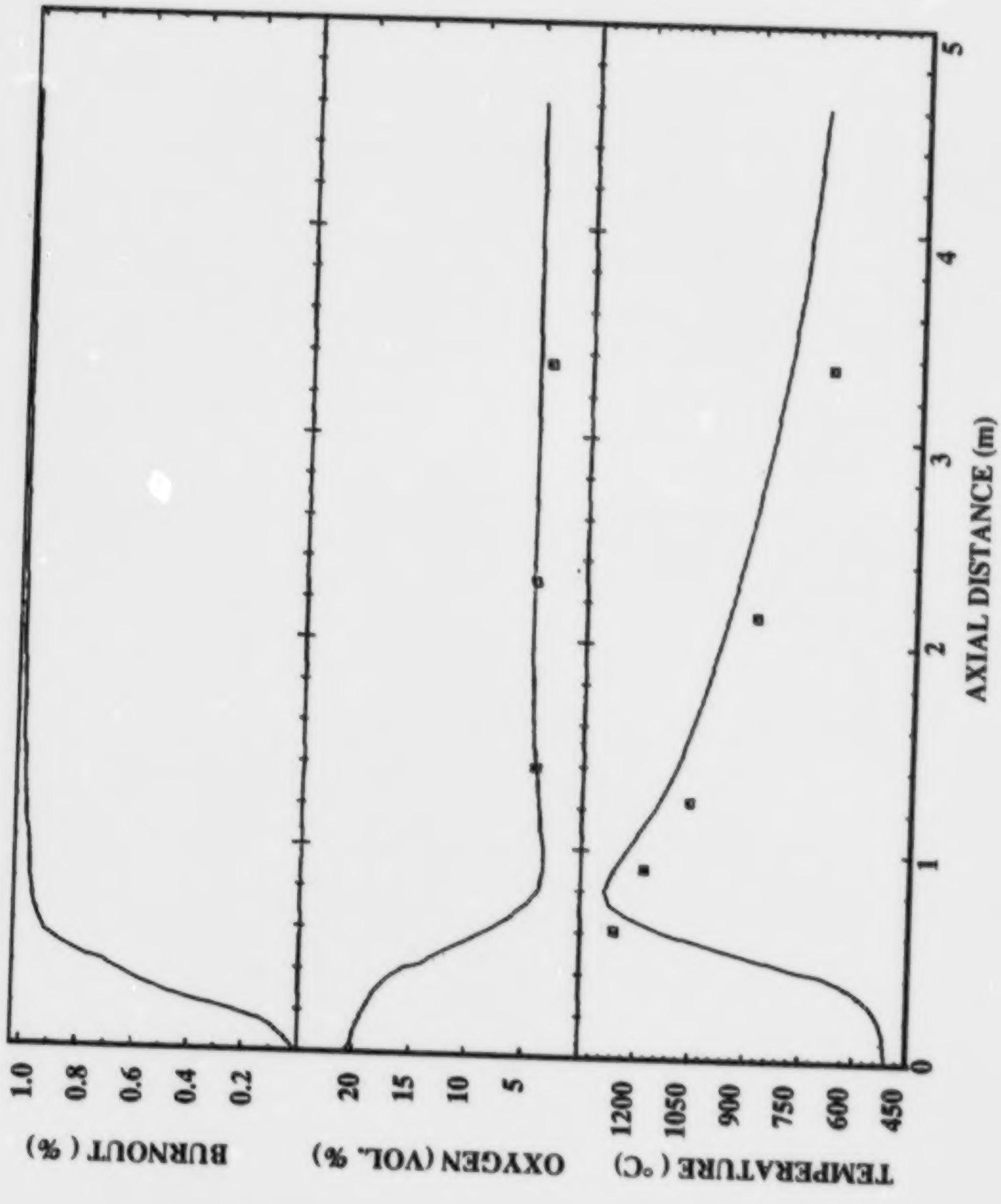

Figure 5.12b The axial distribution of temperature, oxygen concentration and burnout for Case ii-1

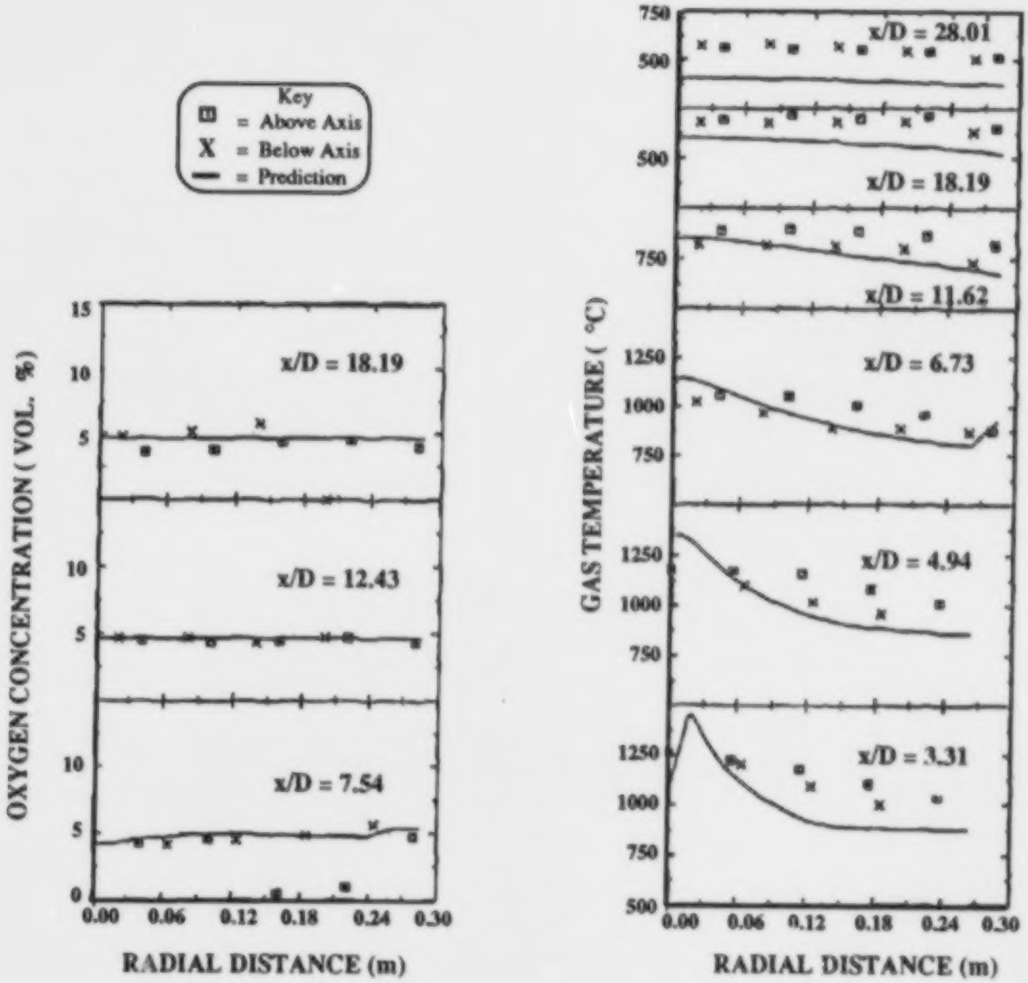

Figure 5.12.c Comparison between the predictions and measured data of the radial profiles for oxygen concentration and gas temperature for Case ii-1

Figure 5.13.a Predicted contours of stream function, oxygen and temperature for case ii-2

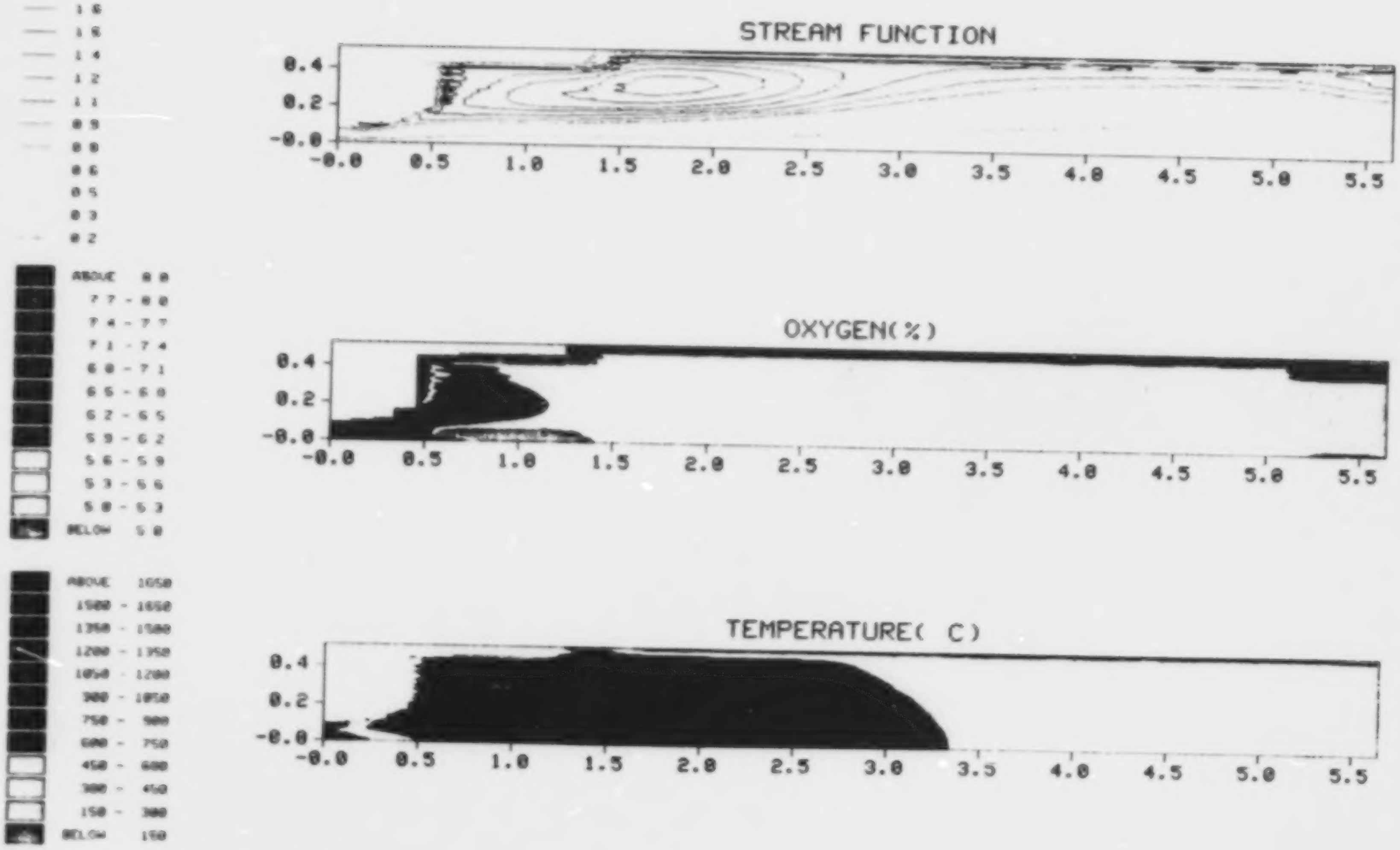

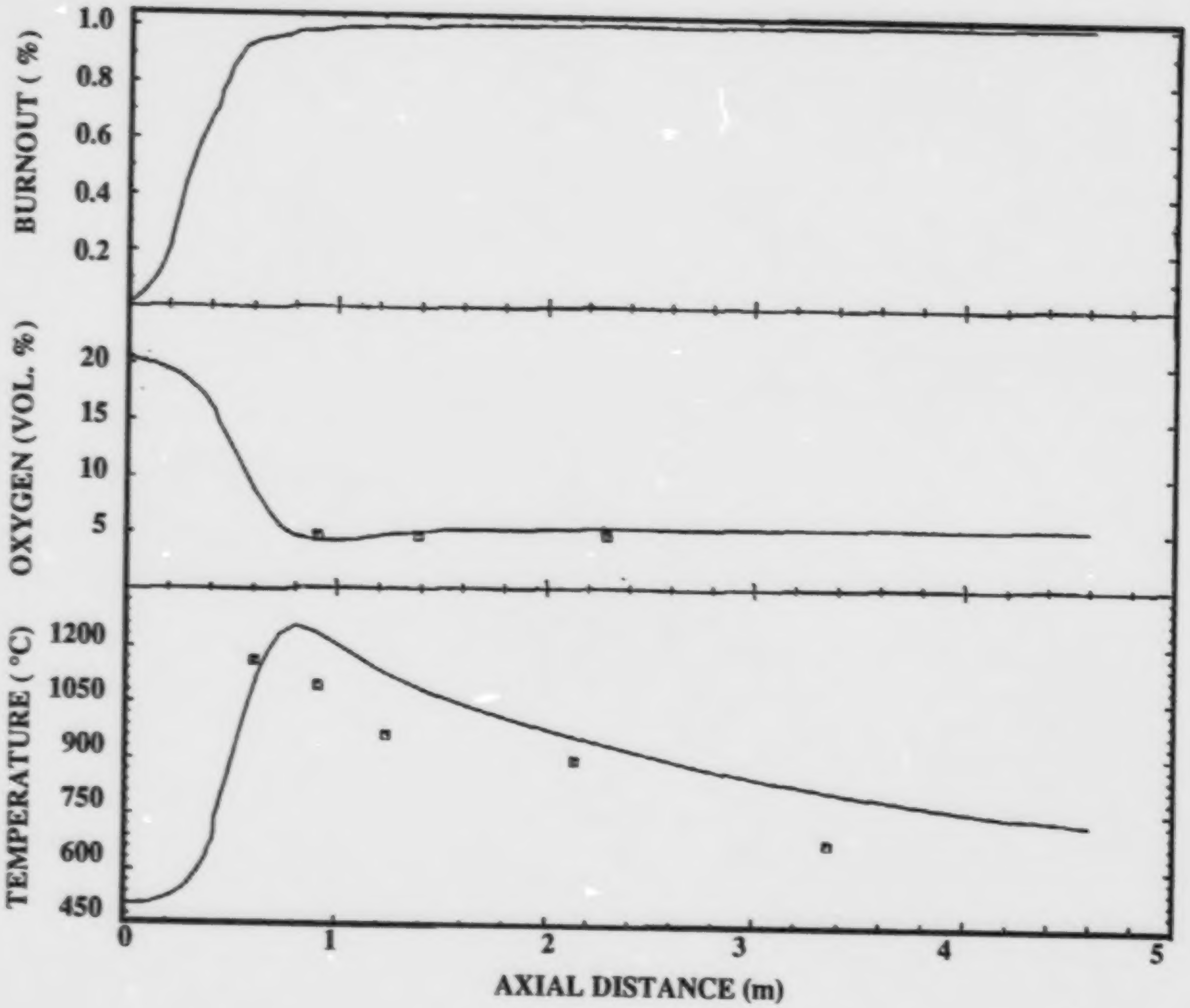

Figure 5.13b The axial distribution of temperature, oxygen concentration and burnout for Case ii-2

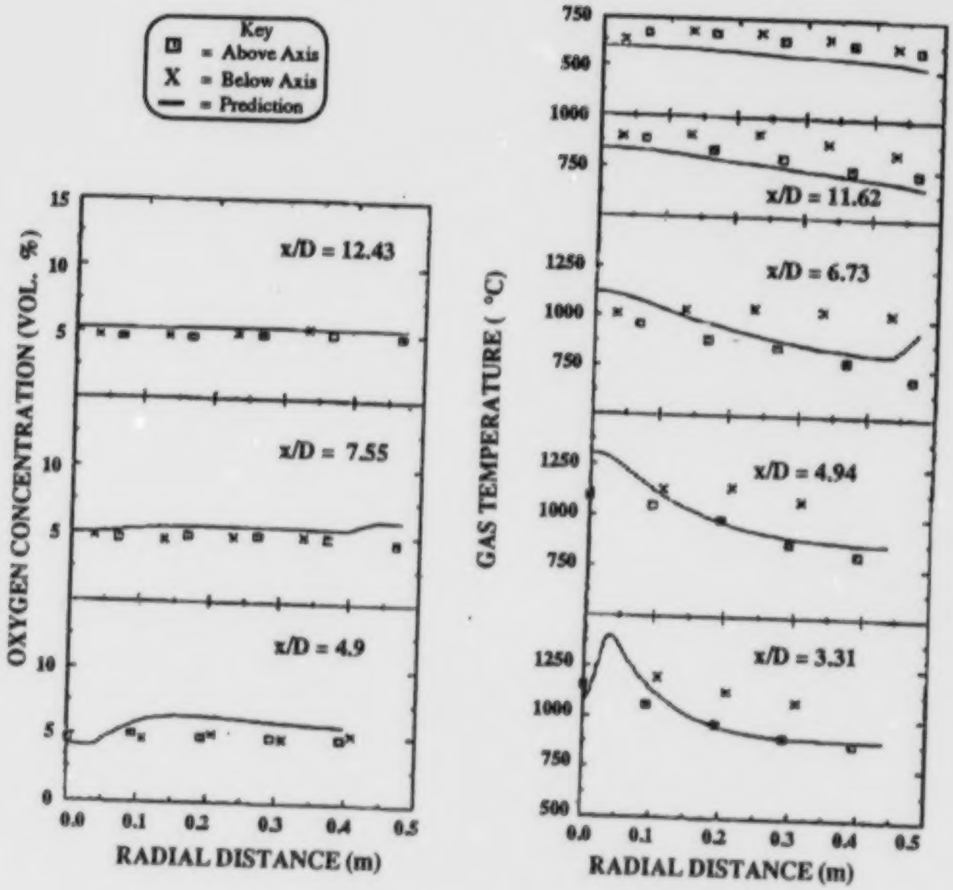

Figure 5.13.c Comparison between the predictions and measured data of the radial profiles for oxygen concentration and gas temperature for Case ii-2.

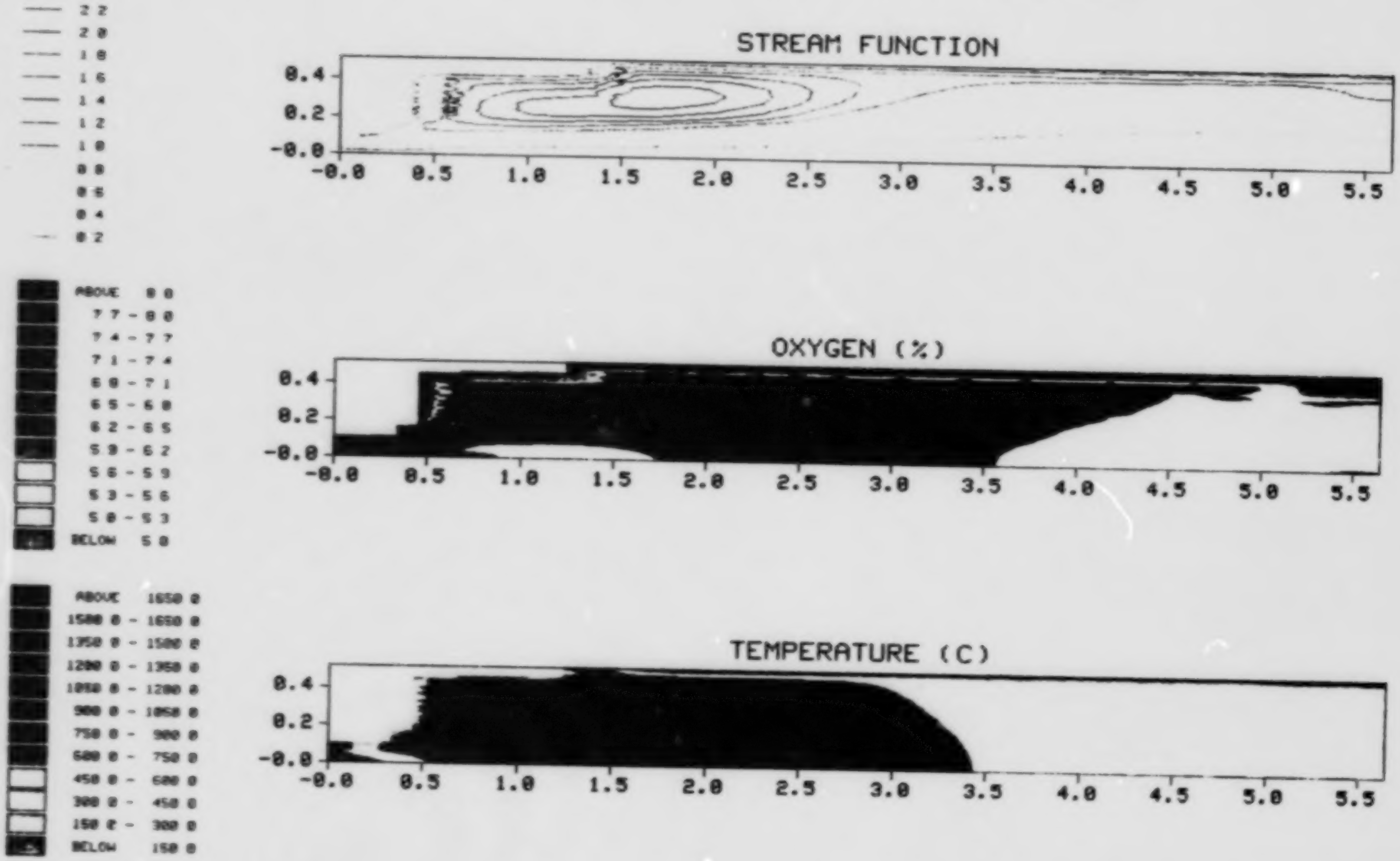

Figure 5.14.a Predicted contours of stream function, oxygen and temperature for case 11-3

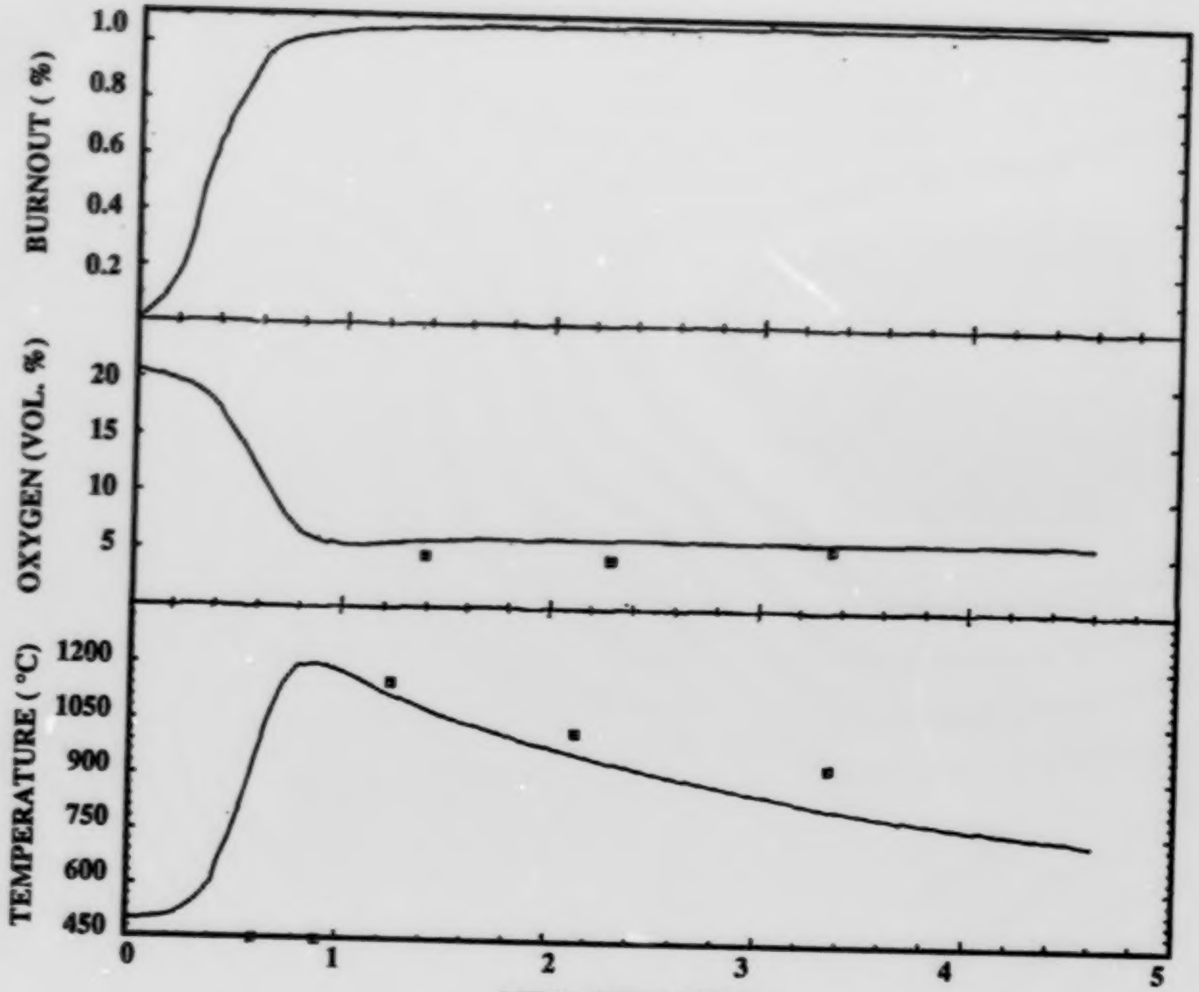

Figure 5.14.b The axial distribution of temperature, oxygen concentration and burnout for Case ii-3

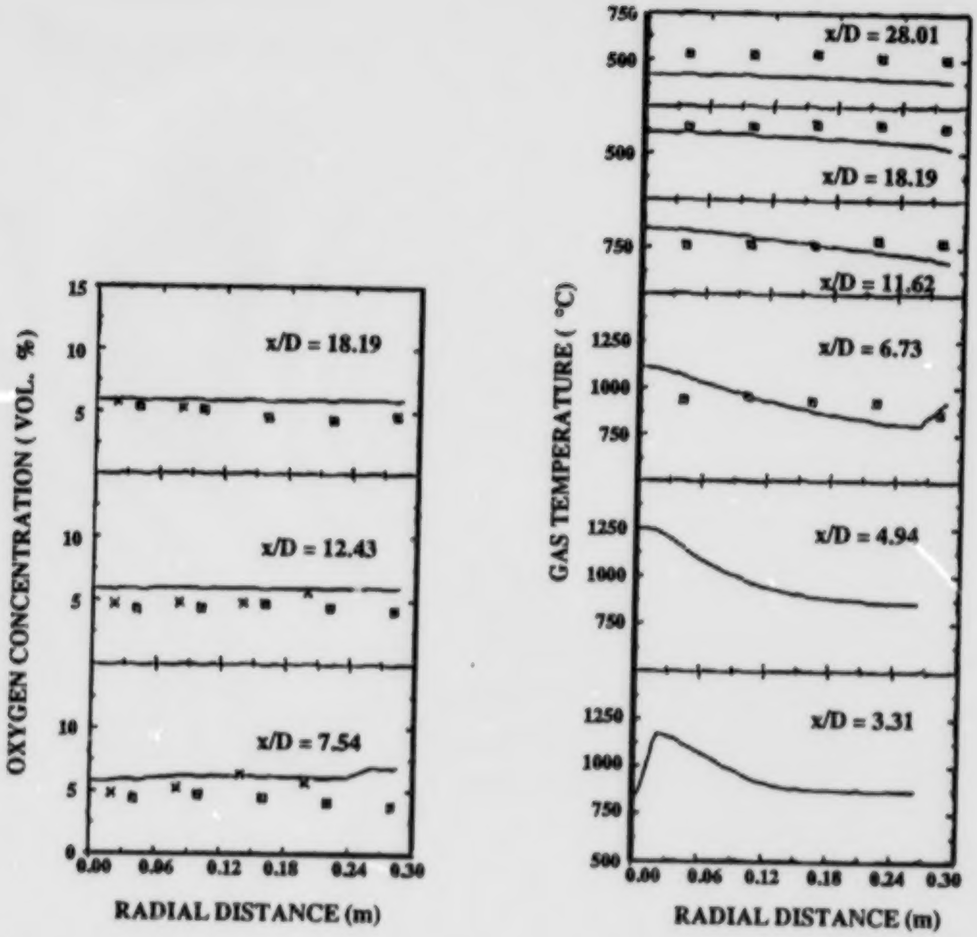

Figure 5.14.c Comparison between the predictions and measured data of the radial profiles for oxygen concentration and gas temperature for Case ii-3

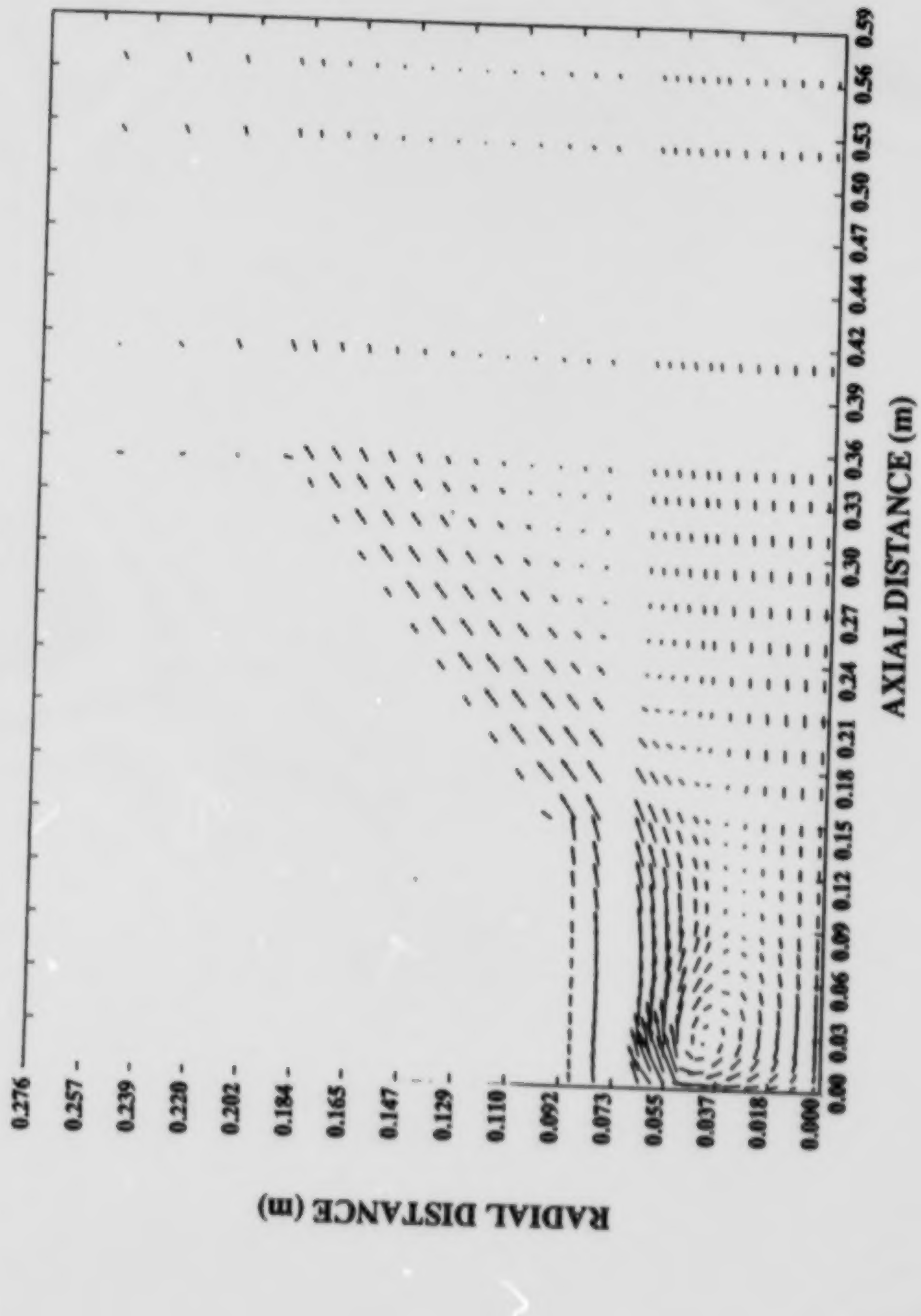

Figure 5.15.a The predicted near burner aerodynamic flow pattern for Case ii-4.

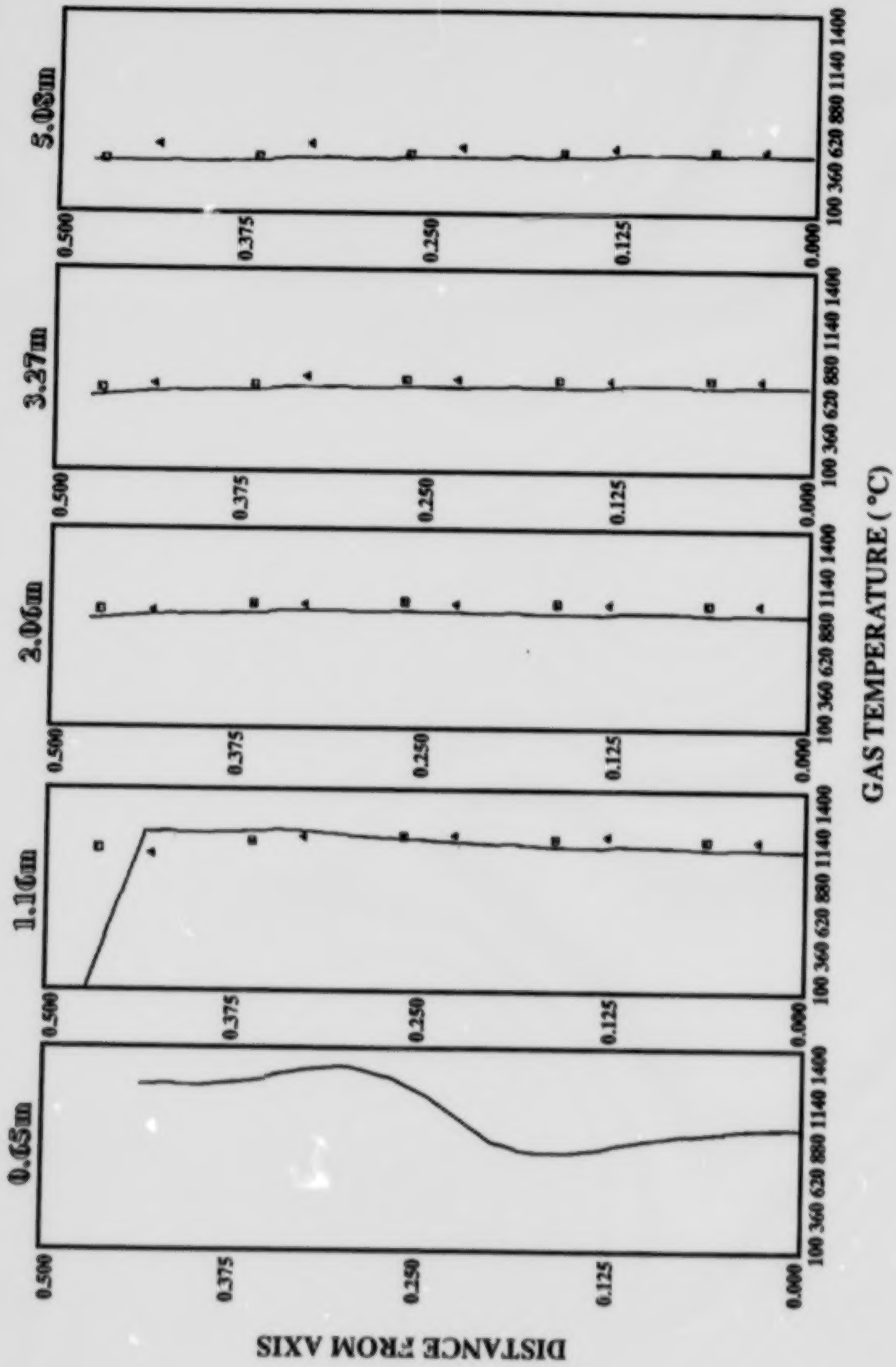

Figure 5.15.b Comparison between the experimental data and the predicted gas temperature for Case ii-4.

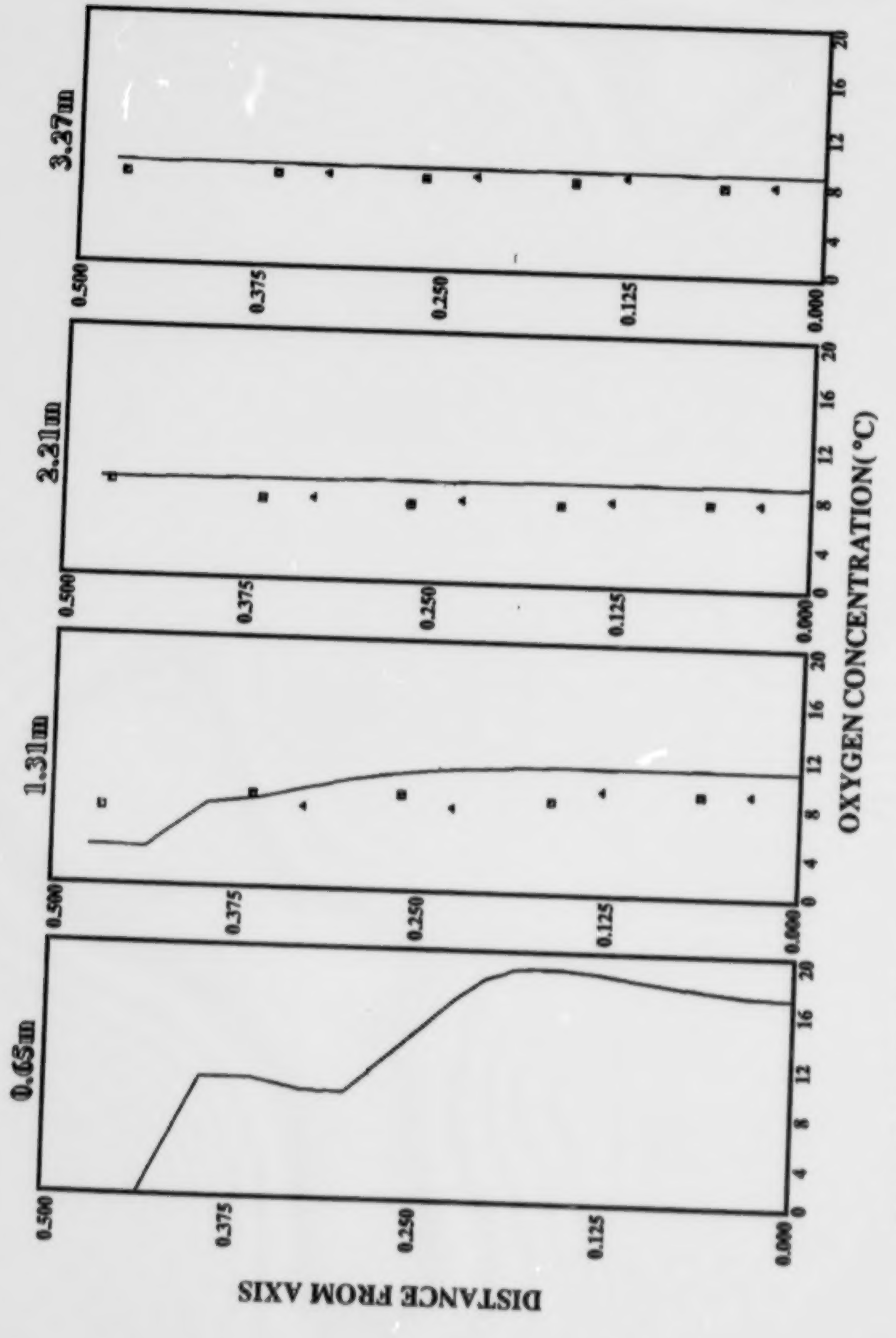

Figure 5.15.c Comparison between the experimental data and the predicted oxygen concentration for Case ii-4.

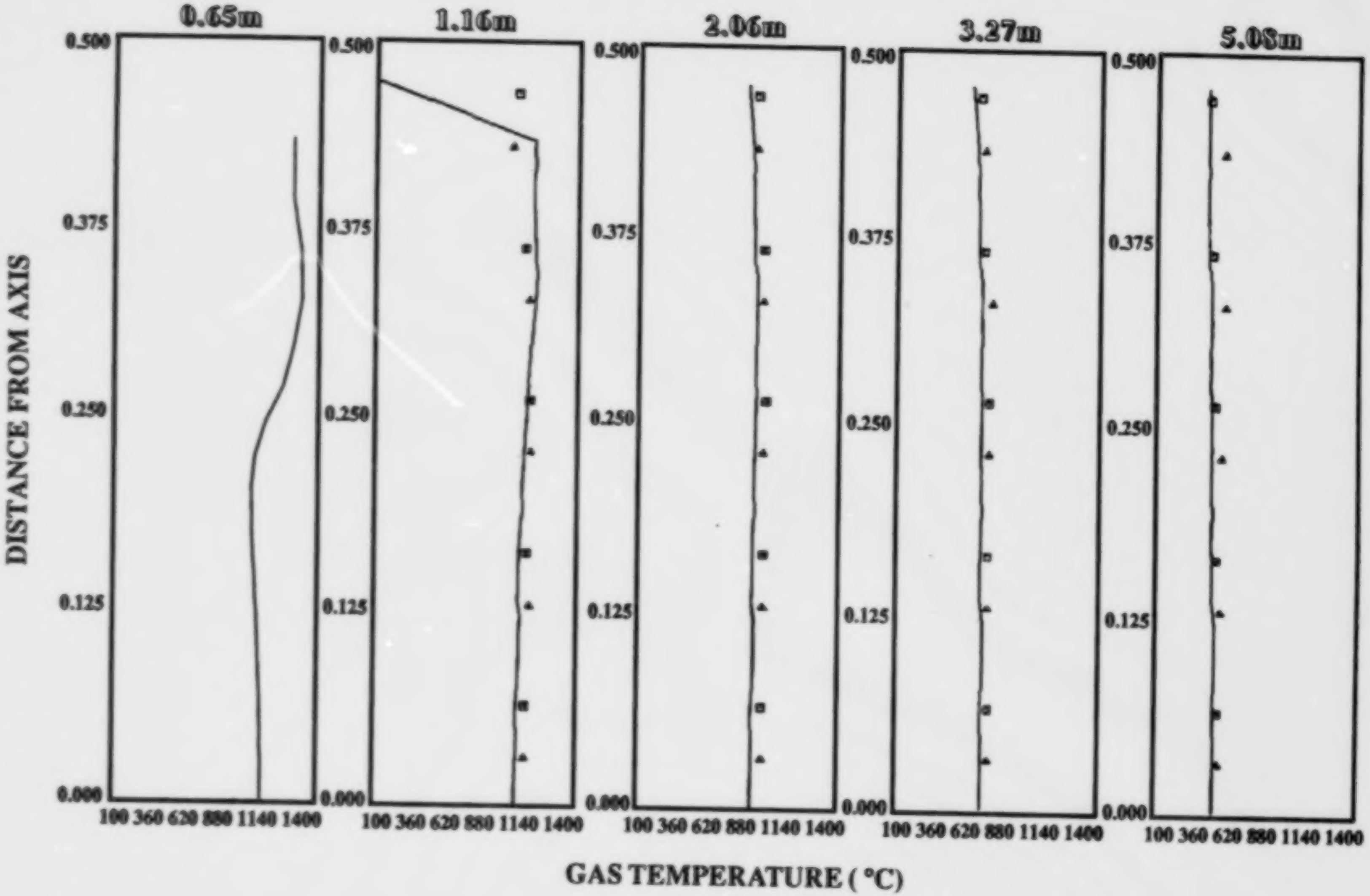

Figure 5.16.a Comparison between the experimental data and the predicted gas temperature for Case ii-5.

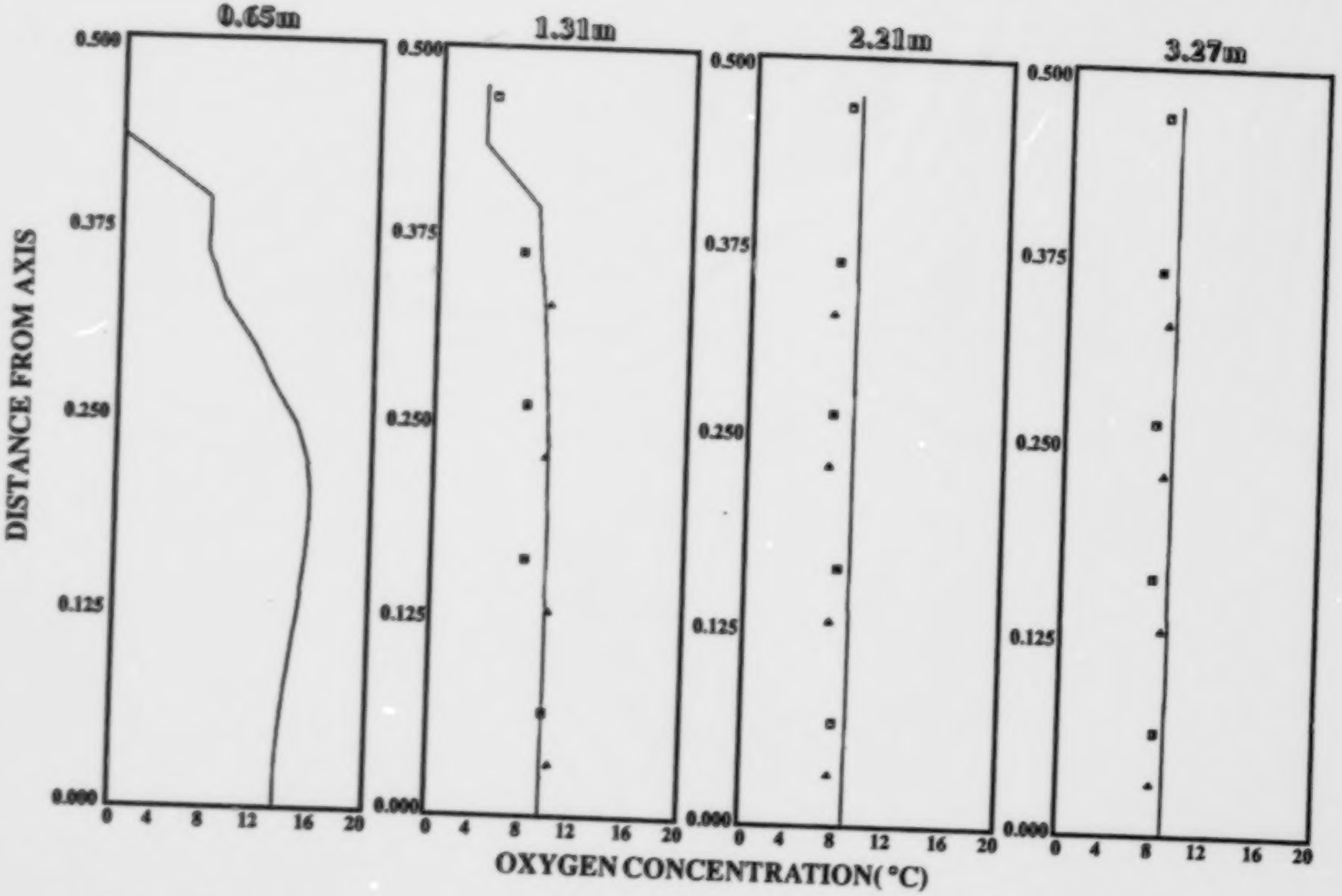

Figure 5.16.b Comparison between the experimental data and the predicted oxygen concentration for Case ii-5.

Figure 5.17.a Predicted contours of stream function, oxygen and temperature for case ii-6

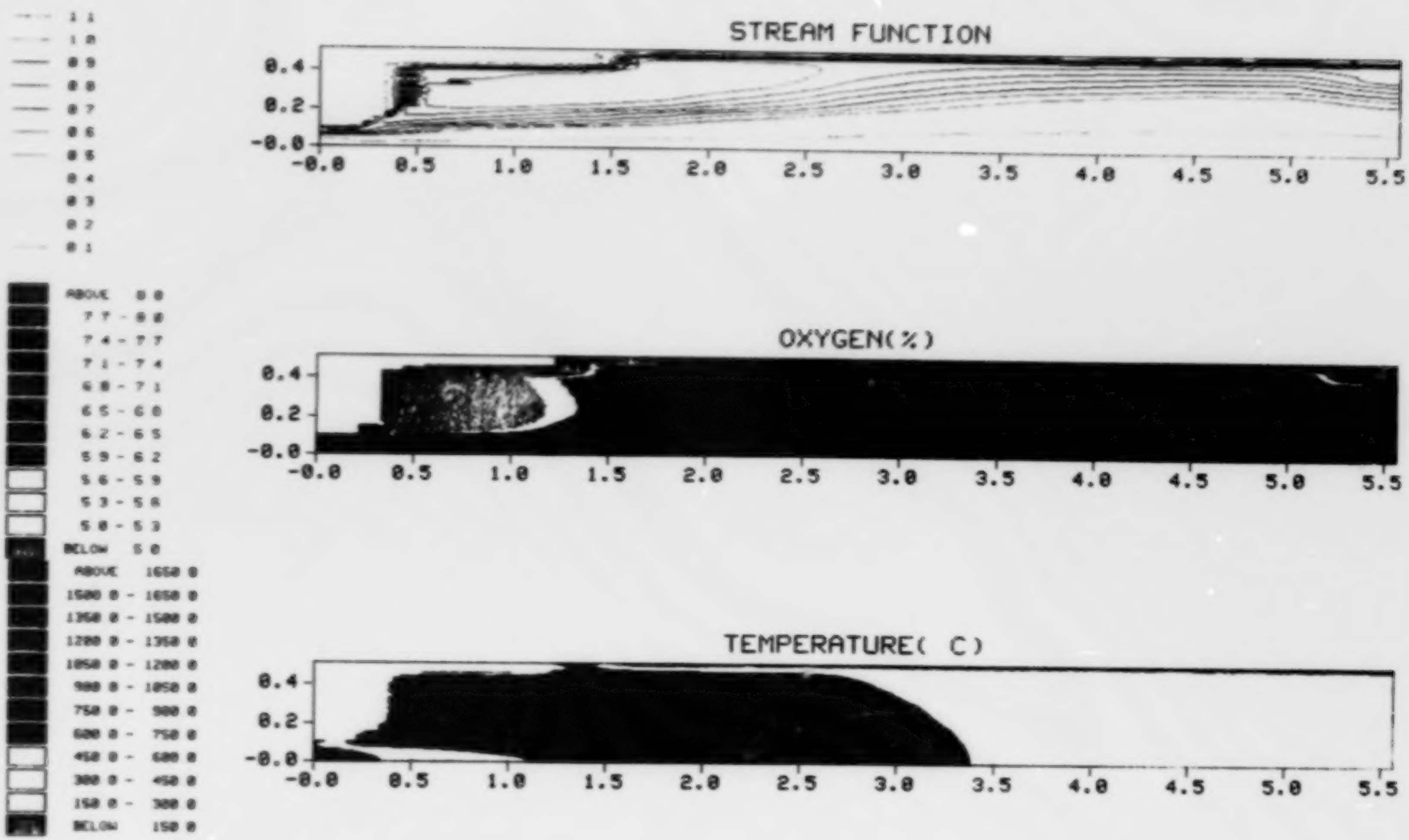

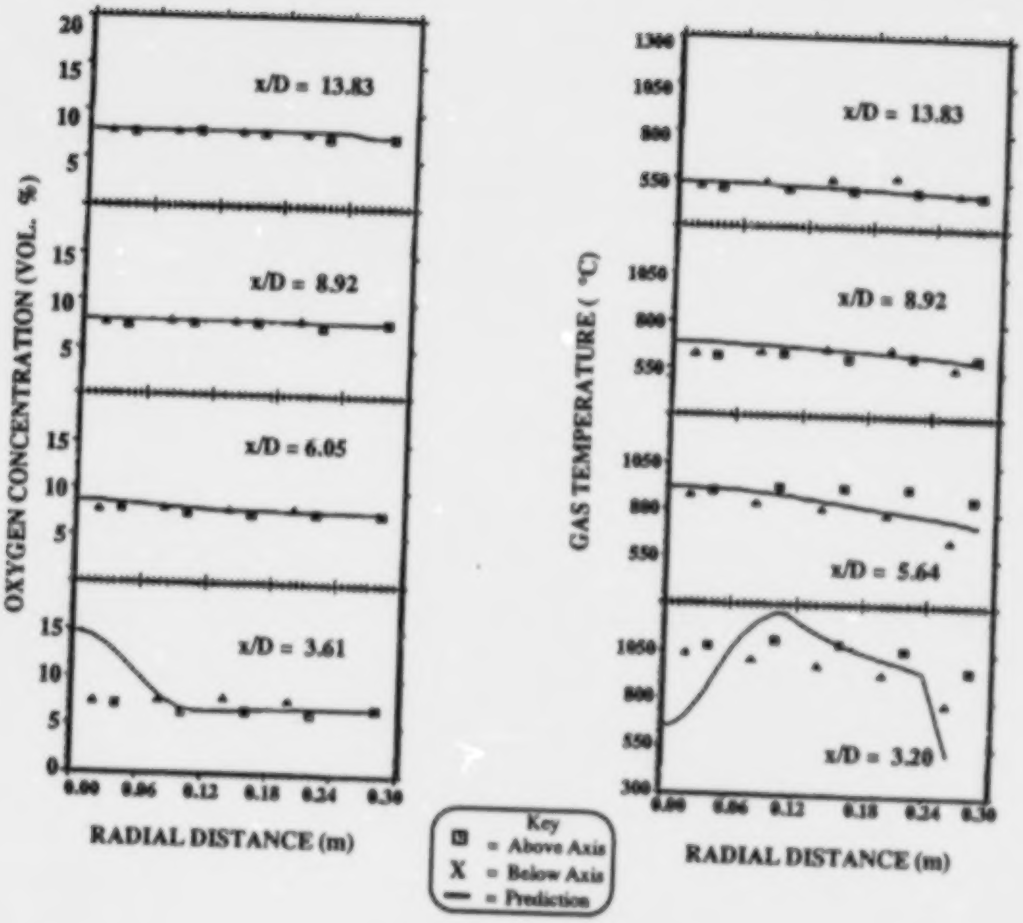

Figure 5.17.b Comparison between the experimental data and the predicted oxygen concentration and gas temperature for Case ii-6.

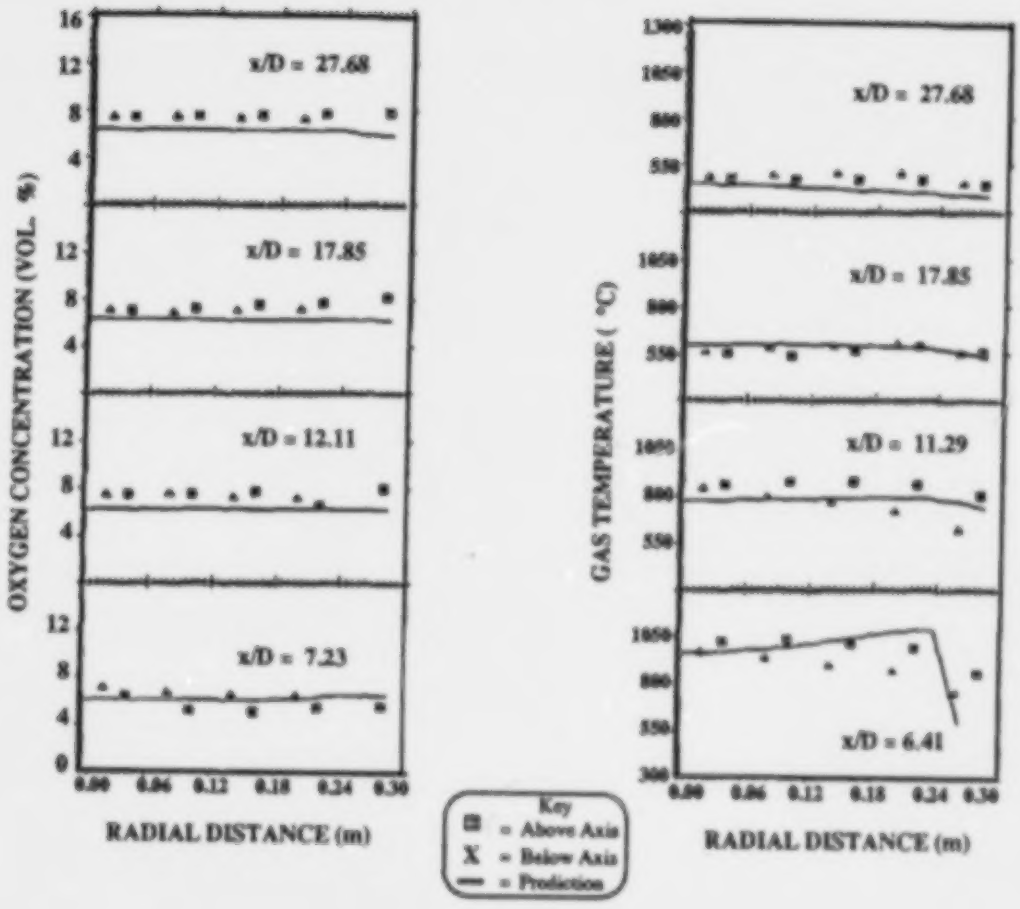

Figure 5.18 Comparison between the experimental data and the predicted oxygen concentration and gas temperature for Case ii-7.

5.4 COMBUSTION CASES FOR FLOW TYPE 2 (STAGE iii)

5.4.1 The IFRF Flame Predictions (Case iii-1)

The predicted gas flow pattern and particle trajectories in the NBR for the IFRF flame of inlet conditions given in Table 4.5 are shown in Fig. 5.19.a. They reveal a strong IRZ anchored to the bluff body. The coal particles penetrate this IRZ to a restricted extent. The smallest particles are "flung" into the ERZ as a result of the swirl where they burn to completion. The predicted boundaries of both recirculation zones generally conform with those mapped out with the aid of a Schreier probe.

Fig. 5.19.b compares the predicted radial profiles of oxygen concentration and gas temperature with the data at four axial locations for the IFRF furnace. In contrast to many of the CCRL measurements, these data pertain to the NBR and provide a much more detailed picture of the flame structure. The overall agreement between predictions and measurements is reasonably good. However, discrepancies occur in the IRZ, particularly near its downstream limits. This can be due to an underprediction of the particles penetration depth. The result is that there are insufficient particles at stations x/D = 2.62 and 4.15 to deplete the oxygen and raise the temperature to the levels measured. This argument is supported by the predictions of Fig. 5.19.a which show remarkably little penetration of the IRZ by the particles. There is no straightforward modelling remedy for this defect although a number have been tried such as reasonable alterations to the particles drag coefficient. It may be that a more correct treatment of the particles/turbulence interaction would improve matters, but a suitable and code implemented one does not exist, see Lockwood and Papadopoulos [1989].

5.4.2 The ICSTM Flame Predictions (Case iii-2)

Fig. 5.20.a shows the predicted gas flow pattern and particles trajectories in the NBR of the ICSTM furnace of operating conditions given in Table 4.5. The general features of the flow exhibit, in common with the previous case, a swirl-induced IRZ attached to the bluff body, and an enveloping ERZ. The smaller particles fail to penetrate the IRZ and burn in the oxygen-rich shear layer adjacent to it. However, only the larger particles partially penetrate the IRZ where they release less than half of their volatile content. The estimated residence times for these particles within the IRZ vary between 10-20 ms, depending upon their size. In contrast to the IFRF case (see Fig. 5.19.a), the relative depth of the predicted penetration of the particles into this zone is significantly greater for the conditions of the ICSTM burner.

The performance of the mathematical model is assessed in Fig. 5.20.b where the predicted oxygen concentrations and gas temperatures are compared with the data. Compared with the CCRL and even the IFRF combustion cases, these data are closer to the burner and allow a critical evaluation of the model. The measured oxygen concentration profiles show the structure of the flame more clearly than do the ones of the gas temperature which are rather flat due to the smoothing effect of the thermal radiation. The quality of the predictions may be described as fair.Very near the burner at x/D = 1.1, the oxygen concentrations are well predicted. At the next two stations downstream a predictive difficulty arises which appears to emanate from the shear region adjacent to the IRZ boundary. The temperature near the axis at the station x/D = 2.2 nearest to the burner (which due to probe geometry distinctions does not coincide with the near burner station for the oxygen concentration profile) is underpredicted. This discrepancy between the quality of the oxygen and temperature predictions most likely arises from the particles/gas phase interactions. For purely gas phase combustion the good prediction of oxygen would be mirrored by the similarly good prediction of temperature unless the thermal radiation simulation were grossly erroneous. In a two phase flow correspondence between oxygen and temperature cannot always be anticipated due to movement of the particulate phase relative to the gaseous one. In the absence of experimental information about the gas and particles velocities it is concluded that the major sources of the discrepancies of Fig. 5.20.b is the poor prediction of the responses of particles to the mean gas velocity field, or more probably, of the particles dispersion due to the fluctuating component of the gas velocities and possibly also the poor prediction of ignition. Of course these arguments presume that the data are correct. It can be claimed that the oxygen measurements are reliable. The temperature measurements were however performed with fine wire thermocouples. Since the thermocouples are heavily bombarded with particles, especially in the NBR, these measurements must reflect some average of the gas and particles temperatures, probably some what in favour of the former to which the predictions shown here pertain. The mean gas and particles temperatures in the NBR can, according to our predictions and once ignition of the char has occured, differ by up to 200°C.

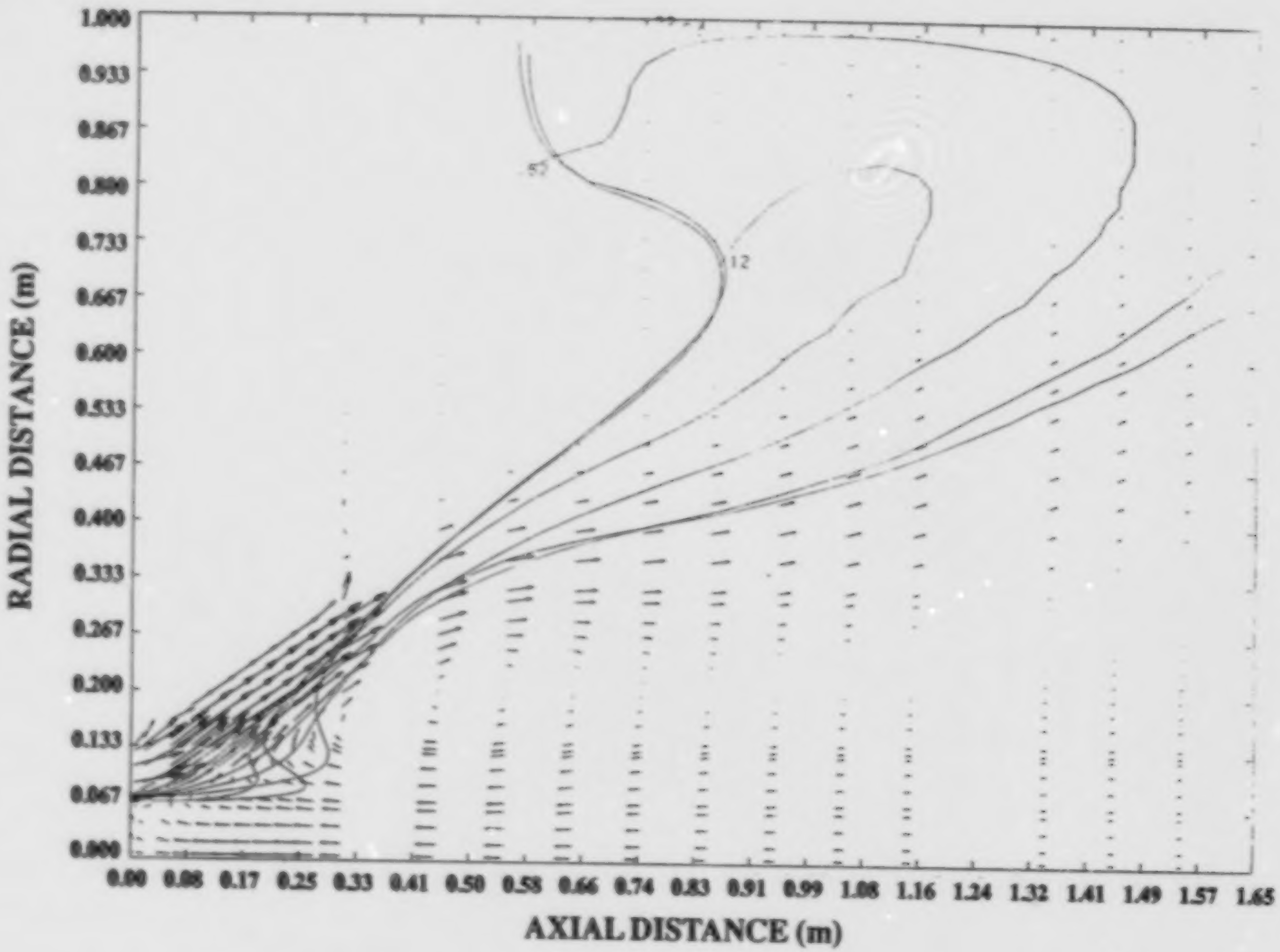

Figure 5.19.a The predicted gas flow pattern and particle trajectories in the NBR for the IFRF flame (Case iii-1).

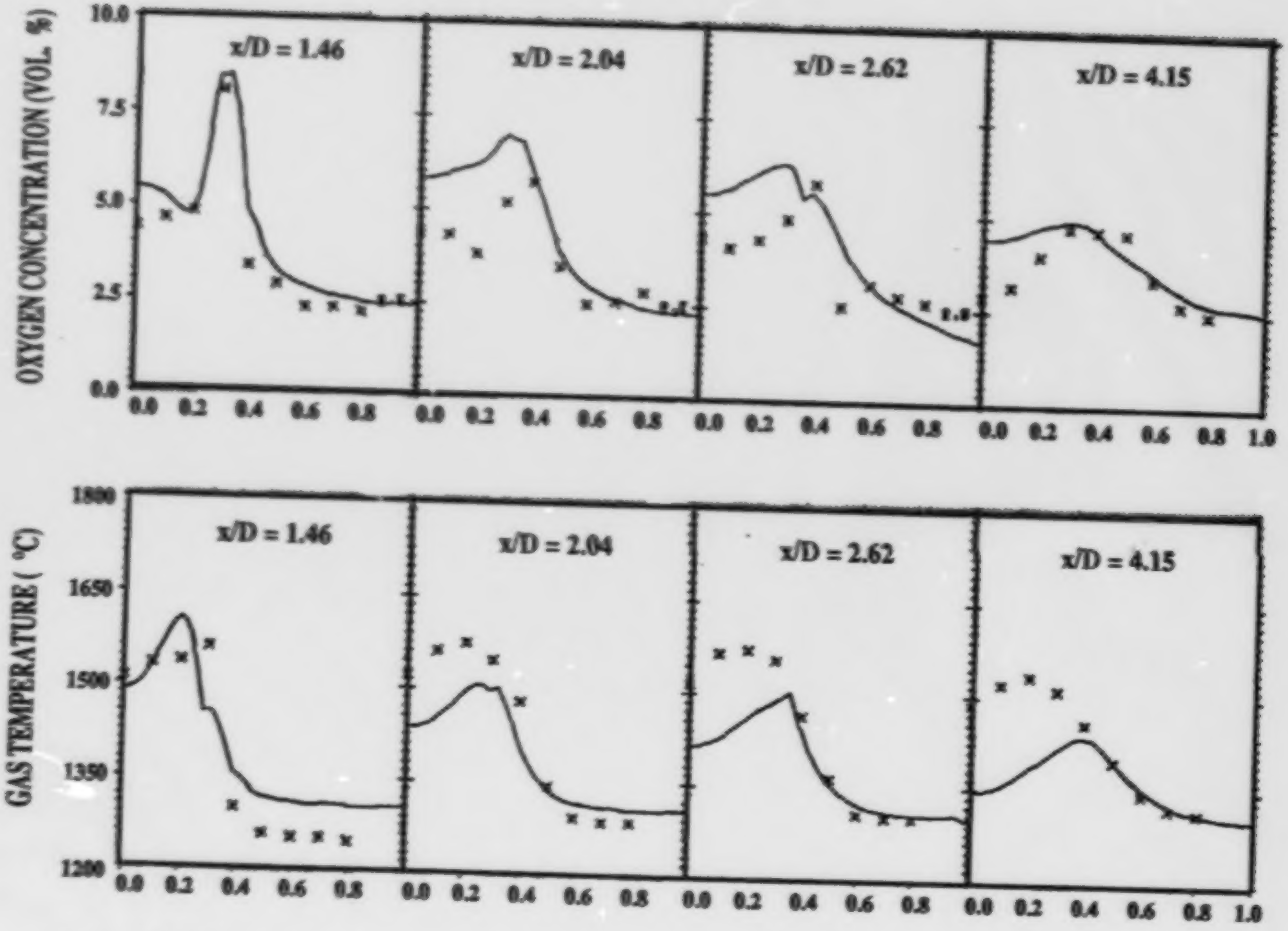

Figure 5.19.b Comparison between predicted radial profiles of oxygen concentration and gas temperature and the experimental data for the IFRF flame (Case iii-1).

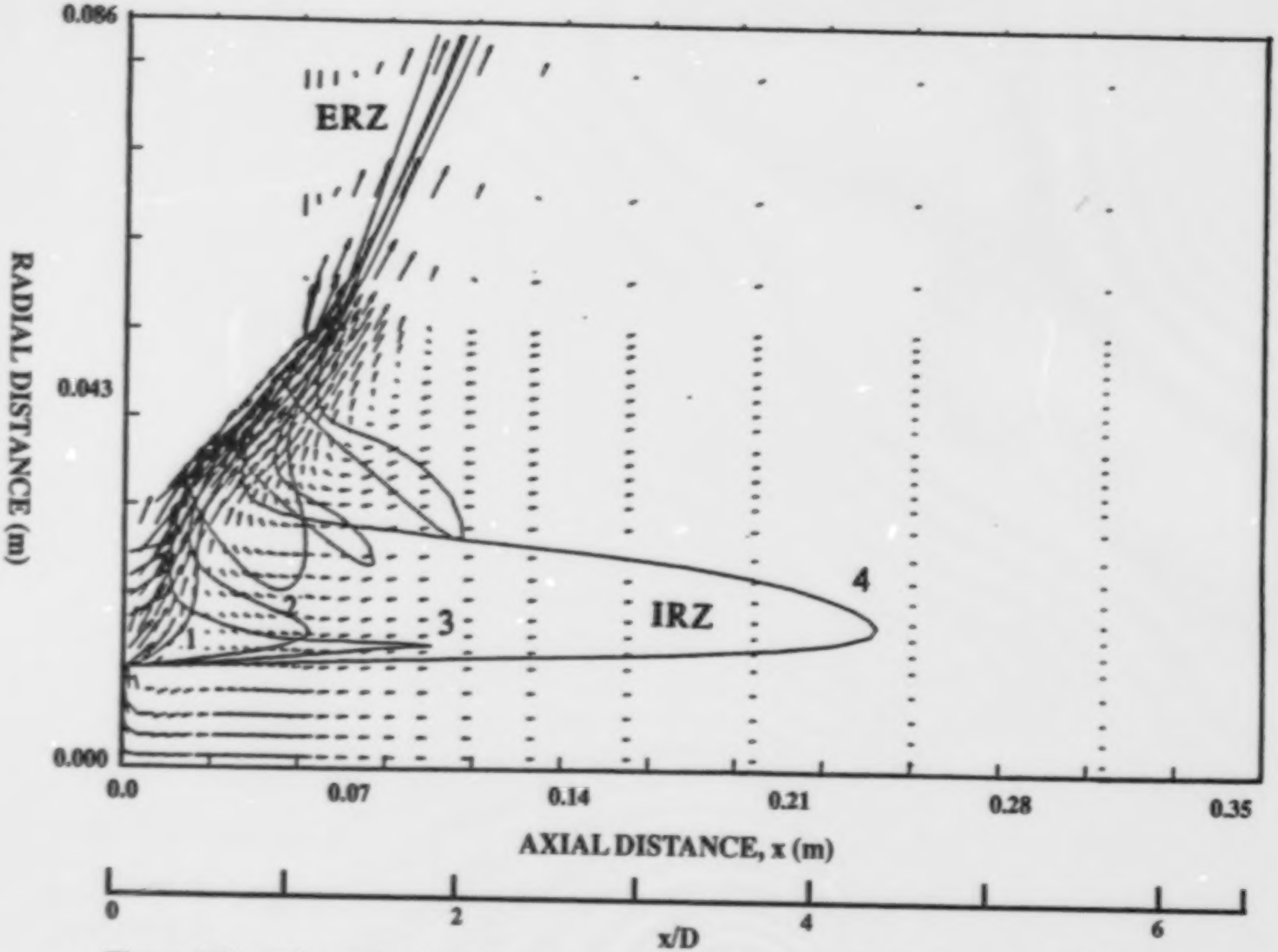

Figure 5.20.a The predicted gas flow pattern and particle trajectories in the NBR for the ICSTM flame (Case iii-2).

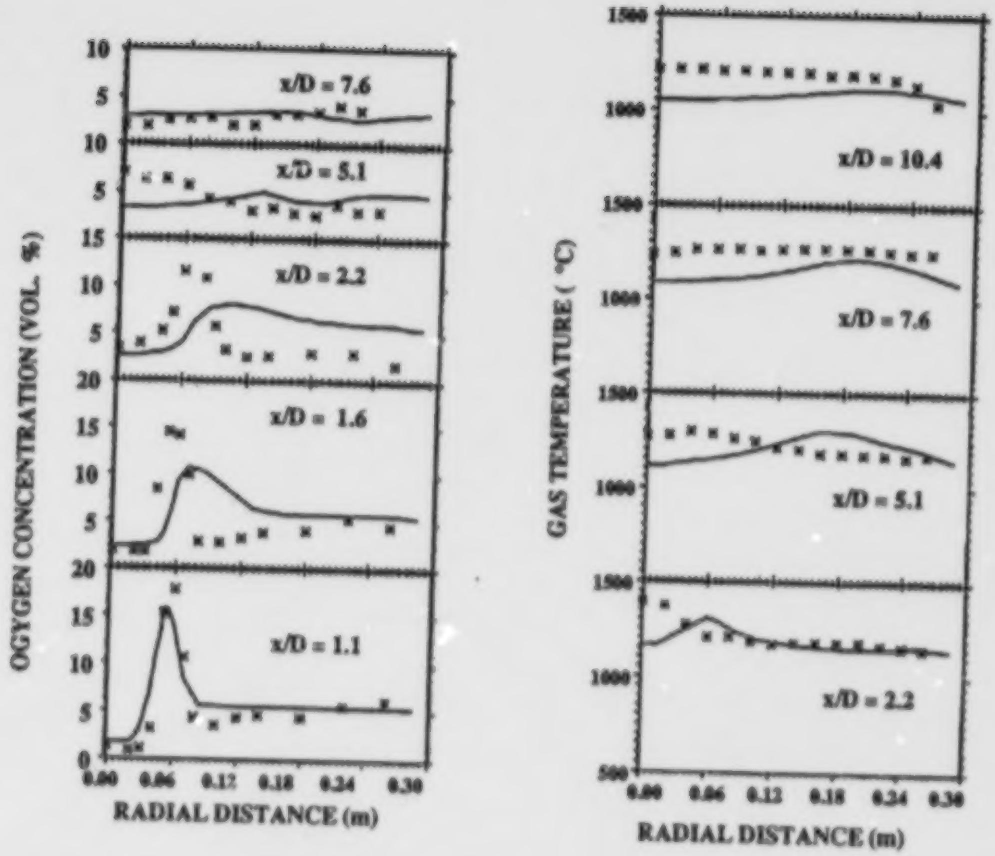

Figure 5.20.b Comparison between predicted radial profiles of oxygen concentration and gas temperature and experimental data for the ICSTM flame (Case iii-2).

5.5 COMBUSTION CASES FOR FLOW TYPE 3 (STAGE iv)

Flames produced by the burner without a central bluff body have been the subject of extensive measurements in the ICSTM furnace. A good review of most of the experimental work has been given by Costa et al [1991].

The present study involved the assessment of the performance of the PF combustion model against most of the data gathered from the ICSTM furnace using the SCO burner in Fig. 4.4. Both the experimental data and the predictions for a wide range of inlet conditions for this burner have revealed that the basic aerodynamic characteristics are very similar. The comparisons with data produced for different swirl levels and coal feed rates are entirely analogous. Emphasis is placed upon the effect of volatile content for the first two cases where the inlet conditions are the same except for the type of coal.

5.5.1 Aerodynamic Flow Pattern and Particle Trajectories

The predicted aerodynamic flow pattern and particle trajectories for Case iv-1 and Case iv-3 are shown in Figs. 5.21.a and 5.23.a respectively. The main features of the flow are a strong IRZ induced by the swirl imparted to the secondary air and an ERZ due to the sudden enlargement of the furnace chamber. The unswirled and coal particle laden primary jet penetrates the hot IRZ to a significant extent in contrast with the SAO case. The IRZ retards and reverses the primary jet containing the coal particles as illustrated in both figures. As the coal particles mix with the hot recirculated gas, their temperatures increase sharply resulting in rapid pyrolysis and initial burnout. For the higher swirl case, Fig. 5.21.a, with secondary air swirl level of 1.43 the particles which are less penetrated into the IRZ are retarded back into the quarl wall where they bounce back into the ERZ. The reduction in penetration depths of the particles into the hot IRZ for the higher swirl level results in reduced IRZ residence times and suppressed burnout, Costa et al [1990]. In the lower swirl case, shown in Fig. 5.23.a, it is observed that the small particles burn fully inside the IRZ. The particles residence times before exiting the IRZ range between 100-200 ms. depending on their sizes, leading to almost complete devolatilisation thereby creating a fuel-rich environment.

It should be noted that the flow pattern obtained for Case iv-2 is very similar to that obtained for Case iv-1 shown in Fig. 5.21.a implying the little or no effect of the volatile content of the coal on the aerodynamic features of the corresponding flame.

In the light of the differences of flow patterns of the SAO and SCO burners of the ICSTM furnace as displayed in Fig. 5.20.a and Fig. 5.23.a respectively, it can be concluded that in the case of the SAO burner, the faster reaction rates maintain a higher flame temperature and a more active ignition zone which allow the flame to remain lit back at lower swirl numbers. This conclusion was confirmed experimentally in the stability studies performed by Costa et al [1991c] and Abbas et al [1991b].

It should be noted that these predictions provide only a qualitative picture of the complex NBR flow pattern. In the absence of quantitative gas velocity data, the quality of the predicted flow field cannot be ascertained. However, limited comparisons with the LDA particles velocity data, [Milosavljevic [1991]] and previously obtained flow directions with a small acetylene flame, Lockwood and Mahmud [1988], suggest that the predicted length of the IRZ is somewhat too long and that the penetration depth of the particles into it may be underpredicted. Nonetheless, the predicted general features of particles trajectories are in qualitative agreement with the LDA data.

5.5.2 Particle History

The operating conditions for both cases iv-1 and iv-2 are identical except for the type of coal where in the former the lower volatile content Oakdale coal was used while the Gedling was used in the latter, as can be revealed from Table (4.6). The

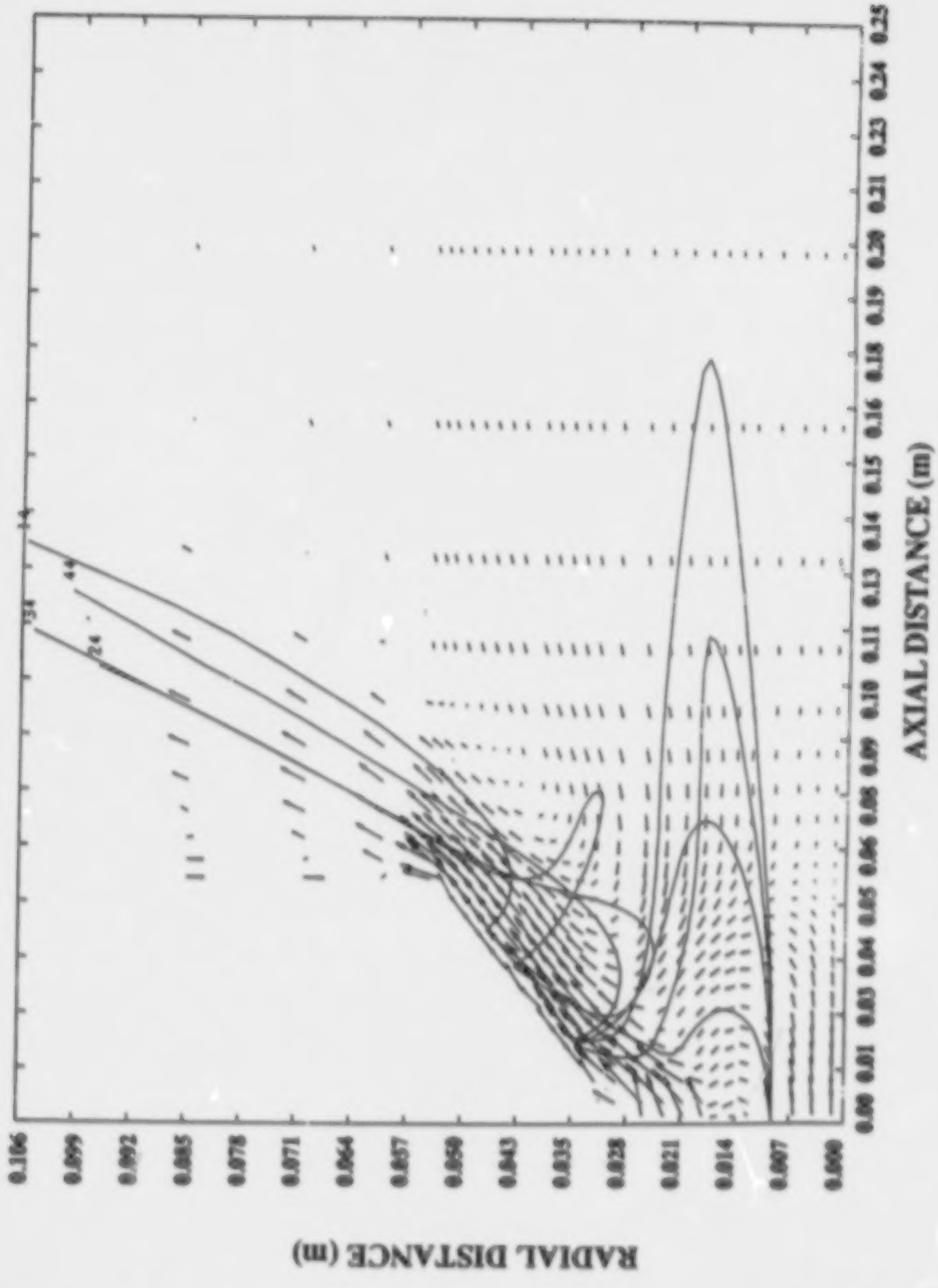

Figure 5.21.a The predicted gas flow pattern and particle trajectories in the NBR for Case iv-1.

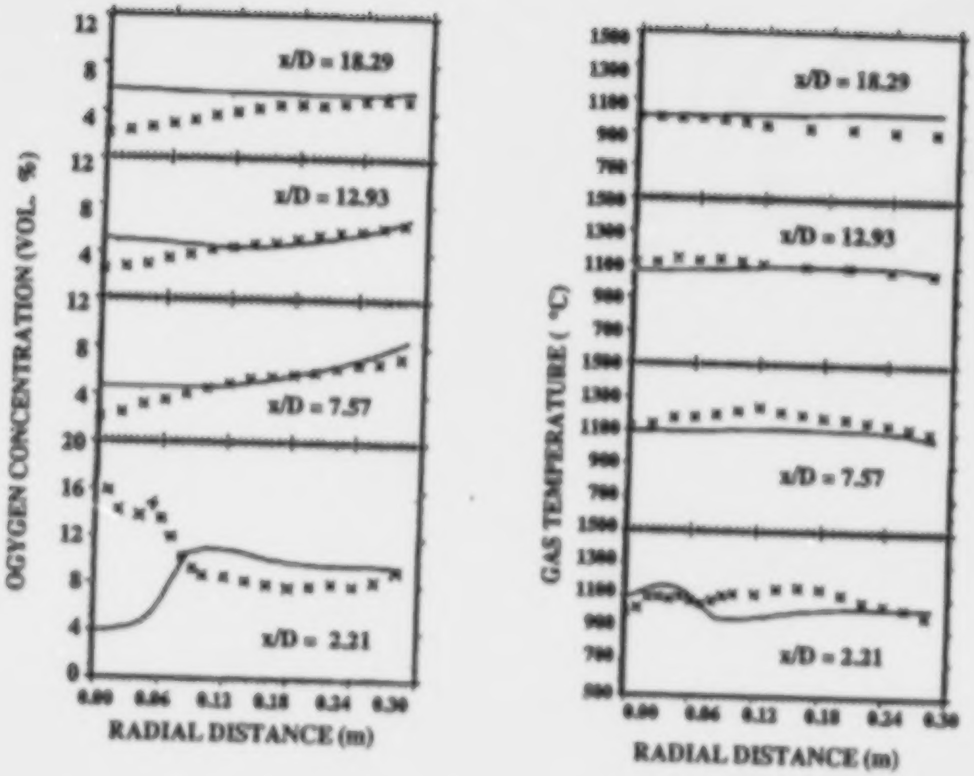

Figure 5.21.b Comparison between the predictive and experimental radial profiles of oxygen concentration and gas temperature for Case iv-1

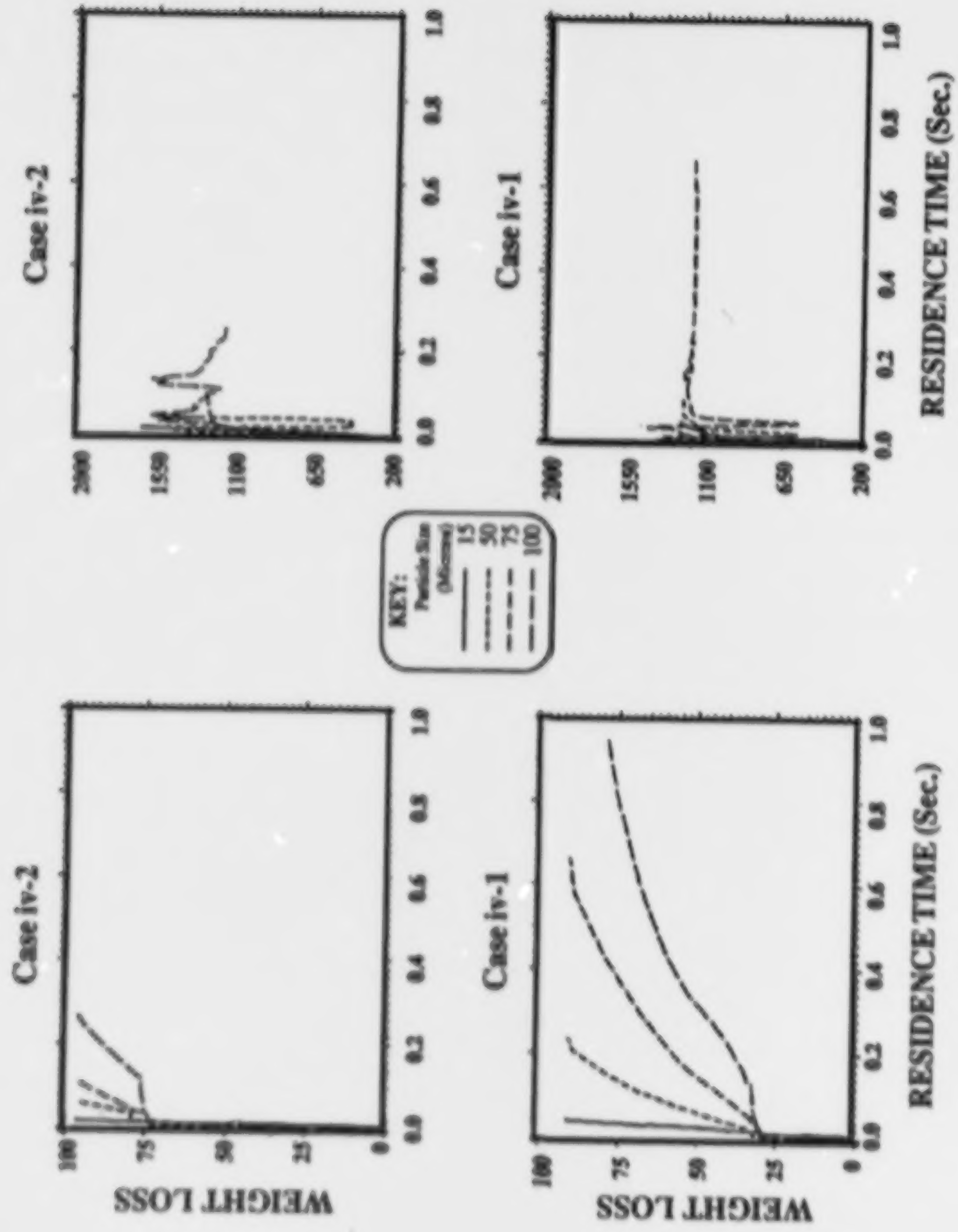

Figure 5.22 The particles weight losses and temperature versus residence time for Case iv-1 and Case iv-2.

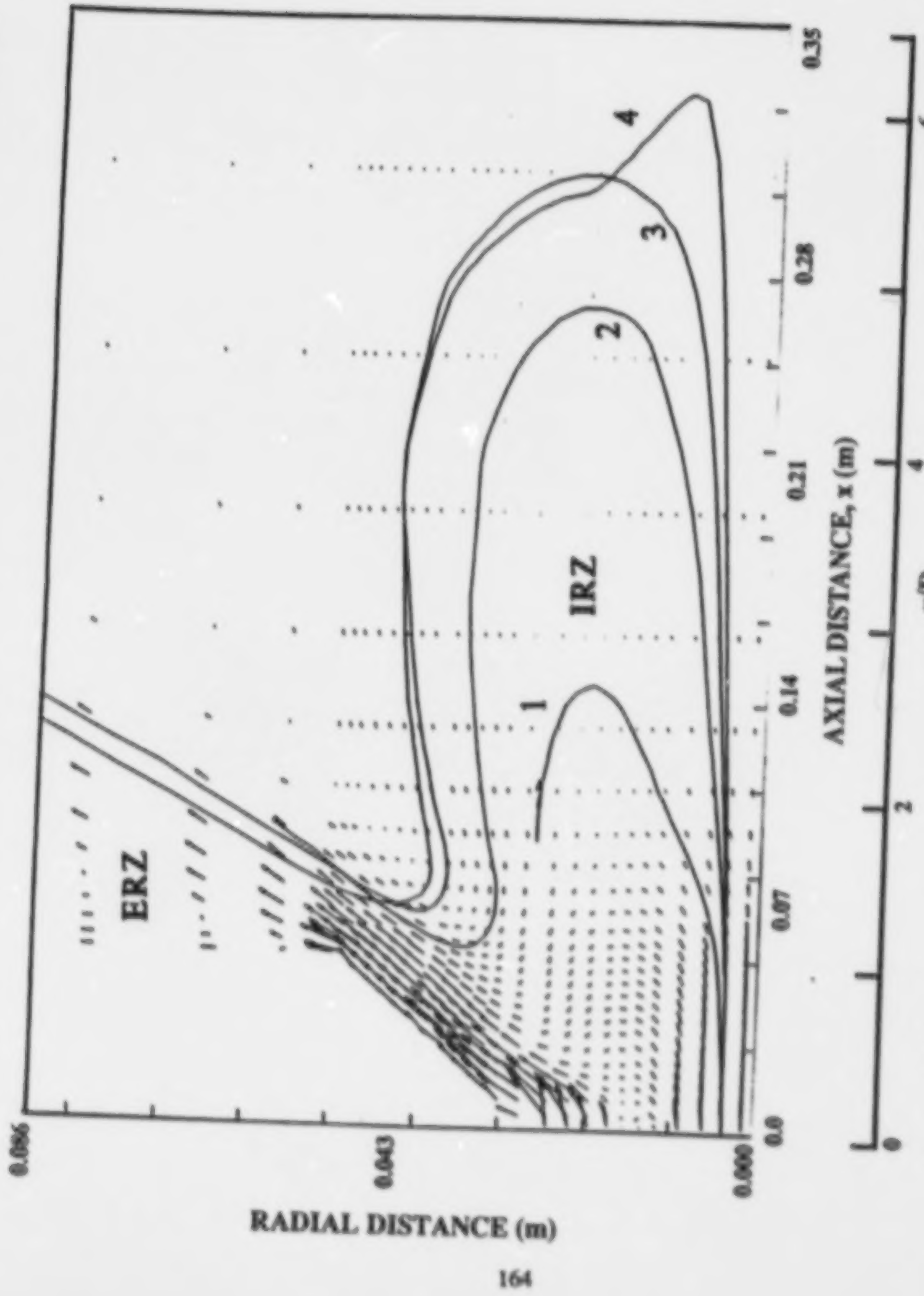

Figure 5.23.a The predicted gas flow pattern and particle trajectories in the NBR for Case iv-3.

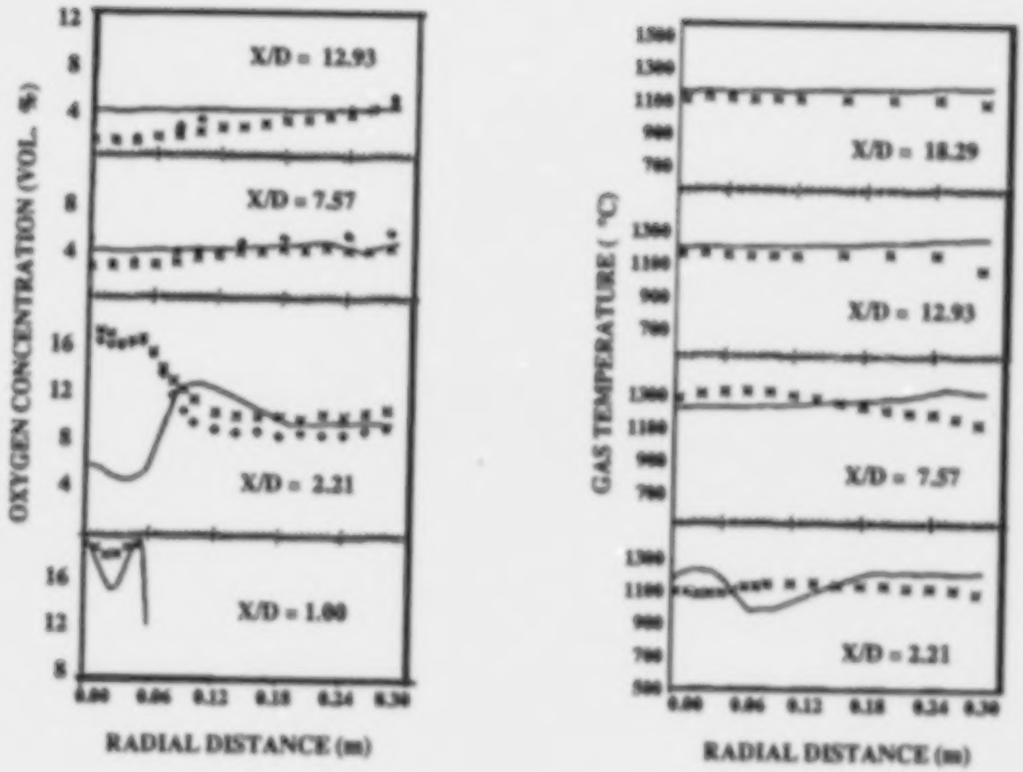

Figure 5.23.b Comparison between the predictions and experimental radial profiles for oxygen concentration and gas temperature for Case iv-3.

experimental data for both flames show similarity in both axial and radial profiles for the gas temperature and species, Costa et al [1991c]. The major difference between the performance of both flames was the reduced exit burnout for the low volatile flame of Case iv-1: specifically 86.3% as compared with 94.3% for case iv-2. In order to explain this difference the particle histories for both flames were studied.

Fig. 5.22.a and Fig. 5.22.b illustrate the particle weight losses and temperature versus the residence time for four sizes for Cases iv-1 and iv-2, respectively. It is to be remarked that, in the panels corresponding to the weight loss histories, the end of the coal devolatilisation (time scale less than 0.01 s) which, incidentally, coincides with the start of the heterogeneous combustion is readily revealed by a decrease in the slope of the curve. This is more pronounced for the larger particles, regardless of the coal type. It is also to be remarked that the temperature-time curves for both flames show a different behaviour from that obtained for one dimensional single particle studies,as for example that of Huang et al [1986] who measured both the particle temperature and the surrounding gas during coal pyrolysis and combustion. Huang et al [1986] reported an initial fast temperature increase after the particle ignition followed by an almost constant temperature during char combustion and until the final quenching when the particle is fully burned. On the other hand, the history shown in the present study for both flames suggest that the particles burning is interrupted by quenching as a result of the surrounding low temperature zones that the particle move through and the particles reignite again completing their combustion. This might imply either the strong and dominating effect of the particle trajectory through different thermal zones on its temperature and thus the rates of devolatilisation and char combustion or the simplicity of the models used.

Although the particles follow approximately the same trajectories, it is seen that the particle weight losses experienced in Case iv-1, Fig.5.22.b, are much slower than those in Case iv-2, Fig.5.22.a. This is due to the lower amounts of volatiles release in Case iv-1, no doubt as a consequence of its lower proximate content which explains the lower temperatures that the particles achieve at the IRZ. In the post flame region, where the temperature drops significantly, the heterogeneous reaction is limited in the model by the chemical factor and thus the lower pre-exponential factor measured by Wall et all [1986] slow down the reaction resulting in the lower burnout associated to Case iv-1 as evidenced by the experimental data. It is worth-noting that the lower pre-exponential factor used for the low volatile coal in Case iv-1 can be attributed to the reduced porosity in the remaining char as suggested by Laurendeau [1978] and Smoot and Smith [1985]. Additionally and more obviously, is that the coal of Case iv-1 has relatively more carbon to burn thus requiring longer residence times.

5.5.3 Radial Profiles

Fig.5.21.b and 5.23.b show comparisons between the predictive and experimental radial profiles of gas temperature and oxygen concentration for Case iv-1 and iv-3 respectively. In Fig.5.23.b, the pairs of data points represent measurements at either sides of the axis and demonstrate the degree of flow symmetry. The measured oxygen concentration profiles show the structure of the flame more clearly than do the ones of the gas temperature which are rather flat due to the smoothing effect of the thermal radiation. The quality of the predictions, on the whole may be described as fair. At the first measurement station of Case iv-3, located at the quarl exit ($x/D = 1.0$), the oxygen concentrations are well predicted. However, at the next station downstream significant discrepancies exist between the measured and predicted oxygen concentrations, particularly near the axis. Detailed measurements in the NBR have revealed that rapid devolatilisation occurs in the near axis region. The decrease in oxygen concentration in this region is due to the combined effects of volatiles ignition and mixing with the recirculated combustion products; both these processes are significantly overestimated by the existing physical models. Further downstream, discrepancies neat the axis are due to the less penetration of coal particles into the IRZ as confirmed by the LDA measurements. The predicted gas temperatures are generally in better agreement with the data. The discrepancy observed in oxygen concentrations at x/D = 2.21 is also reflected in the predicted gas temperatures.

Previous modelling of this type of flames has not been particularly successful, Sloan et al [1986] stressing the difficulty to understand wether the discrepancies in the data comparisons are due principally to the recirculation zone aerodynamics, to the limitations in combustion chemistry, the point of ignition or the empirical deficiency in the particle dispersion model.

5.6 PARAMETRIC TESTS

A detailed parametric study of model predictions has been effected in order to try and identify the deficiencies of the mathematical model.

5.6.1 The Discretisation Scheme

The presence of numerical diffusion resulting from the use of hybrid scheme might be damaging to the solution accuracy even with the use of a relatively fine grid (51x37). As it was aimed to validate the physical models incorporated in the mathematical model, it was necessary to upgrade the discretisation scheme used. We have thus introduced the quadratic upstream-weighted differencing scheme known as QUICK, Leonard [1979], to the momentum equations. It was not incorporated in the k-ε equation and the scalar equations as these are source dominated and thus the effect should not be large and in any case debilitating overshoots can result. The details of the method used in incorporating the QUICK scheme was previously explained in section 3.3.1.4.

The effect of the discretisation scheme on the present cases was studied through comparing their performance in calculating the aerodynamic features of the ICSTM furnace for the SCO burner. Fig. 5.24 shows the different flow patterns resulted from each of the two schemes for an isothermal case of inlet conditions identical of the combustion case iv-1. As can be seen from the stream lines plots the hybrid scheme solution fails to predict an IRZ and only shows the ERZ unlike the QUICK scheme solution that shows both bubbles. The difference in performance of the two schemes illustrates the damaging effect of numerical diffusion for the cases under consideration and justifies the additional computational costs brought by the use of the QUICK scheme.

The performance of both schemes was studied for the combustion case. Fig. 5.25 shows the effect of the discretisation schemes on the gas temperature and oxygen concentration as compared with the experimental measurements of case iv-1. It is evident that there is a difference in the oxygen predicted. This difference is a result of a slightly different prediction of the size of the recirculation zone and a longer primary jet and particle penetration into the IRZ. The comparison shows less effect on the predicted gas temperature which is less dominated by the effect of aerodynamics as a result of the radiation. The oxygen concentration predictions obtained for x/D = 7.57 and x/D = 12.93 are in better agreement with the measurements for the QUICK scheme. The lower oxygen levels obtained are a consequent of the larger IRZ predicted resulting in higher devolatilisation and char combustion rates. However, the improvement brought to the nearer to the burner oxygen concentration of the station at x/D = 2.21 is less definitive. The QUICK scheme results only show better agreement with the measurement at the ERZ. The overall comparison between the two schemes is thus debatable showing that the discrepancies experienced at x/D = 2.21 are more a result of physical modelling than of the numerical methods applied.

5.6.2 The Inlet Conditions

The sensitivity of the predictions to the shapes of the inlet velocity profiles and turbulence levels were examined for several cases and the results shown here are for Case iv-3. The uniform initial velocity profiles for the primary and secondary streams were replaced by a scaled profile from the isothermal measurements for the cases of the CCRL furnace and a one-seventh power-law profile for the primary stream and measurements at a S_0=0.78 given by Lockwood and Mahmud [1988], for the secondary stream of the ICSTM furnace. The predicted flow field and the resulting flame for the CCRL cases were sensitive to the inlet velocity profiles when compared to those obtained using constant profile and swirl numbers suggested by McAscill [1987] while those for Case iv-3 of the ICSTM furnace as shown in Fig. 5.26 were relatively insensitive to the changes. The variations obtained for the CCRL cases may be due to the confusion that is sometimes associated with defining the reported experimental swirl value that can be always cleared in the presence of measured inlet velocity profiles. The effect of the inlet turbulence intensity was also studied. The results were as insensitive to this parameter as to those obtained when varying the velocity profiles. The effect of altering the assumed number of discrete particle size groups was also examined. The results of calculations using four and seven particles differed little.

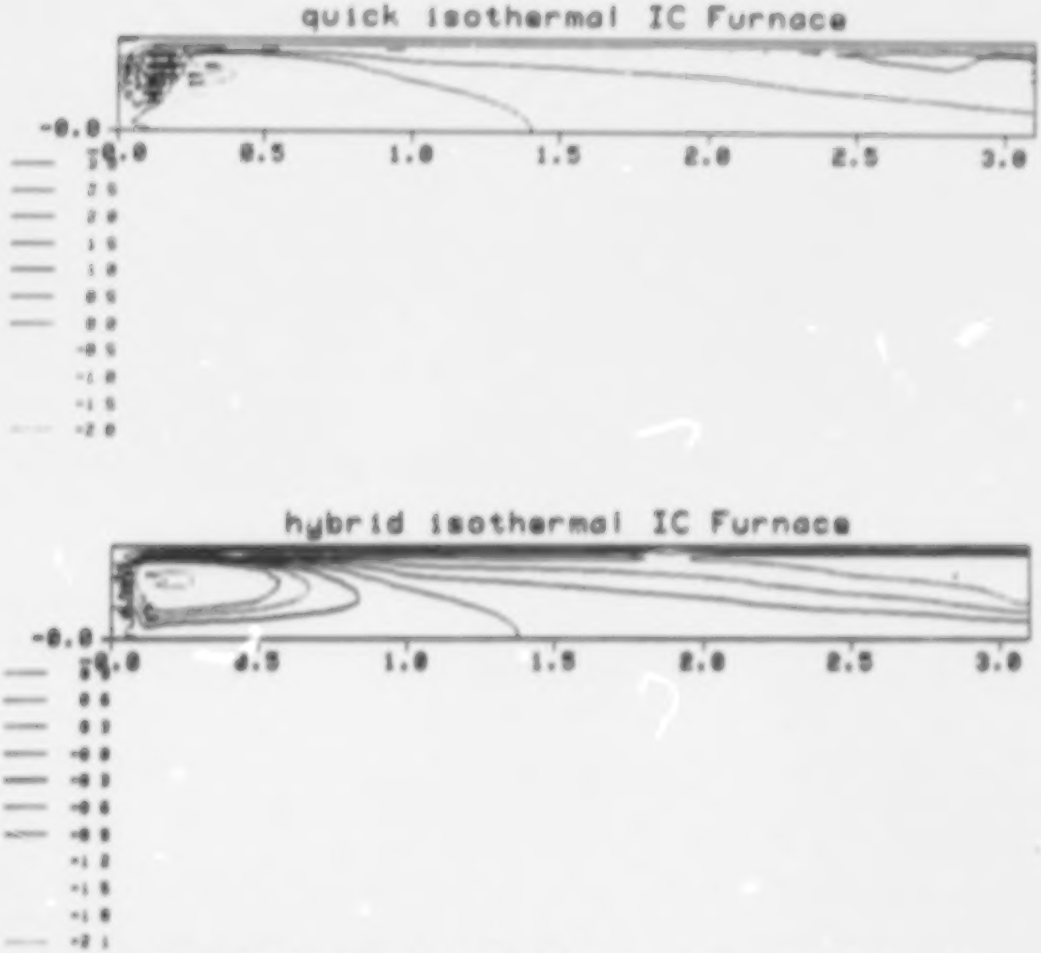

Figure 5.24 Contours of stream function for isothermal prediction of the SCO burner using Hybrid and QUICK discretisation schemes.

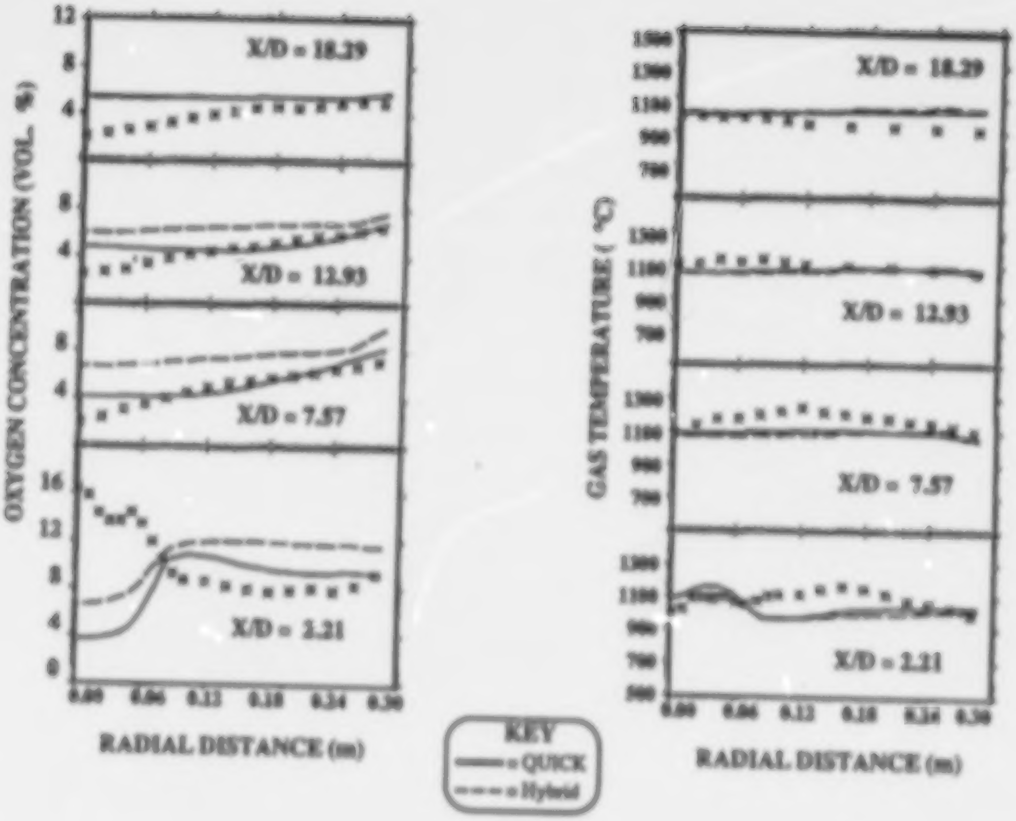

Figure 5.25 The effect of the discretisation scheme on the prediction of Case iv-1.

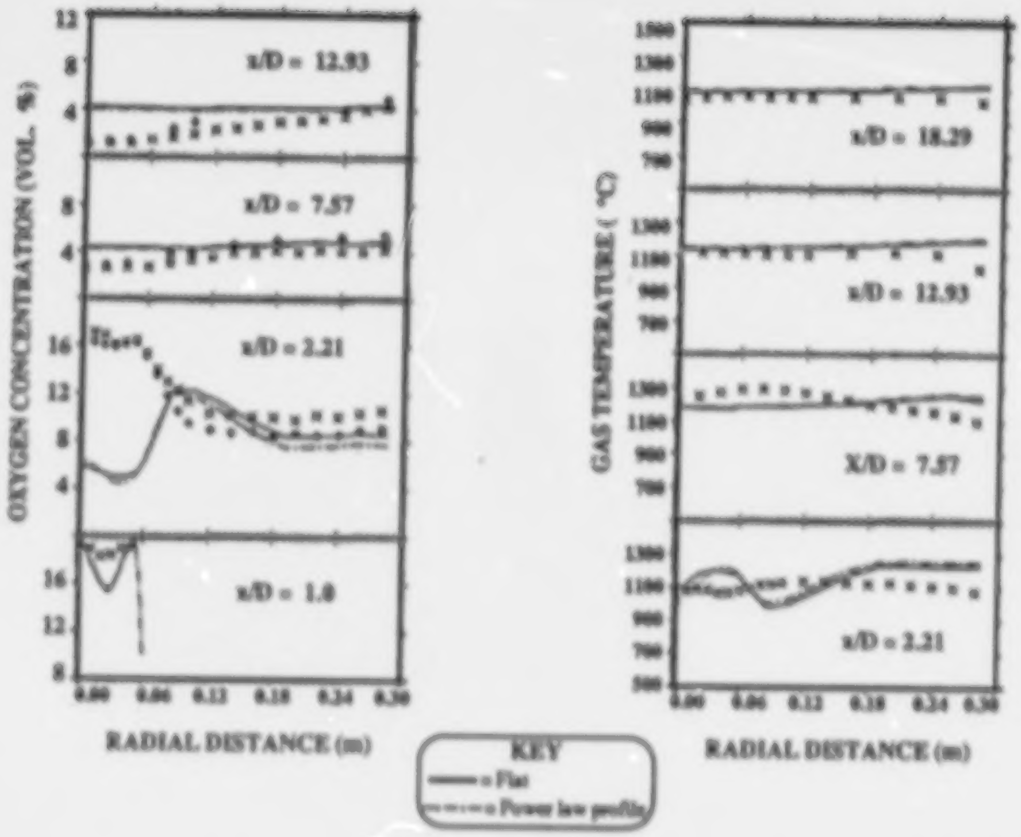

Figure 5.26 The effect of the inlet profile on the prediction of Case iv-3.

5.6.3 Coal Devolatilisation

In the absence of pyrolysis data for the studied coals, the sensitivity of PF flame predictions to the ultimate volatile yield and volatiles kinetic parameters was examined by using a first-order single reaction devolatilisation model.

5.6.3.1 Volatile yield:

The total volatile yield depends upon the heating rate and final temperature. Gibbins [1988] measured the volatile yields for a bituminous coal sized 100-150μm. The heating rates studied were 1 and 1000 °k/s with 30 seconds hold time at peak temperature. The total volatile and tar yields were found to be higher for the higher heating rates. The ultimate volatile yield, V*, for the high heating rates that range between 10^4 and 10^5 °k/s and final temperatures above 1500 °k of coal particles injected into swirling pulverised coal flames is greater than that determined in a proximate analysis, VM. In the present study, the 'Q factor' (defined as V*/VM) was assigned a value of 1.2 for the high volatile coals and 2.2 for the low volatile coals. Wall et al [1986] measured the Q-factor at 1700 °C of 1.48 for a subbituminous coal and 2.38 for a low volatile bituminous coal.The effect of varying the Q factor on the predictions, within the range of 1.2 to 1.7, is shown in Fig. 5.27. In general the predictions are relatively insensitive to the values of Q within the considered range, except very near the burner, at $x/D = 2.21$, where the predictions are somewhat sensitive to the Q factor. The influence of the enhanced volatile yields on the predictions depends on the coal volatile content and level of excess air. The present results conform the findings of Lockwood et al [1984], Truelove [1984], Knill et al [1990] and Visser [1991] for high volatile coals. In contrast, an enhanced sensitivity for volatile deficient coals was reported by Wall et al [1986] which suggest that the influence of volatile yields on the predictions depends on the coal volatile content.

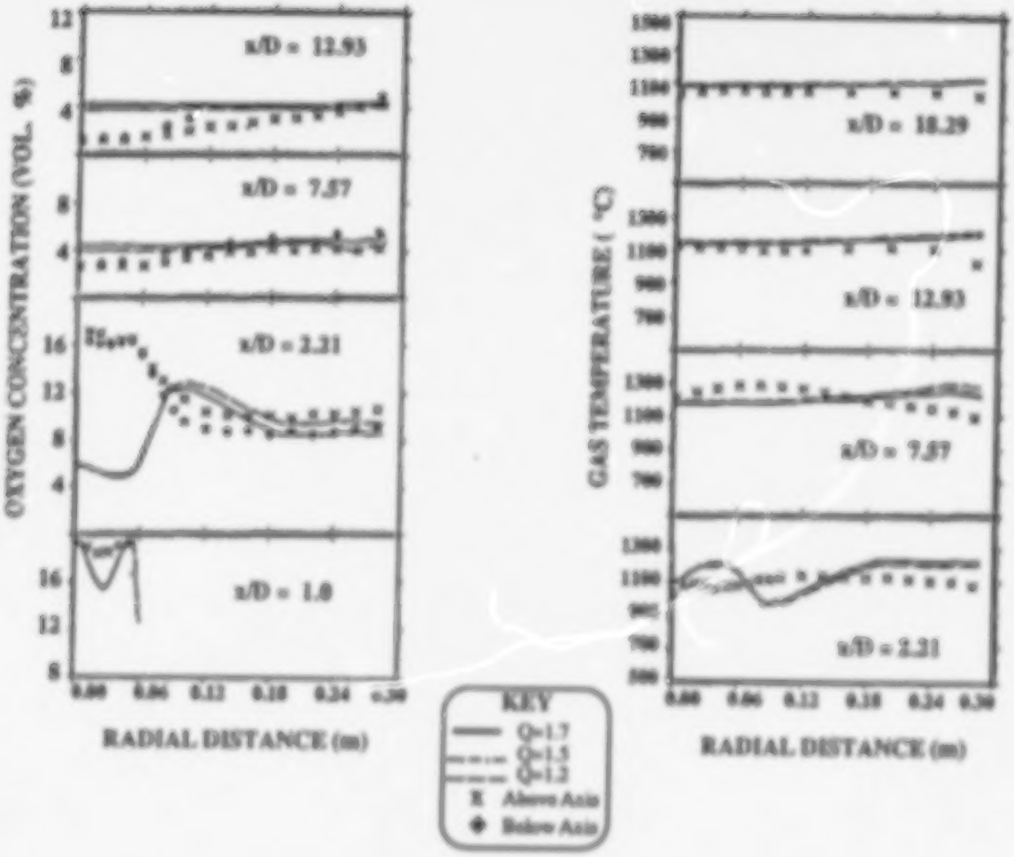

Figure 5.27 The effect of the volatile yield on the prediction of Case iv-3.

5.6.3.2 Devolatilisation kinetics

Pyrolysis kinetic data reported in the literature are generally obtained at heating rates and/or temperatures which are relatively lower than those encountered in furnaces. The reported rates ofdevolatilisation also differ significantly. The predictions using the kinetic parameters for high volatile bituminous coals reported by Badzioch and Hawksley [1970], Golberg and Essenhigh [1979], Anthony et al [1975], Truelove and Jamaludin [1986] and Fletcher [1989], given in Table 5.1, are presented in Fig. 5.28. An insensitivity of the predictions to the kinetic parameters of Badzioch and Hawksley [1970], Golberg and Essenhigh [1979] and Anthony et al [1975], where the rates vary by a factor of about 4, is evident. The kinetic data reported by Solomon et al [1986] and Fletcher [1989] were also unsuccessful; they produced too rapid devolatilisation. Extensive variations of the kinetic constants, within the acceptable limit, produced no significant improvement. It is evident that extraordinarily high values of activation energy or low values of the pre-exponential factor would have to be sought to enhance the quality of the predictions in the NBR. The application of the multiple parallel reaction model also failed to produce any improvement, the rate of devolatilisation was faster than that of the single reaction model.

Table 5.1

Kinetic parameters for the Single Reaction Devolatilisation Model

Ref.	Pre-exponential factor (s^{-1})	Activation Energy (J/kmol)	Experimental Conditions Heating rate,K/s	Temperature,°K
Badzioch & Hawksley [1970]	0.836×10^5	74.0×10^6	$2.5 - 5.0 \times 10^4$	1273
Golberg & Essenhigh [1979]	5.5×10^5	78.7×10^6	10^6	800 - 1700
Anthony et al [1975]	0.2×10^5 *	49.4×10^6	$100 - 1.5 \times 10^4$	670 - 1270
Solomon et al [1986]	4.28×10^4	228.5×10^6	$>2.5 \times 10^4$	873 - 1208
Fletcher [1989]	2.3×10^{14}	230.3×10^6	10^4	1050 -1250

* Original value of pre-exponential factor was modified by Solomon et al [1986].

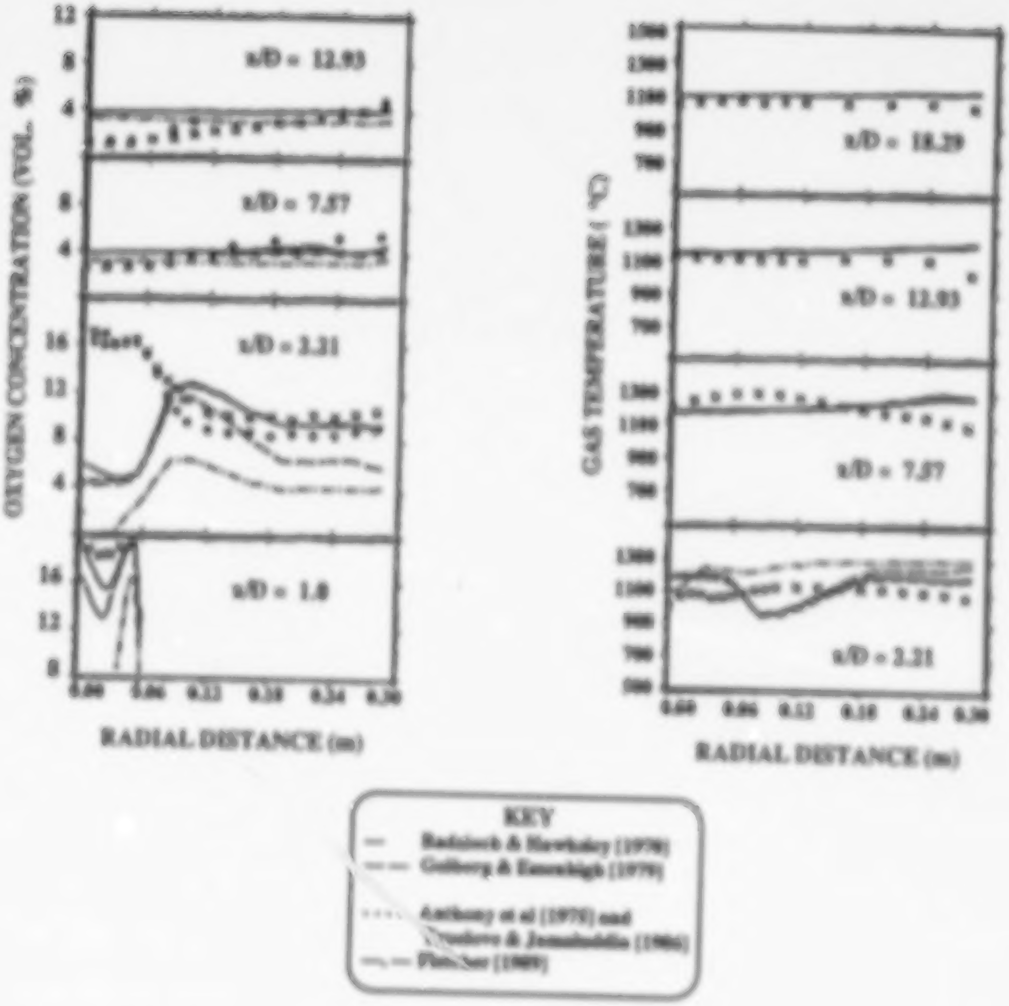

Figure 5.28 The effect of the volatile kinetics on the prediction of Case iv-3.

* Original value of pre-exponential factor was modified by Truelove and Jamaluddin [1986]

5.6.3.3 Ignition Delay

The initial products of the volatiles released from the coal particles are composed of heavy tars which account for up to 70% by mass of the volatile release, see for example Saxena (1990), Stiles and Kandiyoti [1989] and Li et al [1991]. These are decomposed to lighter forms before reacting with the oxidants and igniting. This complicated procedure is not accounted for in the incorporated simple single reacting model. A sensitivity study was made as follows: An amount of volatile matter was allowed to be released and to accumulate before ignition was initiated. A similar approach was followed by Jamaluddin et al [1987] and Agarwal [1986]. The initial amount of volatiles to be released before ignition was altered between 0 and 15% of the total amount of volatiles for Case iv-1. The effect of ignition delay on the prediction as compared to the experimental measurements is shown in Fig. 5.29. It is observed that this alteration had no effect on the qualitative trend of the prediction.

5.6.3.5 Secondary Cracking

A simple model accounting for the the secondary cracking of heavy tars into light hydrocarbons was based upon the proposals of Suuberg et al [1979] which was previously explained in section 2.6.4.2. The procedure suggests that the initial product of coal pyrolysis is in the form of heavy tar. This is latter converted into light hydrocarbons by a secondary reaction. The rate constants for the tar formation, considered to be first-order in the amount of tar yet to be formed, are taken to be that of Table 4.7. The secondary reaction is assumed to have a rate constant expressed in Arrhenius form. A pre-exponential factor of 10^{13} s^{-1}, which is typical of many unimolecular decomposition reactions, and an activation energy of 27.2×10^{7} J/kg-mol have been used.

Figure 5.30 shows the comparison of measurements with predictions with the effects of secondary cracking included in this way. Ignition is delayed resulting in

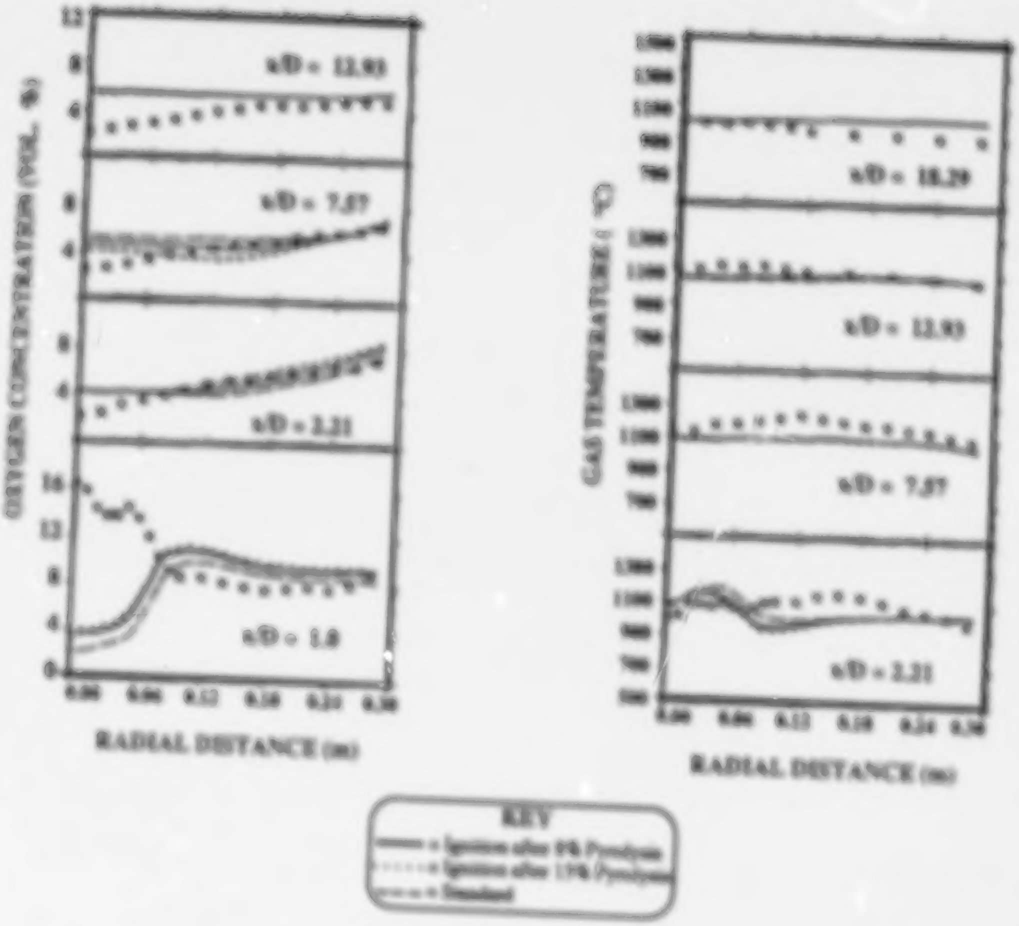

Figure 8.29 The effect of the ignition delay on the prediction of Case ii-2.

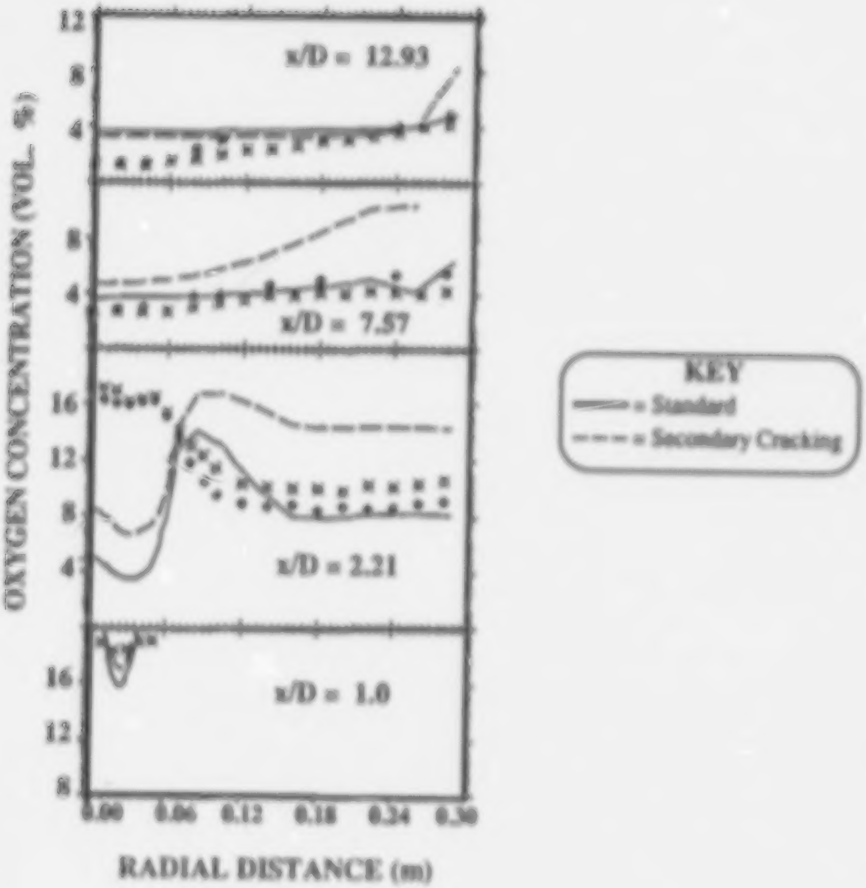

Figure 5.30 The effect of secondary cracking on the prediction of Case iv-1.

higher concentrations of oxygen calculated for the critical station at $x/D = 2.21$ across the whole radial profile. However, the overall predictive quality is not improved. A probable implication is that it is defects in the flow pattern rather than the delayed ignition that is responsible for the predictive discrepancy.

5.6.4 Char Reactivity

In the absence of measured char reactivity data for the Gedling coal, the sensitivity of the predicted burnout of the assumed char combustion kinetics was explored. The pre-exponential factor was varied while the activation energy, E_c, was fixed at 71×10^6 J/kg-mol following the recommendation of Wall et al [1986]. Values of the predicted burnout averaged over the furnace cross-section are compared with the data for this quantity collected along the furnace axis. Burnout is here defined as the ratio of the mass loss of combustibles to the total mass of combustibles in the input coal. Very near the burner, the apparent rapid burnout is due mainly to the release of volatiles. Further downstream, where devolatilisation is essentially complete, the burnout varies slowly with axial distance. Previous numerically optimised, Lockwood et al [1984], char reactivity data overestimate burnout at the furnace exit. The prediction with A_c=0.0006 kg/m^{2}s procures the best agreement with the data. This value is lower than those obtained in drop-tube studies, as reported by Smith [1982] but it is within the range of values extracted from the IFRF plug flow reactor data using a zone type mathematical model by Wall et al [1986]. A recent study of swirling flame in a furnace similar to that of ICSTM by Truelove and Holcombe [1991] burnout is overpredicted at the furnace exit, even when the measured char reactivities for the three coals fired were employed. This can be attributed to the presence of a percentage of coal particles of sizes greater than those specified at the inlet of the burner. Moreover, the drop-tube measurements of char reactivity generally do not include the final 10% of burnout; whereas burnout greater than 90% is controlled by the unreactive coal macerals, Tate et al [1987]. A char combustion model has been proposed by Tate et al [1987], assuming char having reactive and unreactive fractions properties of the coal, possessing different chemical rate constants. Better agreement with the drop-tube burnout has been obtained using this model compared with the conventional one.

5.6.5 Coal Demoisturisation

It is known that the devolatilisation process is preceded by the evaporation of the moisture content of the coal, see for example Suuberg et al [1978]. This fact has not previously been accounted for in our mathematical model. Since this process is likely to cause some delay in the ignition, a modification was modelled to account for demoisturisation. The moisture content has been subtracted from the volatile yield and treated separately. The evaporation of moisture from the particle was modelled as a diffusion controlled process, the rate of evaporation being:

$$R_m = h_m\left(P_{m,p} - P_{m,g}\right)\left(\pi d_p^2\right) \qquad (5.1)$$

h_m represents the mass transfer coefficient, and is given as;

$$h_m = \frac{Sh.D.M_m}{R_g T_g d_p} \qquad (5.2)$$

The Sherwood number of mass transfer for the particle Sh, is a function of the relative velocity between the gas and the particle calculated in the same way as the Nusselt number. $P_{m,p}$ and $P_{m,g}$ are the partial pressure of water vapour at the particle surface and in the bulk gas respectively. $P_{m,p}$ is approximated by the vapour pressure of water at the prevailing particle temperature using Antoine's equation following Jamaluddin et al [1987].

The source term representing the vapour evolved is added directly to the products concentration of the corresponding cell. The latent heat absorbed from the particle as the evaporation takes place is reduced from the particle heat balance.

The effect of this modification was assessed through the prediction of the SCO burner case measured by Abbas et al [1991]. The particle history showed that devolatilisation has been delayed for approximately 0.04 s. The aerodynamic features of the two predictions were almost identical as expected. The volatile concentration in all the domain was reduced, as a consequence of reducing the total yield by the moisture content which was given directly to the product concentration. The comparison shows that accounting for the demoisturisation shifts the location of ignition an axial distance of about 35 mm. Though the mass release of volatiles was reduced in concentration the combustion value is the same since the combustible amounts were preserved. Thus the temperature and oxygen concentration fields are hardly affected.

5.6.6 Gas Phase Combustion

Modelling of gas phase volatiles combustion presents one of the major difficulties in simulation of PF flames. The eddy-dissipation combustion model of Magnussen and Hjertager [1976], the simplicity of which renders it open to criticism, has been employed in the present study.

5.6.6.1 The empirical constant

As being explained earlier in chapter 2, the volatiles burning rate is related to the time scale of the large-scale eddies through an empirical constant, A, which has been assigned a value of 4.0 based on numerical optimisation. The predictions of species concentration and gas temperature are found to be too sensitive to A in the NBR. An extensive sensitivity study of A was carried out and it was found that the optimum value of A ranges between 0.2 and 0.8 for the ICSTM furnace cases. For Case iv-3, a further reduction of A in order to increase the level of on-axis oxygen concentration at x/D = 2.21 resulted in significant over-prediction of oxygen concentration elsewhere in the furnace. A similar value of A has also been used by others,Truelove and Holcombe [1990], Visser et al [1991] and Visser [1990] in order to improve the predictions of species concentration. The originally recommended value of A lacks universality. The physical significance of this modification is that the characterisic life time of the fluid eddies which equal k/Aε, is much longer than assumed. Visser [1991] compared the time scale with other time scales, The Taylor scale and the mean eddy life time as given by Hinse [1975]:

Taylor scale $\tau = 4\frac{k}{\varepsilon}$ (5.3)

Mean eddy life time $\tau = 0.16\frac{k}{\varepsilon}$ (5.4)

Accordingly, if the mixing process of fluid eddies of fuel and oxygen are dominated by the Taylor scale a value of o.25 would be assigned to A. If the process is dominated by the mean eddy life time a value of 6.25 would be assigned to A. Both the present work and that of Visser[1991] suggest that the characteristic life time experienced in the simulation of swirling pulverised coal flames is much closer to the Taylor scale. It should be noted that the higher values of A were suitable in predicting the CCRL cases of stage ii which are of high momentim ratio and low overall swirl level.

It should be noted that the calculation of mixing-controlled volatiles burning rates depends strongly on the accuracy of predicted turbulence quantities. Nevertheless, it can be concluded that further research is required to correlate A in terms of the combustion and aerodynamic parameters.

5.6.6.2 The volatiles chemical kinetic rate

In the present study, the volatiles are assumed to burn in a partially premixed state. The influence of chemical kinetics on the volatiles burning rate was examined by calculating a kinetic rate from an Arrhenious type expression recently given by Shaw et al [1990]; and the lesser of this rate and that of the eddy-dissipation model is used. Fig. 5.31 shows the predictions obtained when employing this formulation for the gas combustion. It is found that the volatiles burning rate was essentially controlled by the rate of mixing as can be concluded from the similarity between these predictions and those obtained for a standard formulation as those shown in Fig. 5.23.b for the same case. This conclusion differs from that of Azevedo and Carvalho [1991] who observed some differences due to small modifications in the flow field when predicting data obtained for the same burner by Godoy et al [1988]. The dissimilar effects of the modification can be attributed to the difference in the values used for the empirical constant A, since these authors employed a value of 3.5, 17.5 times greater than the value employed in the present calculation for that burner.

The examination of the local turbulence Reynolds numbers and time scale; and the good prediction of a natural gas flame for the same burner, Costa et al [1990] indicated that significant retardation of the gas phase combustion due to finite chemical kinetic rate was unlikely at least for the natural gas fuel.

5.6.6.3 The flammability limits

Attempt was also made to delay the volatiles ignition in the NBR by introducing the flammability limits. Unfortunately, due to the complex composition of the volatiles and the extreme variability of the conditions prevailing in PF flames, it was extremely difficult to determine the flammability limits for the volatiles ignition. Calculations were performed using flammability data for methane in air; the imposition of this condition is likely to be an exaggeration of reality. The predictions show an increase in oxygen concentration near the axis at $x/D_b = 2.21$ compared to that shown in Fig. 5.32 but is still less than the data. Further downstream, due to the localised ignition, the predicted oxygen concentrations are considerably higher than the measurements and a significant amount of volatiles escape unburnt from the furnace which is not observed in reality.

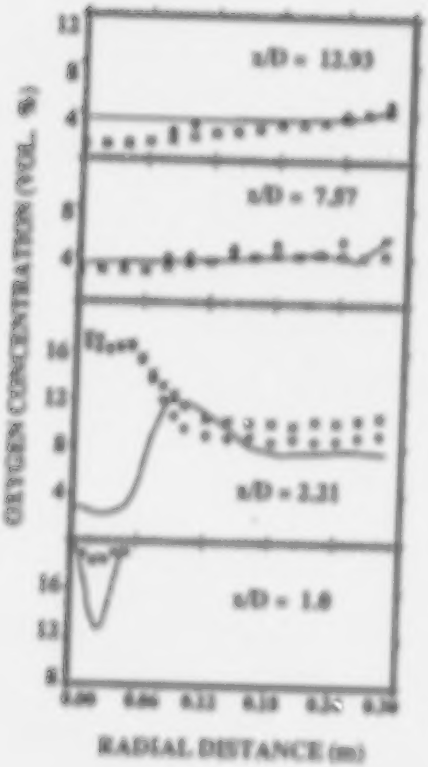

Figure 5.31 Predictions obtained when using the chemical and mixing limitations on gas combustion for Case iv-3.

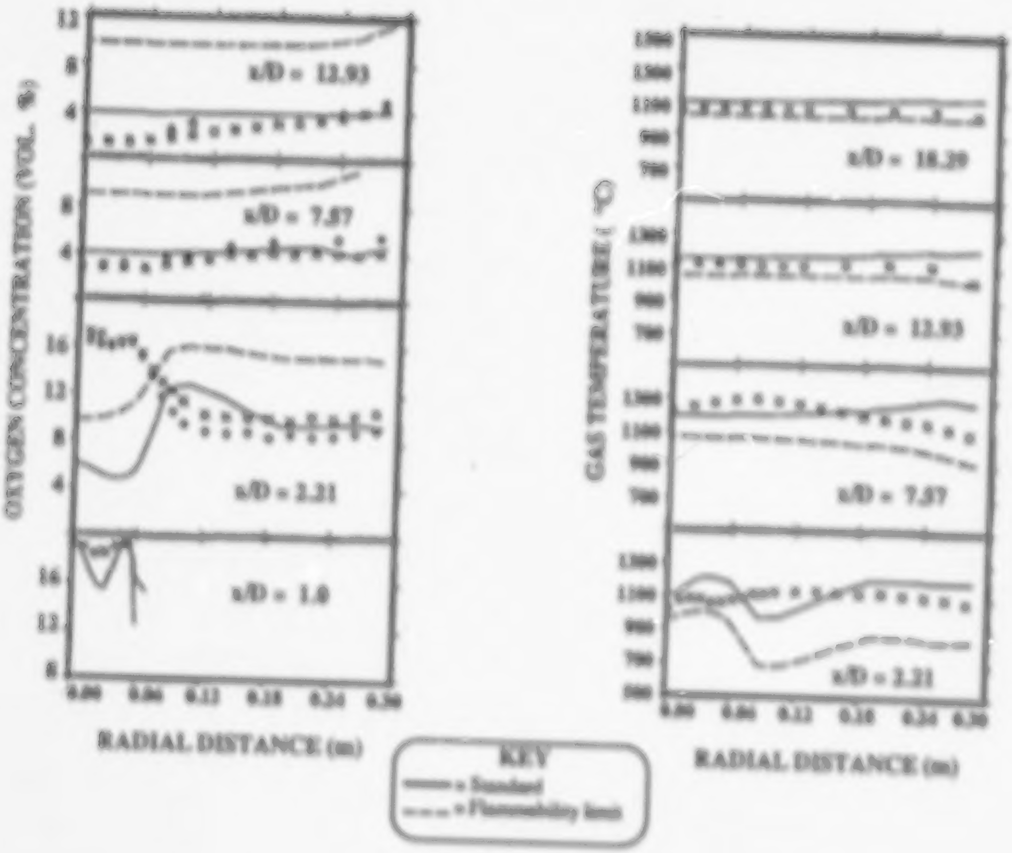

Figure 5.32 The effect of flammability limits on the prediction of Case iv-3.

5.6.7 Effects of Other Parameters

5.6.7.1 Particle size distribution

As mentioned before four particle sizes was used to represent the coal size distribution. Calculations were performed using four sizes with two different distributions and also seven particle sizes; the predictions were somewhat insensitive to the number of particle sizes and their distributions.

Another exercise was performed to assess the effect of particle size on the combustion behaviour. This was undertaken using the experimental data obtained for Case iii-2 for the ICSTM furnace. The particles initiated at the burner pipe were assumed to be mono-sized. The exercise was repeated twice with particle diameter used 125μm and 25μm respectively.

Fig. 5.33 shows the near burner aerodynamic features and the particle trajectories and the comparison between predictions obtained using the 125μm diameter particles and measurements. The large sized particles resulted in longer penetration depths of the particles into the IRZ. The particles larger size also resulted in slowing down the char combustion reaction rate which was pronounced in the lower temperature levels calculated near the axis for $x/D = 5.1$ and 7.6 if compared with those previously obtained for a uniform distribution of particles in Fig. 5.20.b.

Fig. 5.34 shows the near burner aerodynamic features and the particle trajectories and the comparison between predictions obtained using the 25μm diameter particles and measurements. The particles, owing to their small momenta, failed to penetrate the IRZ and very depressed temperatures were calculated and the oxygen concentration was overpredicted inside the IRZ. Comparing the two exercises, it can be concluded that for such aerodynamic flow pattern; although the finer particle sizes improve the exit burnout due to their rapid reaction rates, they might reduce the

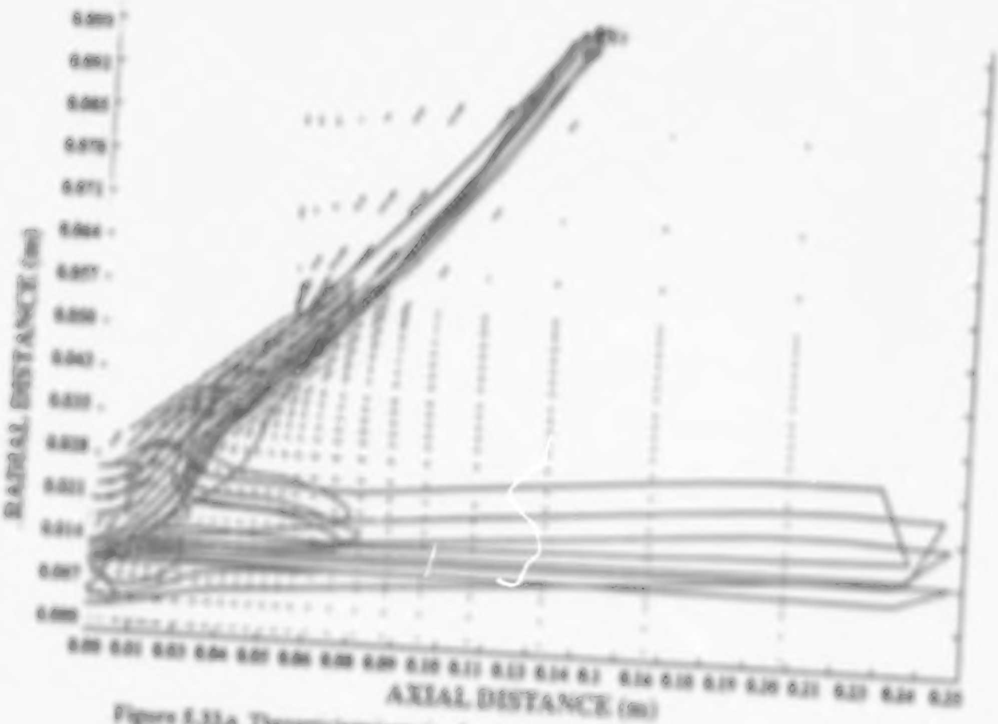

Figure 5.33.a The particle trajectories for the large size particles (dp=125μ) for Case iii-2.

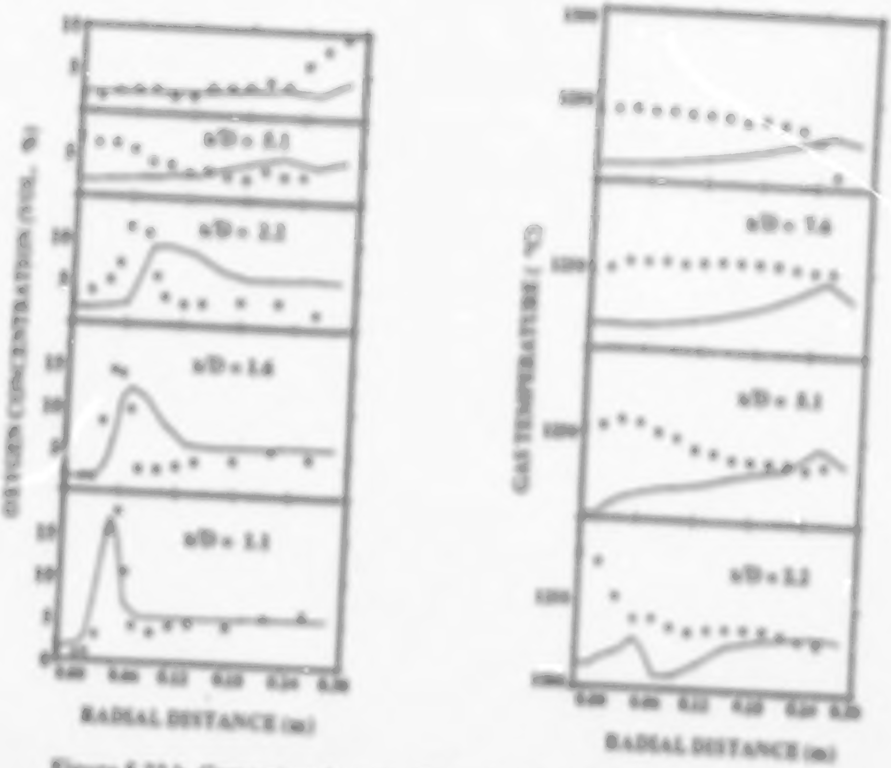

Figure 5.33.b Comparison between the predictive and experimental radial profiles of oxygen concentration and gas temperature for Case iii-2 using large size particles (dp=125 μ)

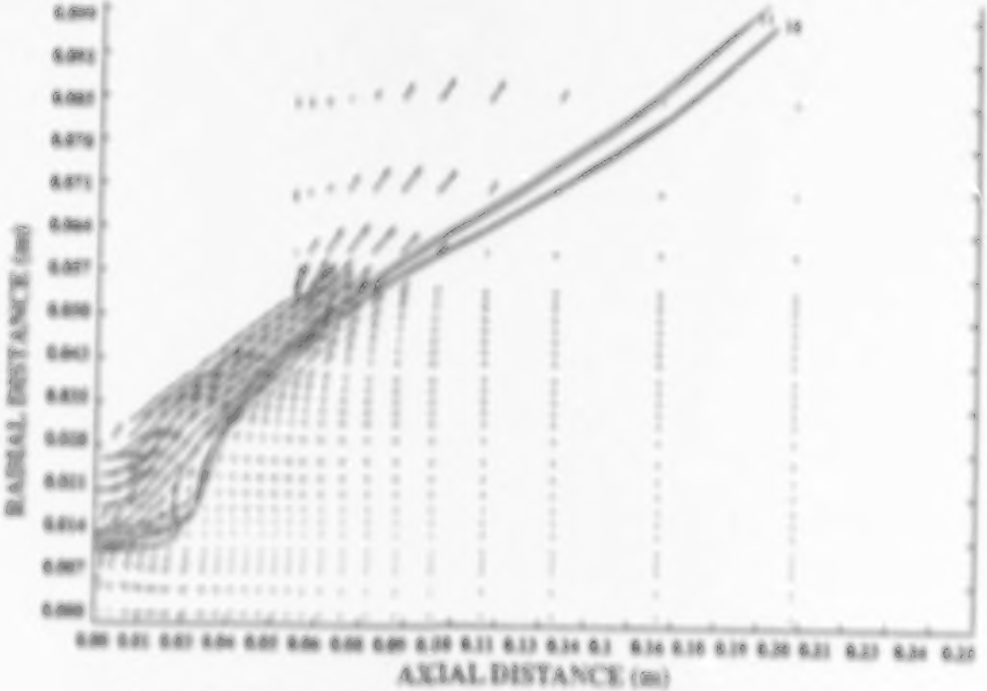

Figure 5.34.a The particles trajectories for the small size particles (dp=25μ) for Case iii-2.

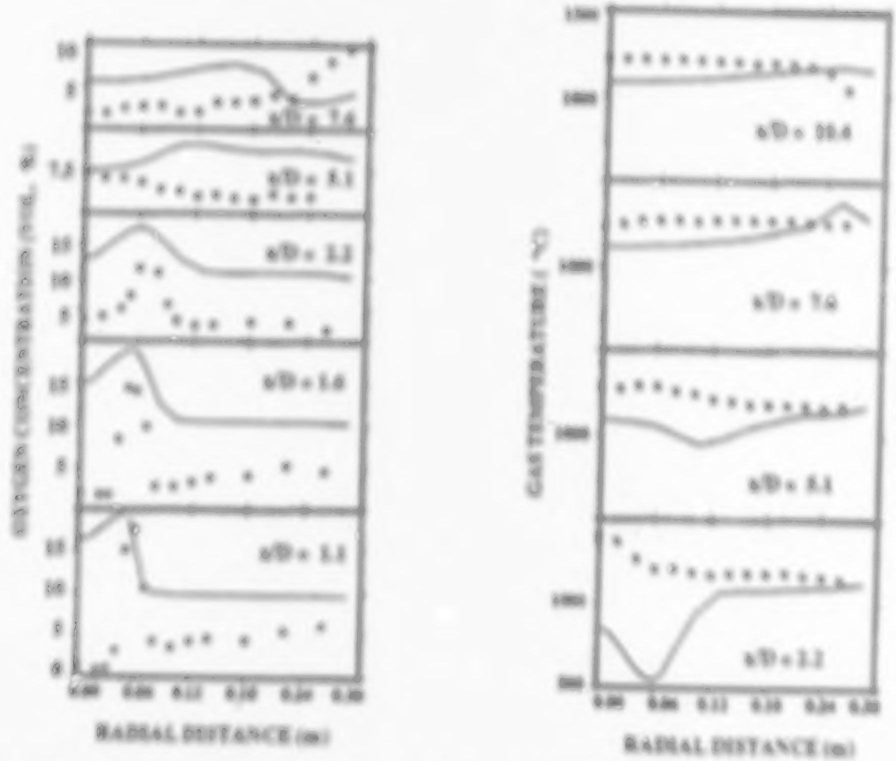

Figure 5.34.b Comparison between the predictive and experimental radial profiles of oxygen concentration and gas temperature for Case iii-2 using small particles (dp=25 μ).

stability since less particle penetration will take place into the IRZ which will, in consequence become relatively cooler.

5.6.7.2 Drag coefficient

The effect of particle drag coefficient on the predictions was studied. A large reduction in the drag coefficient resulted in deeper penetration of the coal particles into the IRZ. This improved predictions of oxygen concentrations further downstream of the burner as can be shown in Fig. 5.35, however, at x/D = 2.21 the predictions are little affected.

5.6.7.3 Effects of soot in radiation heat transfer

The production of soot in the volatiles rich NBR affects the local gas temperature through its effect on the absorption coefficient of the medium. The formation and consumption of soot is a complex process and no attempt has been made to construct a detailed model. An approximate account of the presence of soot in the radiation calculations was achieved by assuming that soot concentration is proportional to the volatiles burning rate. The predicted temperature field in the NBR was somewhat depressed by this action and the oxygen concentration levels were marginally increased. Calculations were also made where the emissivities of the refractory walls and the char particles were altered over an acceptable range, again with small effect.

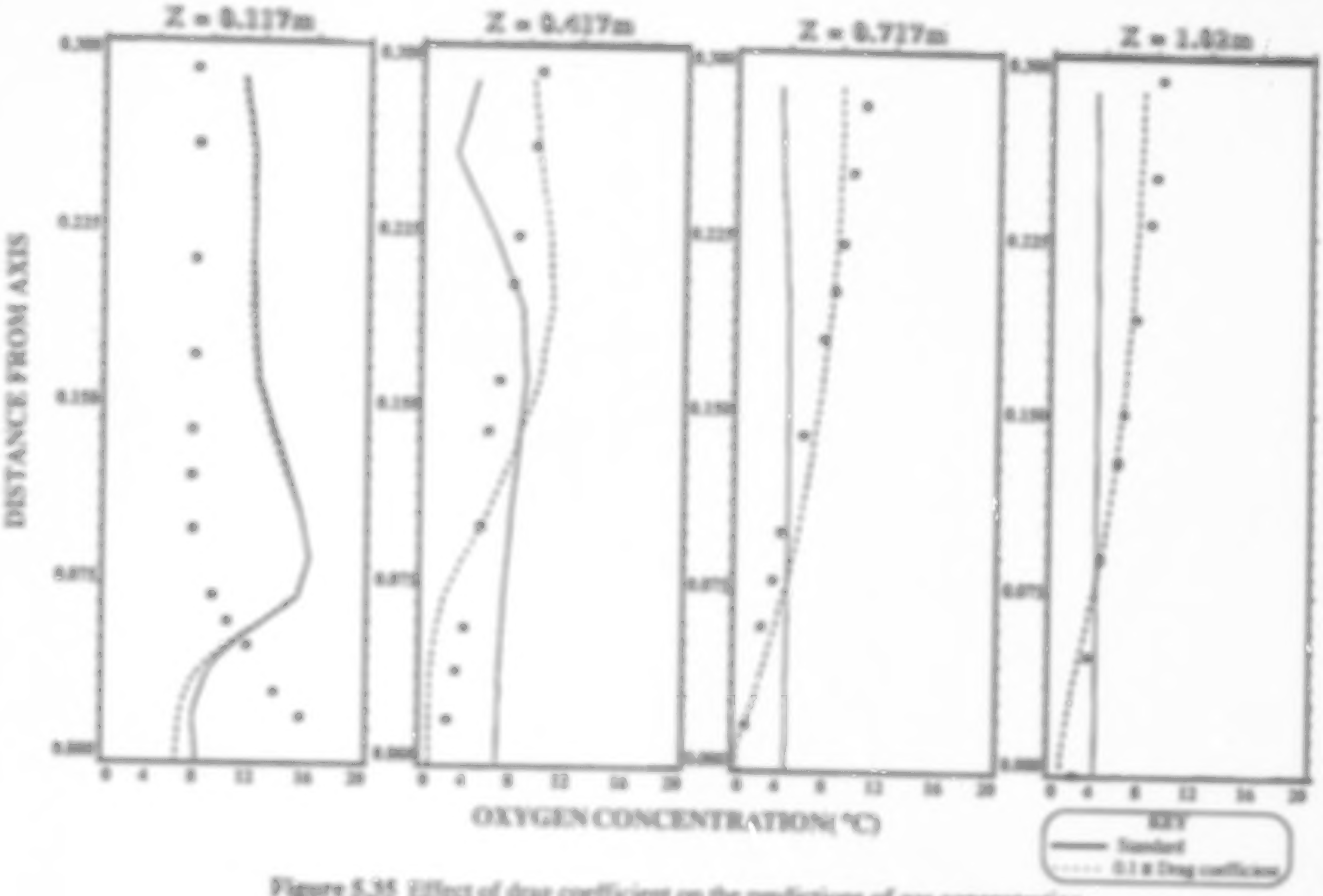

Figure 5.35 Effect of drag coefficient on the predictions of gas concentration.

5.6.2.4. Effect of inlet swirl

Reliable prediction of swirling PF flames in the NBR critically depends on the accuracy of the flow calculation. So far, the eddy-viscosity (k-ε) turbulence model has been widely used for this purpose. In recent studies by Visser et al [1990] the algebraic stress model has been employed but no definite conclusions can be drawn regarding its performance compared to the k-ε model. It is well established that the performance of the k-ε turbulence model is unsatisfactory in predicting swirling flows. In particular, the structure and strength of the IRZ are not predicted correctly. The calculations of swirling natural gas flames for the same burner have shown that the size and strength of the IRZ are significantly overpredicted compared to the LDA measurements taken by Milosevic [1990] and presented in chapter 4. These evidences lead us to suspect that the primary jet penetration is also underpredicted for PF flames. For the type of flow pattern depicted in Fig. 5.21.a, these will have significant effect on the predicted ignition location. In addition, the low oxygen levels predicted near the axis of the x/D = 2.21 station are as a result of this region being located inside the IRZ where the recirculating products of combustion are the main constituent. The measurements, on the other hand, clearly suggest that this region is mainly constituted by the fresh charge of air.

An artificial method of examinig such effect was sought through decreasing the inlet secondary swirl to $S_2 = 0.5$. The aerodynamic flow pattern and particle trajectories obtained for that low swirl is presented in Fig. 5.36.a. Instead of the IRZ being predicted at the proximity of the thickness of the primary pipe and propagated by the quarl and further induced by the effect of the secondary swirl, a much longer penetration of the primary jet was calculated. The particles reverse their direction only at X = 0.235 (X/D = 4.2) with the small size particles burning fully before exiting from it and the larger size particles following trajectories similar to those obtained when using higher swirls with longer axial penetrations. As evidenced in Fig. 5.36.b, the predictions show much better agreement than those obtained previously.

The same reduction of the inlet swirl was applied to the prediction of Case iii-2 (the bluff body burner). Again, Fig. 5.37 showed a better agreement with the measurements than that obtained before using the reported swirl levels.

It can thus be assumed that the k-ε model is over-estimating the swirl decay. However, attempts to improve the performance of the k-ε model through the Richardson number or the variable C_μ as discussed in chapter 2 were unsuccessfull due to the instabilities they brought to the solution algorithm and though the flow pattern was changed to give similar features of those obtained for the reduced swirl case, a fully converged solution was never obtained even when using the hybrid scheme and/or reduced under-relaxation factors.

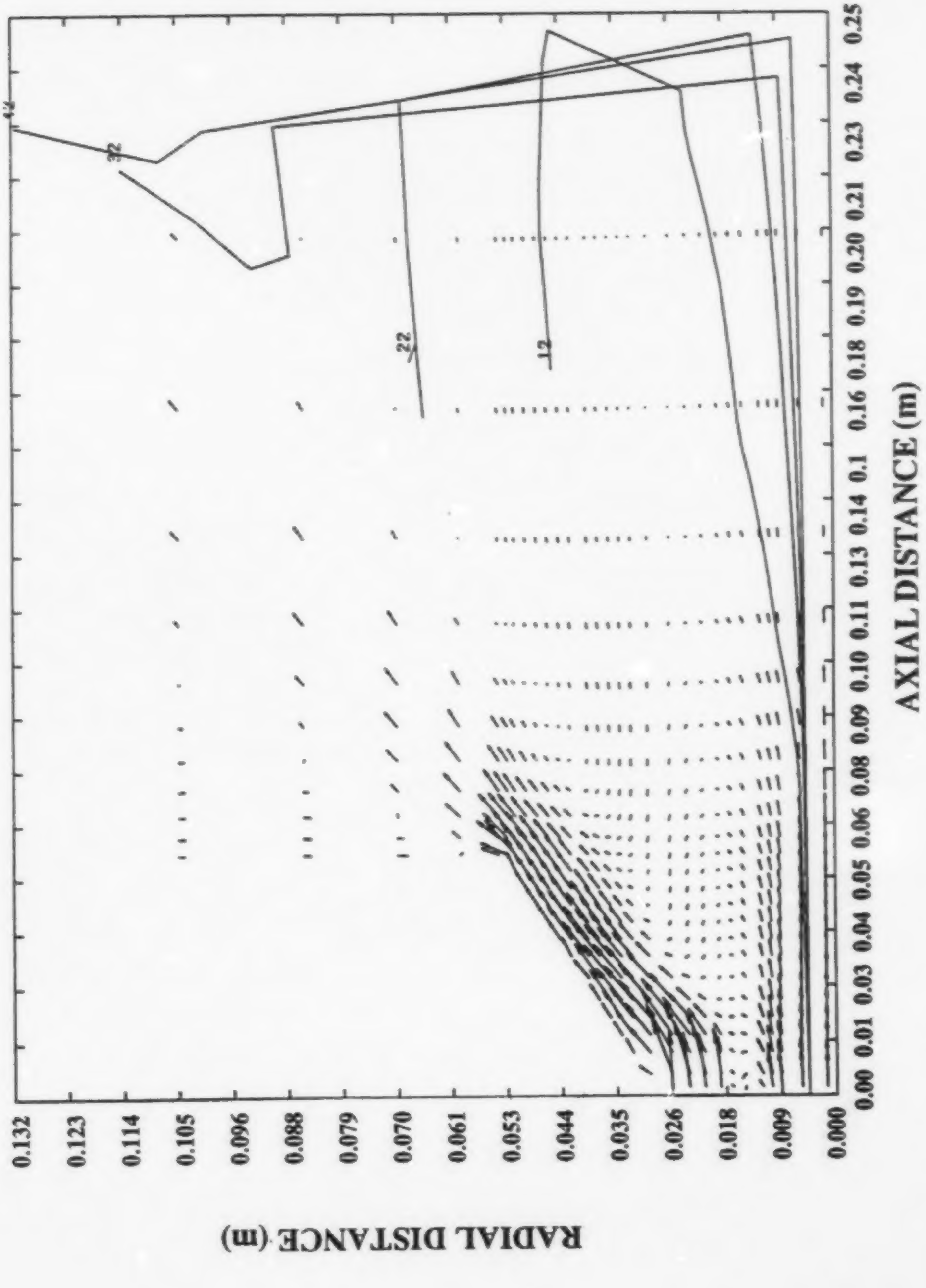

Figure 5.36.a The particle trajectories for Case iv-3 with inlet swirl of 0.5

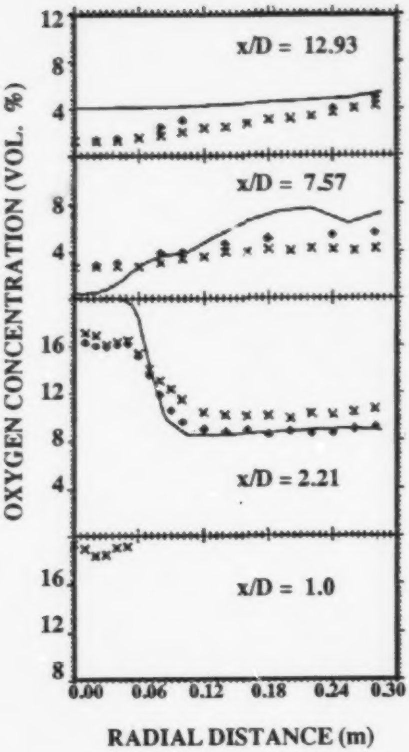

Figure 5.36.b Comparison between the predictive and experimental radial profiles of oxygen concentration and gas temperature for Case iv-3 with inlet swirl of 0.5

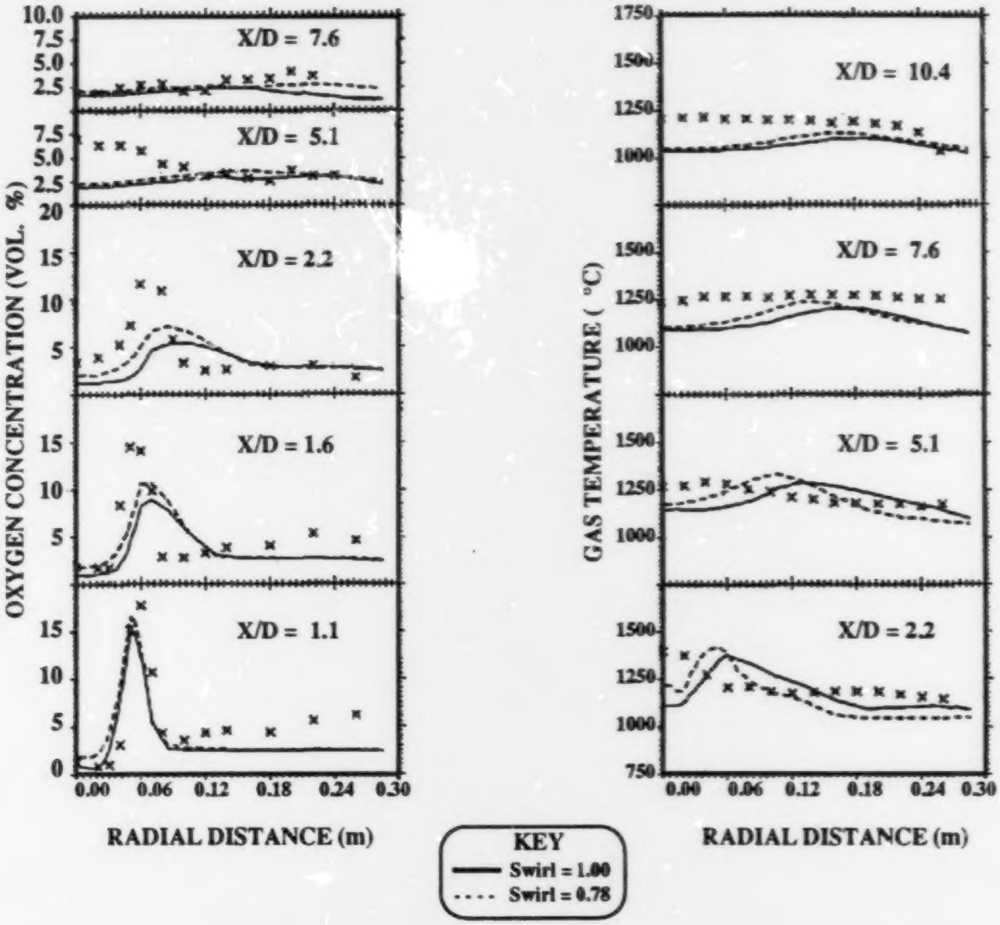

Figure 5.37 Comparison between the predictive and experimental radial profiles of oxygen concentration and gas temperature for Case iii-2, showing the effect of reducing the inlet swirl.

CHAPTER 6

CONCLUSIONS AND SUGGESTIONS FOR FUTURE WORK

6.1 RECAPTULATION

Amongst other applications, the tecniques of computational fluid dynamics are rapidly developing to occupy the front line in the field of research and design of pulverised coal combustors. In this study, the previous efforts in the field of pulverised coal combustion modelling are reviewed. It is observed that most of the prevously available mathematical models are validated only for the overall assessment of the combustor performance without much emphasize of the near burner region. This model is developed with emphasize to this zone as an essential step for succesful prediction of pollution emmisions and stability considerations.

The k-ε turbulence model and a diffusion flux model for radiation are selected. The particle phase is calculated using a lagrangian method where representative particles of different sizes and starting locations are tracked. Demoisturisation is calculated through accounting for diffusional parameters. The particles' pyrolysis is simulated by a first order single reacting devolatilisation model throughout the majority of the cases modelled. A new simple model was formulated to account for the secondary cracking of the initial heavy products of volatiles. The volatiles burn at a rate controlled by the small scale turbulence mixing. The combustion of the char particles is governed by the external diffusion rate of oxygen to the particle surface and by chemical reaction presumed to be first-order in oxygen partial pressure and to occur entirely at the particle surface.

The numerical method involved the finite volume method with the use of the second order QUICK scheme for interpolating the convective coefficients of the momentum equations and the first order hybrid scheme for the rest of the terms. The pressure correction equation is decoupled with the aid of the PISO method formulated by Issa et al [1981]. Special treatment is developed for the boundary conditions. The representative particles are assumed to burn with constant diameter and reducing density.

The validation study comprised four progressive steps that included data gathered from three laboratories of furnaces of different sizes and orientations. The steps consisted of isothermal gas phase data and combustion data. Empasize is devoted to the near burner complicated region.

The results of the validation study showed succesful results for the results obtained from the CCRL furnace for both the single phase isothermal cases and the combustion cases. The validation study gave positive agreement for the single annular orifice burner for both the IFRF and the ICSTM furnaces. A predictive difficulty is discovered when comparing the results with experimental data obtained using a central orifice burner. This testing case is used for a parametric study that involved discretisation scheme, inlet conditions, volatile yield, devolatilsation kinetics, ignition delay, secondary cracking effects, char reactivity, demoisturisation, gas phasae combustion, particle size distribution, drag coefficient, soot inradiation heat transfer and inlet swirl.

6.2 CONCLUSIONS

The number of good data available for the validation of mathematical models of PF flames is small in relation to the complexity and number of involved physical phenomena. Data for the velocities and temperatures of the two phases for furnace conditions are essentially non existant and this fact precludes systematic validation exercises and seriously detracts from the value of the validation studies which can be performed. It is expecting a very great deal of a practicable mathematical model to be able to simulate well such a complex phenomenon as the combusting and turbulent flow in the NBR of a PF swirl burner. Rather the hope is that the simulations will be of sufficient quality to assist the experienced engineer to improve his design.

It is found that this goal is reasonably achieved for the SAO type burner but not for type SCO. The lack of universality is certainly disappointing and has led to numerical experiments with a large number of possible remedies. The task of extracting the right conclusions is not an easy one. The principal difficulty is the continuing absence of reliable velocity measurements. LDA technology seems insufficiently advanced to secure them in the face of non-spherical particles of varying sizes, large fluid density variations, and obscuration problems due to the high particles concentrations.

Although the simple modelling that is incorporated to account for the time-lag associated with the cracking of the primary products of pyrolysis did not bring the anticipated improvements it is nonetheless believed that the failure to allow for this phenomenon is a fundamental failing of existing mathematical models of PF combustion. However, it is clear that this defect is not the sole or principal culprit. The amassed experience leads to the conclusion that the predictive failings for the type SCO burner are aerodynamically linked. The greater tendency of the primary stream to penetrate the IRZ for this geometry renders it inherently more difficult to predict. It may be that the limits of the none too subtle but practicable k-ε turbulence model are excessively exceeded for this flow condition. This presumption can only be tested by the introduction of a multi- equation and state of the art stress-based turbulence model, the superiority of which has been convincingly demonstrated for a range of flows. It would also be reasonable to suggest another possible explanation as to why the quality of the predictions for the two burner types should be so distinctive. The 'roping' phenomenon caused by bends in the primary supply ducting has long plagued power station performance where, effectively, the particles are segregated with the finer ones migrating towards the duct walls and persisting there. The ICSTM experimental furnace suffers bends in the primary supply the effects of which may well not be eliminated by a final long straight run. Regrettably there is not yet an experimental technique which can reveal the radial distribution of the particles' concentrations in the primary duct work. However, if roping exists its effects would certainly be more serious for Burner SCO because of the larger cross sectional area of its primary delivery channel.

Lastly, it might be supposed that the long particles residence times in the fuel rich burner IRZ, which are a predicted feature of the Burner A flow, would lead us to suspect that the NO emissions of this burner will be lower than that for the type B burner. A separate experimental study has shown that this is indeed the case and to a significant extent, {Abbas et al [1991]}.

Inspite of all the failings, at the present time the issue is not so much whether a model is necessarily good or bad in absolute terms but rather whether or not a model has the potential to assist in the process of gaining a better understanding of the physics. We have no doubt that it has.

6.3 SUGGESTIONS FOR FUTURE WORK

This study proved that the dependence of the k-ε model in cases where it is vital to determine accurately the location of the IRZ is unsuitable. Any further development should start with the task of introducing a multi- equation and state of the art Reynolds stress turbulence model, the superiority of which has been convincingly demonstrated

The successful prediction of oxygen concentration in the near burner region should be followed by a through development of NO post-processor to enable the designers of future burners to meet more tight environmental restrictions.

The model should benefit from the new developments in numerical methods that allow better computational economy and more accuracy specially the local grid refinement tecniques, body fitted grids and higher order blended discretisation schemes.

The PISO scheme gave difficulties in converging high swirl cases with high turbulence gradients. It would be advisable to incorporate the SIMPLER scheme to be used for such cases and include the turbulence equations inside the predictor stages of the PISO algorithm.

The particle tracking procedure has adopted simple bouncing techniques. A more realistic model would be required in a further development. The swelling effect is ignored as the application of the model was concentrating on bituminous coals where this effect is of marginal importance. A refined treatment of swelling would be necessary for general use of the model.

When applying the model to large industrial furnaces where the radiative component dominates, the use of the discrete tranfer model instead of the the non-equilibrium diffusion model is advisable.

A parallel three dimensional model that includes all the features of the present one should be formulated for more general application to different geometries specially corner and tangential fired furnaces.

REFERENCES

Abbas, T., Costen, P and Lockwood, F. C. [1991a]. The influence of an aerodynamic change on the formation and emission of nitrogeneous oxides in a pulverized coal-fired furnace. submitted to Combustion and Flame.

Abbas, T., Costen, P , Hassan, M. A and Lockwood, F. C. [1991b]. The effect of the near burner aerodynamics on pollution, stability and combustion in a pf-fired furnace.submitted for publication.

Abbas, A. S., Koussa, S. S. and Lockwood, F. C. [1981]. The prediction of the particle laden gas flows. *18th Symposium [International] on Combustion, The Combustion Institutee.*

Agarwal, P. K. [1986]. A single particle model for the evaluation and combustion of coal volatiles, ***Fuel,*** **65,** 803.

Agrawal, R. K. [1981]. A third-order accurate upwind scheme for Navier-Stokes solutions at high Reynolds numbers. Paper no. AIAA-81-0112, *AIAA 19th Aerospace Science meeting*, St. Louis, Missouri.

Annamalai, K., Durbetaki, P. [1977]. A theory on transition of ignition phase of coal particles. *Combust. Flame,* **29,** 193.

Anthony, D. B. and Howard, J. S. [1976]. Coal devolatilization and hydrogasification. *AIChE journal*, **22, 4,** 625.

Arscott, J. A., Gibb, J. and Jenner, R. [1973]. The application of the diffusion thorey and Monte-Carlo methods to predict the transfer performance of a 500 MW power station boiler from thermal flow data. *European Symposium, The Combustion Institute,* p.675.

Azevedo, J. L. T. and Carvalho, M. G. [1991]. Modelling the near region of a swirling pulverised coal burner. ***presented in the conference of clean combustion***, Algarve, Portugal.

Badzioch, S. and Hawksley, P. G. W. [1970]. Kinetics of thermal decomposition of pulverized coal particles. *Ind. Eng. Chem., Process Des. Develop.*, **9**, 521.

Baum, M. M. and Street, P. J. [1971]. Predicting the combustion behaviour of coal particles. *Combust. Sci. and Tech.*, **3**, 231.

Beer, J. M. and Chigier, N. A. [1974]. *Combustion aerodynamics*. Fuel and Energy Science Series, Applied Science Publishers, London.

Bhattacharjee, S. and Grosshandler, W. L. [1989]. Effect of radiative heat transfer on combustion chamber flows. *Comb. Flame*, **77**, 347.

Bortz, S. [1983]. A further investigation into combined coal/natural gas combustion with a parallel flow burner. International Flame Research Foundation Doc. no. F 090/a/1, Ijmuiden.

Boussinesq, J. [1877]. Theorie de l'ecoulement tourbillant. Mem. par Div. Sav., **23**, Paris

Bradshaw, P. [1971]. The analogy between streamline curvature and buoyancy in turbulent shear flow. *J. Fluid Mech.*, **36**, 1007.

Bradshaw, P. [1973]. Effect of streamwise curvature on turbulent flows. AGARDograph [169].

Bradley, D., Dixon-Lewis, G., Habak, S. and Mushi, E. M. J. [1984]. The oxidation of graphite powder in flame reaction zones. *20th*

Symposium [International] on Combustion, The Combustion Institute. 931.

Choi, S. and Kruger, C. H. [1985]. Modeling coal particle behaviour under simultaneous devolatilization and combustion. *Combust. Flame*, **61**, 131.

Costa, M., Costen, P., Lockwood, F. C. and Mahmud T. [1990]. Detailed measurements in and modelling of an industry-type pulverised-coal flame. *23rd Symposium [International] on Combustion, The Combustion Institute* , 973.

Costa, M., Costen, P. and Lockwood, F. C. [1991a]. Pulverised-coal and heavy-fuel- oil flames: large-scale experimental studies at Imperial College, London*Journal of the Institute of Energy*, **64,** 64.

Costa, M., Costen, P. and Lockwood, F. C. [1991b]. The influence of coal volatility and burner aerodynamics on pulverised-coal flame stability. Proceedings of the second European conference on industrial furnaces and boilers. Algarve - Portugal, 1991.

Costa, M., Costen, P., Lockwood, F. C.and Yehia, M. A. [1991c]. Measurements in and modelling of the near burner region of a swirling pulverised-coal flame. Submitted to Combust. Sci. Tech.

Essenhigh, R. H., Misra, M. K. and Shaw, D. W. [1989]. Ignition of coal particles.*Combust Flame*, **77,** 3.

Fiveland, W. A., Cornelius, D. K. and Oberjohn, W. J. [1984]. A numerical model for predicting furnace performance in axismmetric geometries. *ASME*, 84-HT-103.

Fu, S., Launder, B. E. and Leschziner, M. A. [1987]. Modelling strongly swirling recirculating jet flow with Reynolds-stress transport closures. *Proc. 6th Symp. on Turbulent Shear Flows, Toulouse.*

Fu, S., Huang, P. G., Launder, B. E. and Leschziner, M. A. [1988]. A comparison of algebraic and differential second-moment closures for axisymmetric turbulent shear flows with and without swirl. *J. of Fluid Engineering*, **110**, 216.

Gibbins, J. [1988]. Investigation of primary coal pyrolysis processes using a variable heating rate wire-mesh apparatus. PhD. thesis. Imperial College.

Gibson, M. M. and Launder, B. E. [1978]. Ground effects on pressure fluctuations in the atmospheric boundary layer. *J. of Fluid Mechanics,* **86**, 491.

Gibson, M. M and Morgan, B. B. [1970]. Mathematical model of combustion of solid particles in a turbulent stream with recirculation. *J. Inst. Fuel,* **12,** 512.

Glass, J. and Rodi, W. [1982]. A higher order numerical scheme for scalar transport. *Computer methods in applied mechanics and engineering,* **31**, 337.

Godoy, S., Hirji, K. A. and Lockwood, F. C. [1988]. Combustion measurements in a pulverised coal-fired furnace. *Combust. Sci. and Tech.,* **59**, 165.

Godoy, S., Ismail, M. and Lockwood, F. C. [1989]. Measurements in a cylindrical pulverised coal furnace. Influence of swirl number on combustion performance. *Combust. Sci. and Tech.*, **67**, 59.

Gorner, K. and Zinser, W. [1988]. Prediction of three-dimensional flows in utility boiler furnaces and comparison with experiments. *Combust. Sci. and Tech.*, **58**, 43.

Gosman, A. D. and Ideriah, F. J. K. [1976]. TEACH-2E: A general computer program for two-dimensional, turbulent, recirculating flows. Mech. Eng. Dept.,*internal report, Imperial College*, London.

Gosman, A. D. and Issa, R. I. [1989]. Computational fluid dynamics and heat/mass transfer: an introductory course. Imperial College.

Gupta, R. P., Gururajan, V. S., Lucas, J. A. and Wall, T. F. [1990]. Ignition temperature of pulverised coal particles: experimental techniques and coal-related influences. *Combust. Flame*, **79**, 133.

Hamor, R. J., Smith, I. W. and Tyler, R. J.[1973]. Kinetics of combustion of a pulverised brown coal char between 630 and 2200° K. *Combust. Flame*, **21**, 153.

Harlow, F. H. and Nakayama, P. I. [1968]. Transport of turbulence energy decay rate. Los Alamos Scientific Laboratory report LA-3854, Univ. of California, USA.

Hinze.[1975]. Turbulence. 2nd edition, McGraw-Hill.

Hottel, H. C. and Cohen, E. S. [1958]. Radiant heat exchange for non-uniformity of gas temperature. A.I.Ch. E. J **4**, 3

Howard, J. B. and Essenhigh, R. H. [1967]. Pyrolysis of coal particles in pulverized fuel flames. *Ind. Eng. Chem. Proc. Des. Dev.*, **6**, 74.

Howard, J. B. and Essenhigh, R. H. [1967]. Mechanism of solid-particle combustion with simultaneous gas-phase volatiles combustion. *11th*

Symposium [International] on Combustion, The Combustion Institute, 399.

Huang, G., Vastola, F. J. and Scaroni, A. W. [1985]. Mearsuremen of particle temperatures during coal pyrolysis and combustion. Proceedings of Pittsburg Coal Conference.

Hubbard, E. H. [1958]. Comparison between turbulent jet diffusion flames of gaseous, liquid and pulverised fuels. *Fuel Soc. J.*, **9**, 63

Issa, R., Gosman, A. D. and Watkins, A. P. [1983]. The computation of compressible and incompressible recirculating flows by a non-iterative implicit scheme, Internal report no. FS/83/8, Imperial College.

Jamaluddin, A. S., Truelove, J. S. and Wall, T. F. [1986]. Devolatilization of bituminous coals at medium to high heating rates. *Comb. Flame*, **63**, 329.

Jamaluddin, A. S., Truelove, J. S. and Wall, T. F. [1987]. Modelling of high intensity combustion of pulverised coal in a tubular combustor.*Combust. Sci. and Tech.*, **55**, 89.

Jang, D. S., Jelti, R. and Acharya, S. [1986]. Comparison of the PISO, SIMPLER, and SIMPLEC algorithms for the treatment of the pressure-velocity coupling in steady flow problems. *Numerical Heat Transfer*, **10**, 209.

Jones, W. P. and Launder, B. E. [1972]. The prediction of laminarisation with a two-equation model of turbulence. *Int J. Heat Mass Transfer*, **15**, 301.

Jones, W. P. and Whitelaw, J. H. [1984]. Modelling and measurements in turbulent combustion. *20^{th} Symposium [International] on Combustion, The Combustion Institute* 233.

Khalil, E. E., Spalding, D. B. and Whitelaw, J. H. [1975]. The calculation of local flow properties in two-dimensional furnaces. *Int. J. Heat Mass Transfer*, **18**, 775

Kobayashi, H., Howard, J. B. and Sarofim A. F. [1976]. Coal devolatilization at high temperatures. *16^{th} Symposium [International] on Combustion, The Combustion Institute* 411.

Kollrack, R. and Edelman, R. B. [1987]. Evaluation and assessment of pulverised coal combustion models and data bases. Interim Report No. 2. Submitted to US Department of Energy, SAIC.

Launder, B. E.,Reece, G. J. and Rodi, W. [1975]. Progress in development of a Reynolds stress turbulence closure. *J. Fluid Mech.*, **68** No 3, 537

Launder, B. E.[1977]. Turbulent transport models for numerical computations of complex turbulent flows: Lecture notes for MSc course on Advanced Fluid Dynamics, UMIST.

Launder, B. E. [1982]. Modelling of turbulent flow in gas-turbine blading: achieving and prospects. Int. J. Heat Fluid Flow, **V3 n4**, 171.

Launder, B. E. and Spalding, D. B. [1972]. Mathematical models of turbulence. Academic Press, London.

Launder, B. E. and Spalding, D. B. [1974]. The numerical calculation of turbulent flows. *Computer Methods in Applied Mechanics and Engineering*, **3**, 267.

Laurendeau, N. M. [1978]. Heterogeneous kinetics of coal char gasification and combustion. *Prog. Eng. Comb. Sci.*, **4**, 221.

Leonard, B. P. [1979]. A stable and accurate convective modelling procedure based on quadratic upstream interpolation. *Computer Methods in Applied Mechanics and Engineering*, **19**, 59.

Leschziner, M. A. and Rodi, W. [1981]. Calculation of annular and twin parallel jets using various discretization schemes and turbulence model variations. *J. Fluids Engineering*, **103**, 352.

Levy, J. F. [1991]. Prediction of flow, combustion and heat transfer in coal fired cement kilns. PhD thesis, Mech. Eng. Dept. Imperial College.\

Lockwood, F, C., Salooja, A. P. and Syed, S. A. [1980]. A prediction method for coal fired furnaces. Combust. Flame, **38**, 1.

Lockwood, F, C. and Stolakis, P. [1983]. Assessment of two turbulence models for turbulent round diffusion jets with combustion. *4th Symp. on turbulent shear flows, Univ of Karlsruhe*, FRG.

Lockwood, F, C., Rizvi, S. M. A., Lee G. K. and Whaley H. [1984]. Coal combustion model validation using cylindrical furnace data. *20th Symposium [International] on Combustion, The Combustion Institute* .

Lockwood, F, C., Rizvi, S. M. A. and Shah, N. G. [1986]. Comparative predictive experience of coal firing. *Proc. Instn Mech. Engrs*, **200 no C**, 79.

Lockwood, F.C. and Mahmud, T. [1988]. The prediction of swirl burner pulverised coal flames,*22nd Symposium [International] on Combustion, The Combustion Institute*, 1165.

Lockwood, F.C.and Papadopoulos, C.[1989]. A new method for the computation of particulate dispersion in turbulent two phas flows. *Combust. Flame*, **61**, 131

Lockwood, F.C., Papadopoulos, C. and Abbas, A. S. [1988b]. Prediction of a corner-fired power station combustor. *Combust. Sci. and Tech.*, **58**, 5.

Lockwood, F.C. and Rizvi, S.M.A.[1988]. Prediction of low and high volatiles pulverised coal flames, Int. Rep. FS/88/15, Imperial College.

Magnussen, B. F. and Hjertager, B. H. [1976]. On mathematical modelling of turbulent combustion with special emphasis on soot formation and combustion. *16th Symposium [International] on Combustion, The Combustion Institute*, 719.

Mahmud, T., Truelove, J. S. and Wall, T. F. [1987]. Measurements and calculations of mean velocity in isothermal coaxial jets from swirl burners. *J. Fluids Engineering*, **109**, 275.

McDonald, H. [1979]. *Prog. Energy Comb Sci.*,5,97

McGuirk, J. J., Taylor, A. M. P. K. and Whitelaw, J. H. [1982]. An assesment of numeical diffusion in upwind difference calculation of turbulent recirculating flows, Turbulent shear flows 3, Springer Verlag.

Michel, J. B. and Payne, R. [1980]. Detailed measurement of long pulverised coal flames for the characterization of pollutant formation. Int. Flame Research Foundation, Doc. No. F 09/a/23, Ijmuiden, The Netherlands.

Migdal, D. and Agosta, V. D. [1967]. A source flow model for continuum gas particle flow, Trans. ASME, *J. Applied Mechs.*, **89**, 860.

Mostafa, A. A. and Mongia, H. C. [1988]. On the interaction of particles and turbulent fluid flow. *Int. J. Heat Mass Transfer*, **31**, 2063.

Musarra, S. P., Fletcher, T. H., Niksa S. and Dwyer, H. A. [1986]. Heat and mass transfer in the vicinty of a devolatilizing particle. *Combust. Sci. and Tech.*, **45**,289.

Patankar, S. V. and Spalding, D. B. [1972]. A calculation procedure for heat, mass and momentum in three-dimensional parabolic flows. *Int. J. Heat Mass Transfer*, **15**, 1787.

Patankar, S. V. [1980]. Numerical heat transfer and fluid flow. Hemisphere Publishing Corporation, Washington.

Patankar, S. V. [1988]. Recent developments in computational heat transfer. *J Heat Transfer*, **110**, 1037.

Prado, G., Froelich, D. and Lahaye, J. [1987]. Heterogeneos combustion of residual coke particle. Fundamentals of the physical-chemistry of pulverized coal combustion. Ed. Lahaye and Prado. Nato ASI series.

Prandtl, L. [1925]. Bericht uber Untersuchungen zur ausgenbildeten Turbulenz. ZAMM, 5, 136 English Translation: Spalding, D. B. [1980], Imperial College, Mech. Eng. report HTS/TN/80/1.

Pratt, D. T. [1976]. ***Prog. Energy Comb. Sci,*** **1, 73.**

Raithby, G. D. [1976]. Skew-upstream differencing schemes for problems involving fluid flow. *Computer Methods in Applied Mechanics and Engineering*,**9**

Reece, G. J. [1977]. Development and application of a generalized Reynolds stress model of turbulence. PhD thesis, Imperial College.

Rizvi, S. M. A. [1985]. Prediction of flow, combustion and heat transfer in pulverized coal flames. Ph.D. thesis, Mech. Eng. Dept. Imperial College.

Roache, P. J. [1982]. Computational fluid dynamics. Hermosa Publishers, Albuquerque

A two-parameter model of turbulence and its application to free jets. Warme und Stofubertragung, **3**, 85

Rodi, W.[1979]. Influence of buoyancy and rotation on equation for the turbulent length scale. *Proc. 2nd Symp. on Turbulent Shear Flows,* London.

Rodi, W.[1980]. Turbulence models and their application in hydraulics- a state of the art review. Int. Association for Hydraulic Research Publication, Delft.

Salooja, A. P. [1978]. Mathematical modelling of an experimental studies in axi-symmetrical combustors. PhD thesis, University of London.

Saxena, S. C. [1990]. Devolatilization and combustion characteristics of coal particles. *Prog. Energy Comb. Sci,* **16**, 55.

Schlichting, H. [1968]. Boundary layer theory. McGraw-Hill Book Co., New York.

Shaw, D. W., Zhu, X., Misra, M. K. and Essenhigh, R. H. [1990]. Determination of global kinetics of coal volatiles combustion. *23rd Symposium [International] on Combustion, The Combustion Institute,* 1155.

Sloan, D. G., Smith, P. J. and Smoot, L. D. [1986]. Modelling of swirl in turbulent flow systems. *Prog. Energy Combust. Sci.*, **12**, 163.

Smith, I. W. [1978]. The intrinsic reactivity of carbons to oxygen. *Fuel*, **57**, 409

Smith, I. W. [1982]. The combustion rates of coal chars: a review.*16th Symposium [International] on Combustion, The Combustion Institute* .1045.

Smith, P. J. and Fletcher, T. H. [1988]. A study of two chemical reaction models in turbulent coal combustion. *Combust. Sci. and Tech.*, **58**, 59.

Smith, P. J. and Smoot, L. D. [1980]. One-dimensional model for pulverised coal combustion and gasification. *Combust. Sci. and Tech.*, **23**, 17.

Smith, P. J., Sowa, W. A. and Hedman, P. O. [1990]. Furnace design using comprehensive combustion models. *Combust. Flame,* **79,** 111.

Smoot, L. D. [1981]. Pulverised coal diffusion flames: a perspective through modelling. *18th Symposium [International] on Combustion, The Combustion Institute,* 1185.

Smoot, L. D. and Horton, M. D. [1978]. Exploratory studies of flame and explosion quenching, Final Report, Bureau of Mines Contract 10122052, Brigham Young University, Provo, Utah.

Smoot, L. D. and Smith, P. J. [1985]. Coal combustion and gasification. The Plenum Chemical Engineering Series, Ed. Dan Luss, Plenum Press, New York.

Solomon, P. R., Chien P. L., Carangelo, R. M., Serio, M. A. and Markham [1990]. New ignition phenomenon in coal combustion. *Combust. Flame,* **79,** 214.

Speziale, G. C., Gatski, T. B. and Mhuiris, N. M. [1989]. A critical comparison of turbulence models for homogeneous shear flows in a rotating frame. ICASE report no. 89-43,NASA contractor report 181864.

Stewart, F. R. and Cannon, P. [1971]. The calculation of radiative heat flux in a cylindrical furnace using the Monte Carlo method. *Int. J. Heat Mass Transfer,* **14**, 245.

Strugess, G. J. and Syed S. A. [1985]. A calculation of confined swirling flows. AIAA-85-0060. AIAA 23rd Aerospace Science Meeting, Reno, NV Jan. 14-17.

Syed, S. and Chiapetta, L. M. [1985]. Finite difference methods for reducing numerical diffusion in TEACH-type calculations. AIAA-85-005, AIAA 23rd Aerospace Science Meeting, Reno, NV Jan. 14-17.

Suuberg, E. M., Peters, W. A. and Howard, J. B. [1979]. Product compositions and formation kinetics in rapid pyrolysis of pulverised coal implications for combustion. *17th Symposium [International] on Combustion, The Combustion Institute* , 117.

Syed, S., Gosman, A. and Peric, M. [1985]. Assessment of discretisation schemes to reduce numerical diffusion in the calculation of complex flows. *AIAA -85-0441*.

Taniguchi, H., Kudo, K., Hayasaka, H., Yang, W. J. and Tashiro, H. [1984]. Fundamentals of thermal radiation heat transfer, T. C. Min and J. L. S. Chen [Eds.] ASME HTD, 40, 29, Newyork.

Thomas, G. R., Harris, J. J. and Evans, D. G. [1968]. The ignition of pulverized brown coal. *Combust. Flame*, **12,** 391.

Thurgood, J. R., Smoot, L. D. and Hedman, P. O. [1979]. Rate measurements in a laboratory-scale pulverized coal combustion. *Combust. Sci. and Tech.*, **21**, 213.

Truelove, J. S. [1986]. Prediction of the near-burner flow and combustion in swirling pulverised-coal flames. *21st Symposium [International] on Combustion, The Combustion Institute* 275.

Truelove, J. S. and Holcombe, D. [1990]. Measurement and modelling of coal flame stability in a pilot-scale combustor. *23rd Symposium [International] on Combustion, The Combustion Institute*, 963.

Tsai, C. Y. and Scaroni, A. W. [1987]. The structural changes of bituminous coal particle during the initial stages of pulverised-coal combustion, *Fuel*, **66**, 200.

Ubhayakar, S., Stickler, D. B., Von Robenberg, C. W. and Gannon, R. E. [1976]. Rapid devolatilization of pulverized coal in hot combustion gases. *16th Symposium [International] on Combustion, The Combustion Institute* 427.

Viskanta, R. and Menguc, M. P. [1987]. Radiation heat transfer in combustion systems. *Prog. Energy Combust. Sci.*, **12**, 163.

Visser, B. M., Smart, J. P.,Van De Kamp, W. L. and Weber, R. [1990]. Measurements and predictions of quarl zone properties of swirling pulverised coal flames. *23rd Symposium [International] on Combustion, The Combustion Institute*, 949.

Visser, B. M. [1991]. Mathematical modelling of swirling pulverised coal flames. PhD thesis, Technisch Universiteit Delft.

Wall, T. F., Phelan, W. J. and Bortz, S. [1986]. Coal burnout in the IFRF no. 1 furnace. *Combust. Flame*, **66**, 137.

Wall, T. F. and Gurarajan, V. S. [1986]. Combustion kinetics and the heterogeneous ignition of pulverized coal. *Combust. Flame*, **66**, 151.

Wallis, G. B. [1979]. One-dimensional two-phase flow. McGrawHill, NewYork.

Weber, R., Boysan, F., Swithenbank, J. and Roberts [1986]. Computations of near field aerodynamics of swirling expanded flows. *21st Symposium [International] on Combustion, The Combustion Institute*, 1435.

Weber, R., Visser, B. M. and Boysan, F. [1990]. Assessment of turbulence modelling for engineering prediction of swirling vortices in the near burner zone. *Int. J. Heat Fluid Flow*, **11**, no. 3.

Wen, C. Y. and Chen, L. H. [1979]. A model for coal pyrolysis. Paper presented at ACS National Meeting, Washington D. C.

Xieu, D. V., Masuda, T., Cogoli, J. G. and Essenhigh, R. H. [1981]. A mathematical model of a one dimensional char flame: a comparison of theorey and experiment. *18th Symposium [International] on Combustion, The Combustion Institute*, 1641.

Young, B. C. and Smith, I. W. [1981]. The kinetics of combustion of petroleum coke particles at 1000 to 18000 K: The reaction order. *18th Symposium [International] on Combustion, The Combustion Institute*, 1249.